

# 博士論文

*In-Situ* Chemical Structure Analysis of Cured Glue-Line of Aqueous Vinyl Polymer-  
Isocyanate Adhesive for Wood Using FT-NIR and FT-IR Spectroscopy

(FT-NIR および FT-IR による水性高分子-イソシアネート系木材接着剤の接着層の  
*in-situ* 化学構造分析)

凌 志剛



1	Introduction .....	1
1.1	Aqueous Vinyl Polymer-Isocyanate Adhesive for woods.....	1
1.1.2	Advantage and Disadvantage .....	1
1.1.3	Components.....	2
1.1.4	NCO Reactions.....	5
1.1.5	Cross-Linking Attributed to NCO Reactions .....	5
1.1.6	Curing and Post-Curing.....	7
1.1.7	Previous Researches .....	7
1.2	Fourier Transform Near Infrared Spectroscopy .....	9
1.2.1	Fourier Transform Infrared Spectroscopy .....	9
1.2.2	Fourier Transform Near Infrared Spectroscopy .....	11
1.2.3	Derivatization .....	13
1.2.4	Two-Dimensional Correlation Spectroscopy .....	14
1.3	Purpose .....	16
2	Post-Curing Process of API Adhesive.....	17
2.1	Introduction .....	17
2.2	Experimental .....	18
2.2.1	Materials.....	18
2.2.2	Sample Preparation.....	19
2.2.3	Characterizations .....	21
2.3	Results and Discussion.....	21
2.3.1	TGA.....	21
2.3.2	DSC .....	24
2.3.3	DMA.....	27
2.3.4	FT-IR .....	30
2.3.5	Bond strength .....	36
2.4	Conclusions .....	36
3	In-situ Analysis of API Adhesive glue-line by using FT-NIR .....	39
3.1	Introduction .....	39
3.2	Experimental .....	40
3.2.1	Materials.....	40
3.2.2	Sample Preparation.....	40
3.2.3	Characterizations .....	41
3.3	Results and Discussion.....	42
3.3.1	DSC Thermograms of model Compounds .....	42
3.3.2	FT-IR Spectra of Model Compounds .....	42

3.3.2 FT-NIR Spectra of Model Compounds .....	46
3.3.3 FT-NIR Spectra of API paper.....	52
3.4 Conclusions .....	59
4 Influence of Adhesive Components and Aging Conditions on The Chemical Structure of API Adhesive Glue-Line .....	61
4.1 Introduction .....	61
4.2 Experimental .....	62
4.2.1 Materials .....	62
4.2.2 Adhesive Preparation .....	62
4.2.3 Sample Preparation.....	63
4.2.4 Aging Humidity.....	64
4.2.5 Heat Treatment .....	64
4.2.6 Characterizations .....	64
4.3 Results and Discussion.....	64
4.3.1 Different PVAs.....	64
4.3.2 Different SBR latex Mass Ratios .....	67
4.3.3 Different Humidity conditions .....	71
4.3.4 Heat Treatment .....	74
4.4 Conclusions .....	77
5 Further Studies on NCO self-reactions and Urethane Generating Reactions.....	79
5.1 Introduction .....	79
5.2 Experimental .....	80
5.2.1 Materials .....	80
5.2.2 Synthesis.....	80
5.2.3 Characterizations .....	82
5.3 Results and Discussion.....	82
5.3.1 Uretdione and Isocyanurate.....	82
5.3.2 Difference on Band Location Between Urethane and Isocyanurate.....	84
5.3.3 Uretdione and Isocyanurate in API thin Film.....	86
5.3.4 Thermal degradation of urethane.....	87
5.3.5 Urethane formation in ambient condition.....	92
5.4 conclusions .....	95
6 Summary .....	96
References .....	99
Acknowledgement.....	108

# **1 Introduction**

## **1.1 Aqueous Vinyl Polymer-Isocyanate Adhesive for woods**

### **1.1.1 History**

Aqueous Vinyl Polymer-Isocyanate Adhesive for woods (API adhesive) has been defined as one adhesive prepared using aqueous polymer solution or water-based emulsion as base resin and isocyanate component as cross-linker. <sup>[1, 2]</sup>

Before the appearance of API adhesive, the widely utilized adhesives for furniture and housing construction are formaldehyde-based products such as urea resin. As VOCs (Volatile Organic Compounds) pollution had been taken into account more and more, non-formaldehyde-containing adhesive was requested strongly by industry. In 1970s, API adhesive was first developed by Kuraray Co., Ltd, Koyo Sango Co., Ltd and Asahi Plywood Co., Ltd and patented then in Japan.

API adhesive is also named as 'WPI', which is the abbreviation of 'Water Based Polymer-Isocyanate Adhesive for Woods', based on Japanese Industrial Standard. In Europe, this adhesive is abbreviated as 'EPI', based on the name of 'Emulsion Polymer Isocyanate'.

### **1.1.2 Advantage and Disadvantage**

API adhesive has the advantages:

- Non-formaldehyde emission, environmentally friendly
- High bond strength, durability and thermal resistance
- Various operating conditions due to room temperature curing
- Less damage to wood due to neutral pH

It also has disadvantage:

- Higher price
- Short pot life
- A little bit of toxicity

### 1.1.3 Components

Normally, API adhesive is prepared from three components, base resin, cross-linker and filler. Originally, Polyvinyl alcohol (PVA) aqueous solution was employed as base resin. Styrene-butadiene rubber (SBR) latex and ethyl vinyl acetate (EVAc) latex are also added to improve the performance of adhesive. Cross-linker consists of highly reactive NCO (isocyanate) group, and therefore can react with other components. Filler, such as CaCO<sub>3</sub> and wheat flour, are used to reduce the price and improve gap filling property.

- PVA (Scheme 1.1)

PVA, one of water-soluble polymers, is used widely in adhesion industry in consideration of its low price and innocuity. PVA is produced by the saponification of polyvinyl acetate. Degree of saponification is one important factor that concerns physical properties. In API adhesive, PVA hydroxyl reacts with NCO, generating cross-linking structure. Further, PVA could be used to adjust the performance of API adhesive.

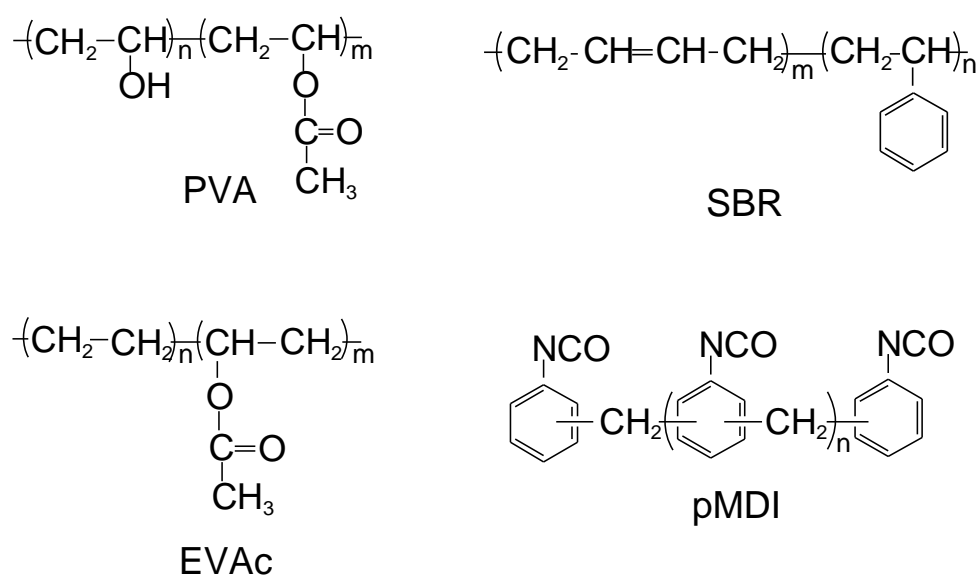
PVA with high degree of saponification has more hydroxyls attaching onto molecular chain, and could produce a better water resistant glue-line. On the other hand, PVA with low degree of saponification has more lipophilic acetyl groups attaching onto molecular chain, which could lead to a better compatibility of PVA with other components <sup>[2]</sup>. Therefore, most of PVAs used for API adhesives are partially saponified.

· SBR latex (Scheme 1.1)

In industry, SBR latex is synthesized by the emulsion copolymerization of styrene and butadiene. SBR latex can act as a softer, improve the elastic property of API adhesive, adjust initial bond strength and reduce cost. The lipophilicity of SBR allows it to promote the miscibility of base resin and cross-linker and further accelerate the formation of cross-linking structure.

· EVAc latex (Scheme 1.1)

EVAc is copolymerized from ethylene and vinyl acetate. It also has excellent flexibility and bond strength and can improve initial bond strength more than SBR latex. However, considering the more CO<sub>2</sub> releasing of API adhesive caused by EVAc, the usage of EVAc latex is limited [3].



Scheme 1. 1

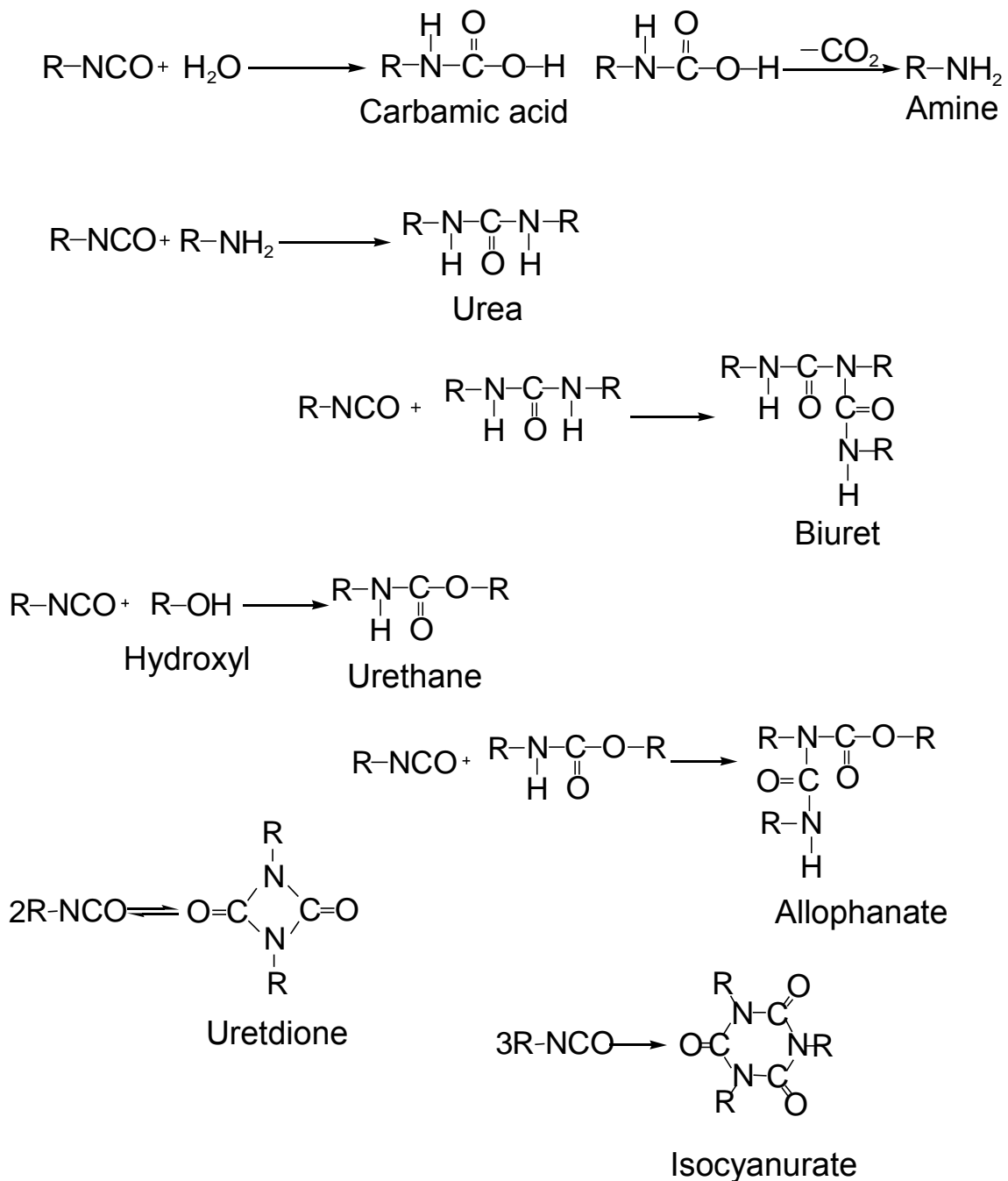
· NCO cross-linker

Cross-linker employed for API adhesive has more than two NCOs on molecular chain, such as diphenylmethane diisocyanate (MDI) and Toluene diisocyanate (TDI), which can form cross-linking structure in glue-line. Normally, aromatic isocyanate has better bond strength and durability than aliphatic isocyanate. Widely used polyisocyanate, polymethylene polyphenyl polyisocyanate (pMDI,

Scheme 1.1) <sup>[4]</sup>, is the polymer of MDI, and contains MDI more than half of the weight <sup>[5]</sup>.

· Filler

Fillers, such as CaCO<sub>3</sub> <sup>[6]</sup>, wheat flour and starch, are also added into adhesive to reduce cost, improve gap filling property, and inhibit over-permeation of API adhesive.



Scheme 1. 2. The reactions of NCO. R: the functional group not reacting with NCO.

### **1.1.4 NCO Reactions**

NCO reacts with labile hydroxyl, producing cross-linking structure and generating bond strength. NCO reactions in API adhesive were shown in Scheme 1.2. Reaction between NCO and water is the rapidest one in API adhesive, forming carbamic acid at first. The formed instable carbamic acid soon decomposes, releases CO<sub>2</sub> and generates amine. Then, amine will react with another NCO and form urea. NCO also can react with hydroxyls, generating urethane. Hydroxyls are not only from adhesive components, such as hydroxyl of PVA, but also from adherends. In adhesive-bonding-wood structure, hydroxyls of wood ingredients, for example, hydroxyl of cellulose, can react with NCO. Thus, urethane formations could also generate covalent bond between adhesive and adherend. Actually, NCO can further react with the produced urea and urethane and generate biuret and allophanate, as it was shown in Scheme 1. 2. However, those reactions were regarded as side reactions and barely occur at ambient temperature <sup>[7]</sup>.

Also, self-reactions of NCO rise, producing dimer (uretdione) and trimer (isocyanurate) (Scheme 1. 2). It seems like that the self-reactions will wastefully consume NCO in API adhesive, but for the isocyanate compounds which has more than two NCO groups on molecular chain, such as MDI and pMDI, self-reactions could form cross-linking structure, too.

### **1.1.5 Cross-Linking Attributed to NCO Reactions**

After API adhesive was applied onto wood, initial bond strength relies on PVA and SBR performances. In the first 24h, evaporation and permeation of water as well as NCO reactions lead to the curing process of API adhesive and finally form a glue-line. NCO reactions still can continue for several days in glue-line, contributing to the increasing of physical property, which is called post-curing process.

Cross-links produced in glue-line could be summarized as following:

- NCO-water: NCO reacts with water, release  $\text{CO}_2$  and forms urea linkage. Two NCOs are consumed in this process, so if the two NCOs are from two different molecules, then this reaction will generate one cross-linking.
- NCO-hydroxyl of adhesive components: This reaction produces urethane linkage inside API adhesive, which contributes to the increasing of cohesion.
- NCO-hydroxyl of wood: Wood consists of cellulose, hemicellulose, lignin, etc. that contain hydroxyl on molecular chain, so it can react with NCO. This reaction generates urethane linkage between NCO and wood, contributing to the increasing of adhesion.
- Cross-linking attributed to others reactions: Other reactions of NCO, such as biuret and uretdione generating reactions, also can form cross-links. However, those reactions are very limited at ambient temperature <sup>[7]</sup>.

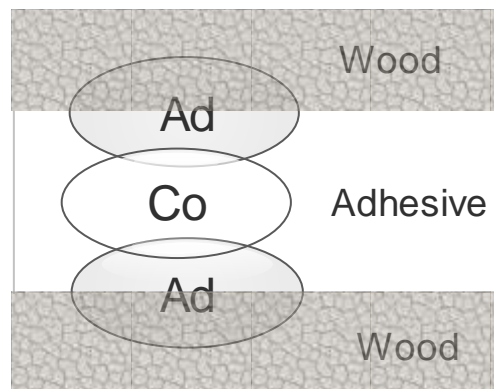


Fig. 1.1. Glue-line. Ad: adhesion; Co: cohesion.

Glue-line structure was shown in Fig. 1.1. There are two kinds of primary strength existing in glue-line: the one inside adhesive is called cohesion that is due to the aggregation of adhesive, the other one between adhesive and wood is named as adhesion which is due to the interaction of adhesive and wood. <sup>[8, 9]</sup>

### **1.1.6 Curing and Post-Curing**

After adhesive was applied on adherend, it is commonly cured at room temperature for at least 12h. In curing process, cross-linking structure is formed to a certain extent. Post-curing is a subsequent process, in which one elevated temperature is normally performed on adhesive to accelerate cross-linking forming reactions. Post-curing process can improve mechanical properties of adhesive, such as bond strength and flexural strength.

In this experiment, API adhesive was prepared from aqueous solution and emulsion of base polymers and cross-linker. Then, the prepared API adhesive was aged in thermostatic chamber (RH50%, 23°C). At first, water in API adhesive evaporated, and the reactions of NCO carried on gradually. The first step, called as curing, lasted for 24h, after which API adhesive solidified into block. Here, the cured API adhesive was continuously aged for much longer time in thermostatic chamber, and this period was called post-curing. Even though no heating, NCO reactions still carried on in post-curing process, forming urethane, urea, etc., which aroused the motion of molecular chain as well as the increasing of mechanical property.

### **1.1.7 Previous Researches**

Initial studies on API adhesive mostly focused on production and performance. Afterwards, Taki <sup>[10]</sup> firstly started a research on chemical structure analysis, and then this subject was carried on gradually.

#### **· Components**

Due to NCO reactions, specially, urea and urethan generating reactions, cross-linking structure forms. According to Takis' research, NCO reaction with water consists of three steps: first, NCO react with water, generating carbamic acid; second, generated carbamic acid soon decomposes, releases CO<sub>2</sub> and forms amine;

third, amine reacts with another NCO and forms urea linkage<sup>[11]</sup>. NCO reacts with hydroxyl, generates urethane linkage and contributes to the increasing of water resistance. While, the generating rate of urethane is much lower than that of urea<sup>[12]</sup>. In order to investigate the reactivity between NCO and PVA hydroxyl, Yamada et al<sup>[13]</sup> used acetoacetylated PVA to react with NCO compound. They found out that lipophilic group, acetoacetyl, can accelerate the mixing and the reaction of NCO with hydroxyl.

Hori et al.<sup>[3]</sup> reported that the addition of EVAc can increase CO<sub>2</sub> releasing in API adhesive. Maehara<sup>[14]</sup> investigated the effects of SBR and EVAc latexes on rheological property of initially cured API adhesive.

CaCO<sub>3</sub> used as filler can reduce cost, increase solid content and improve gap filling property<sup>[15]</sup>. Donate-Robles et al.<sup>[16]</sup> studied the interaction between CaCO<sub>3</sub> and adhesive using ATR-IR.

#### · Reaction Rate of NCO

According to previous studies<sup>[17]</sup>, NCO can remain and react in glue-line for a long time in post-curing process. Taki et al.<sup>[18]</sup> reported that the amount of residual NCO in adhesive film after 1-3 weeks aging was 40% of the initial amount. Yamada et al.<sup>[19]</sup> heated cured API adhesive and confirmed the steep reaction of residual NCO.

#### · Aging Condition of Post-curing

After API adhesive was coated onto wood, post-curing process continues for several days. In this period, aging conditions, such as temperature and humidity, can affect chemical structure as well as mechanical property of adhesive<sup>[5, 20]</sup>. Ling et al.<sup>[21]</sup> studied the effect of heat treatment on dynamic viscoelastic property and chemical structure. He et al.<sup>[22]</sup> used differential scanning calorimetry to investigate the effect of aging humidity on pMDI reaction.

#### · The Analysis of Chemical Structure

There were several methods used to analyze the chemical structure of API adhesive. Taki et al. confirmed NCO-cellulose reaction peak at  $\approx 270^\circ\text{C}$  on DSC thermogram [23]. Frazier et al. labelled pMDI by using  $^{15}\text{N}$  and analyzed the product generated from the reaction of between  $^{15}\text{N}$ -pMDI and wood using CP/MAS NMR. Reaction rate increasing of NCO was confirmed by using differential scanning calorimetry by He et al. [22]. Gao et al. [24] used FT-IR to study the reactions of pMDI in protein-based API adhesive.

However, it is difficult to analyze the chemical structure of adhesive applied onto adherend. Omura et al. [25] used filter paper as adherend and *in-situ* detected the adhesive glue-line sandwiched between two pieces of filter paper by using FT-NIR.

## 1.2 Fourier Transform Near Infrared Spectroscopy

### 1.2.1 Fourier Transform Infrared Spectroscopy

Infrared spectrum (FT-IR) is generated from the fundamental infrared absorption of chemical bond, by which molecular structure can be discussed [26]. In ambient environment, all atoms are vibrating at a lowest energy level through chemical bonds, and the vibration can transform into a higher energy level by absorbing infrared light. Here, the infrared light absorbed by each chemical bond is quantized, i.e. wavenumber is specific. Therefore, the existence of each chemical bond can be designated, respectively.

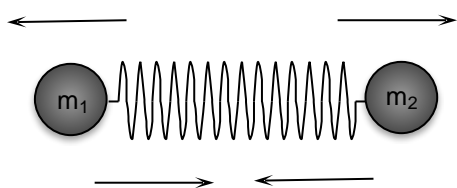


Fig. 1.2. Vibration of diatomic molecule.

$$\mu = \frac{m_1 m_2}{m_1 + m_2}$$

$$\nu = \frac{1}{2\pi} \sqrt{\frac{K}{\mu}}$$

Scheme. 1.3. Hooke's law.

The simplest vibration model is stretching of diatomic molecule, which was shown in Fig. 1.2. Two atoms, with the masses of  $m_1$  and  $m_2$ , respectively, were bonded by electrons and vibrated. Vibrational frequency  $\nu$  can be calculated using Hooke's law in Scheme 1. 3 where  $K$  is force constant of bond and  $\mu$  is reduced mass. Atoms can vibrate at different energy levels, and the energy levels are discrete.

$$E_n = h\nu(n + \frac{1}{2}), \quad (n=0, 1\dots) \quad (1)$$

$$\Delta E = E_1 - E_0 = h\nu = \frac{h}{2\pi} \sqrt{\frac{K}{\mu}} \quad (2)$$

$$\bar{\nu} = \frac{1}{\lambda} = \frac{h}{2\pi c} \sqrt{\frac{K}{\mu}} = 1307 \sqrt{\frac{K}{\mu}} \quad (3)$$

Scheme 1. 4. Fundamental absorption.  $h$ , Planck's constant;

$E$ , energy;  $\bar{\nu}$ , wavenumber.

Scheme 1. 4 indicated the calculations of vibrational energy,  $E_n$ , the energy of absorbable infrared light;  $\Delta E$ , the wavenumber of infrared light;  $\bar{\nu}$ , corresponding to fundamental absorption. Diatomic molecular at ground level has the energy of  $E_0$ . After it absorbed infrared light energy,  $\Delta E$ , atoms will vibrate at a higher energy level,  $E_1$ . Absorbable energy for each chemical bond is specific, so is the wavenumber of infrared light. Thus, the information of each chemical bond can be confirmed on spectrum separately.

Infrared spectroscopy is widely used in industry, agriculture, etc., due to admirable capability to detect the molecular component and structure. Normally used FT-IR (Fourier Transform Infrared) spectroscopy tests the wavenumber range between 400 and 4000  $\text{cm}^{-1}$ , which is called mid-infrared (Fig. 1.3).

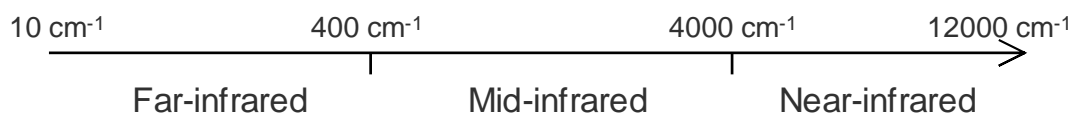


Fig. 1.3. Different infrared ranges.

### 1.2.2 Fourier Transform Near Infrared Spectroscopy

Different from IR spectroscopy, NIR (Near Infrared) Spectroscopy tests the near-infrared range of 4000-12000 $\text{cm}^{-1}$  (Fig. 1.3). Moreover, the mechanism of near-infrared absorption is also distinct from the former. In other words, only overtone and combination tone could be observed on NIR spectrum.

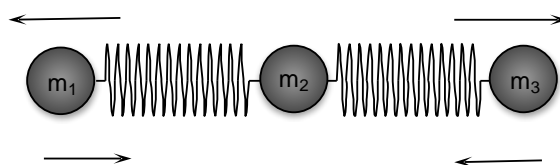
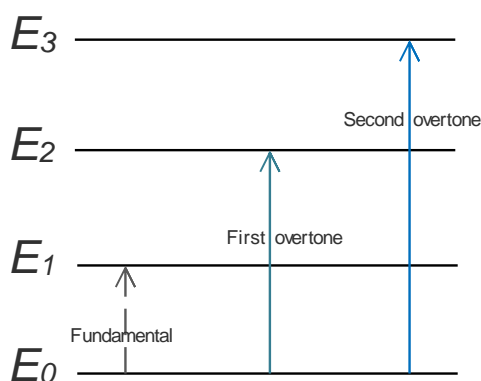


Fig. 1.4. Energy levels of vibration.

Fig. 1.5. Vibration of triatomic molecule.

#### · Overtone

IR absorption (fundamental absorption) arises in the situation that atom vibration transmits over only one energy level, changing from  $E_0$  to  $E_1$ . On the other hand, a few part of atom vibrations can transmit over more than one energy level, changing from  $E_0$  to  $E_2$ ,  $E_3$ , or even higher energy level, and this action causes first, second, or higher overtone absorption (Fig. 1.4). In the case of overtone absorption, wavenumber of absorbed infrared light can be calculated using Scheme 1. 5 where  $\nu_n$  is the wavenumber in overtone absorption,  $\nu_1$  is the wavenumber of fundamental absorption,  $\chi$  is the anharmonicity constant considering anharmonic vibration, and  $n$  is 2 for first overtone, 3 for second

overtone, etc. However, the value of  $\chi$  is too small to have a significant effect on the consequent wavenumber.  $\chi$  values of some common chemical bonds are listed in Table 1.1. [27]

Table 1. 1. Anharmonicity constants.

$$\nu_n = \frac{\nu_1 n - \nu_1 \chi n(n+1)}{1 - 2\chi}$$

$\chi\nu(\text{CH})$	$1.9 \times 10^{-2}$
$\chi\nu(\text{CD})$	$1.5 \times 10^{-2}$
$\chi\nu(\text{CF})$	$4 \times 10^{-3}$
$\chi\nu(\text{CCl})$	$6 \times 10^{-3}$
$\chi\nu(\text{C=O})$	$6.5 \times 10^{-3}$

#### Scheme 1. 5. Overtone absorption.

- Combination tone

Combination tone arises in polyatomic molecule on condition that more than two absorptions occurs at the same time. In other words, it is generated from the sum and difference of fundamental absorption [27]. Fig. 1.5 demonstrated the stretching vibration of triatomic molecule, which is the simplest model of combination tone. If the bond between  $m_1$  and  $m_2$  has the fundamental infrared absorption at wavenumber  $\nu_1$ , and the bond between  $m_2$  and  $m_3$  has the absorption at  $\nu_2$ , then combination absorption of these two bonds can give rise to a combination tone at around  $\nu_1 + \nu_2$ . Combination tone is relevant to the molecular symmetry so it is more unique than overtone for the distinguishment of chemical bonds.

- Characteristic of FT-NIR

NIR absorption has a lower probability of occurrence than IR absorption, due to which the applied sample amount for FT-NIR spectroscopy is more than that for FT-IR spectroscopy. In addition, NIR light has an admirable penetration ability that allows it to be performed on un-pretreated sample. Comparing to other analysis methods, e.g., DSC and NMR, FT-NIR has a shorter test time. However, on FT-NIR spectrum the overlapping of bands occurs significantly, which

complicates the assignment of chemical bond, so, normally, some treatment methods are applied, such as derivatization.

### 1.2.3 Derivatization

$$x_{ik} = a_i \bar{x}_k + b_i + e_{ik}$$

Scheme 1. 6. Components of spectrum.

Original spectrum consists of several components, which was shown in Scheme 1. 6 where  $x_{ik}$  is original spectrum,  $\bar{x}_k$  is average spectrum,  $a_i$  is multiplied fluctuation,  $b_i$  is additive fluctuation, and  $e_{ik}$  is error. By 1<sup>st</sup> derivatization the effects of  $b_i$  and  $e_{ik}$  can be eliminated, and by 2<sup>nd</sup> derivatization the effect of  $a_i$  can also be dissolved. In NIR test the obtained spectrum is frequently influenced by physical differences, for example, particle size and thickness of sample. Derivatization can reduce the effect of physical difference and clarify the chemical difference between spectra, which is particularly useful in *in-situ* analysis [27].

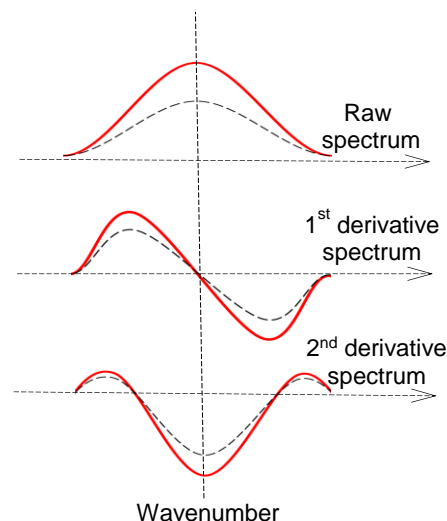


Fig. 1.6. Derivatizations of spectrum. Solid and dot lines represent two different spectra.

Fig. 1.6 illustrated the bands on raw, 1<sup>st</sup> derivative and 2<sup>nd</sup> derivative spectra, respectively. 1<sup>st</sup> derivatization calculates the gradient of raw spectrum, therefore

the upward peak on raw spectrum turns into vertical-axis origin point on 1<sup>st</sup> derivative spectrum. 2<sup>nd</sup> derivative spectrum is obtained by performing another derivatization on 1<sup>st</sup> derivative spectrum, on which a downward peak shows up at the same wavenumber as that of raw spectrum peak [28]. On the other hand, the change of band intensity can also be confirmed using derivative spectra. When some variations arise on molecular structure, caused by physical or chemical factor, the band intensity will vary accordingly. On raw spectrum (Fig. 1.6), band intensity increases from dot line to solid line. The increasing will arouse a variation of derivative spectra, also from dot to solid line. Based on this phenomenon, the variation of chemical structure could be discussed by using 2<sup>nd</sup> derivative spectrum.

#### 1.2.4 Two-Dimensional Correlation Spectroscopy

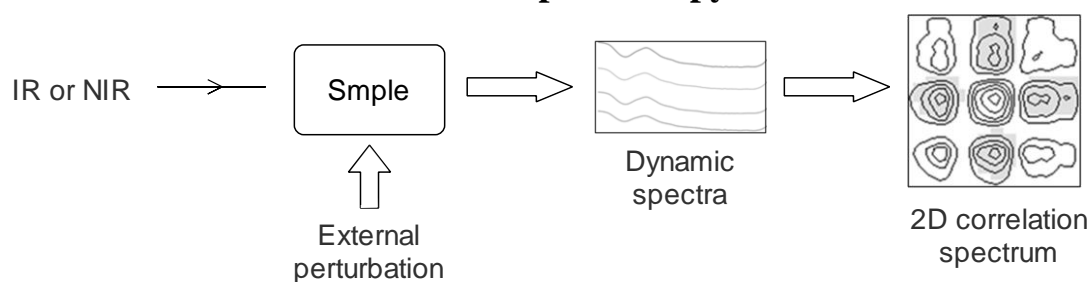


Fig. 1.7. Process of 2D correlation spectrum.

2D (two-dimensional) correlation spectroscopy for IR was started by Noda in 1990s [29], which could be utilized to study the molecular interaction. After an external perturbation, e.g., varying temperature, is applied to the sample, some dynamic variations will demonstrate on IR spectra, due to intra and intermolecular interaction. 2D correlation spectrum is obtained by spreading dynamic IR spectra over two dimension and protruding the correlation (Fig. 1.7). 2D correlation spectroscopy can also be applied on NIR spectra, by which resolution is enhanced and, hence, overlapping band can be distinguished. The cross-correlation function of 2D correlation spectroscopy was demonstrated in Scheme 1.7 where  $\tilde{Y}_1(\omega)$  and  $\tilde{Y}_1(\omega)$  are generated from the Fourier transforming of absorbance,  $T$  is excitation time, and  $\Phi(\nu_1, \nu_2)$  and  $\psi(\nu_1, \nu_2)$  are the intensities of synchronous

and asynchronous spectrum, respectively. The calculation generates synchronous and asynchronous spectrum (Fig. 1.8) by which the degree of coherence of dynamic spectra can be studied.

$$\Phi(\nu_1, \nu_2) + i\Psi(\nu_1, \nu_2) = \frac{1}{\pi T} \int_0^\infty \tilde{Y}_1(\omega) \cdot \tilde{Y}_2(\omega)$$

Scheme 1. 7. Calculation of 2D correlation spectra.

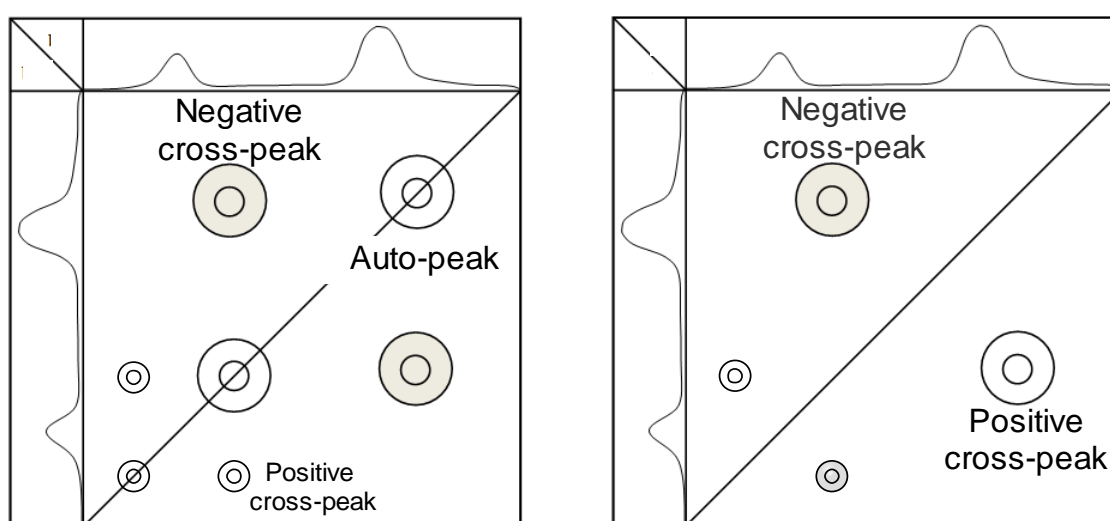


Fig. 1.8. 2D correlation spectra. Left, synchronous; Right, asynchronous.

On synchronous spectrum, there are two kinds of peaks: one is auto-peak, showing up on diagonal, generated from the same band variation; the other one is cross-peak, locating off the diagonal, generated from the correlation between different bands. Auto-peak sign is always positive (white), and, on other hand, cross-peak signs are symmetrical about diagonal, positive (white) or negative (grey) (Fig. 1.8 left). On asynchronous spectrum, just cross-peaks occur and their signs are antisymmetrical about diagonal (Fig. 1.8 right). Synchronous spectrum demonstrates the synchronicity of bands. On the contrary, asynchronous spectrum research the asynchronicity. For example, there are two bands on dynamic spectra at the wavenumber of  $\nu_1$  and  $\nu_2$  ( $\nu_1 > \nu_2$ ), respectively, and their band intensities are varying with external perturbation. Two bands synchronicity can be confirmed

using the cross-peak on synchronous spectrum. Positive cross-peak means that their band intensities change in the same direction, both increasing or both decreasing. Negative peak suggests that their band intensities change in the opposite direction, one increasing and the other one decreasing. Further, the variation rate of the two band intensities can also be compared: if synchronous cross-peak and asynchronous cross-peak have the same sign, both positive or both negative, it implies that band  $\nu_1$  has a higher variation rate than band  $\nu_2$ ; if synchronous cross-peak and asynchronous cross-peak have different signs, one positive and the other one negative, it suggests that band  $\nu_1$  has a lower variation rate than band  $\nu_2$  [30, 31].

### 1.3 Purpose

Residual NCOs in API adhesive glue-line can react with hydroxyl and moisture during post-curing process, contributing to the variations of both chemical and physical properties. However, NCO reactions in API adhesive glue-line sandwiched between two adherends are difficult to be studied by using normal methods (such as FT-IR and NMR). In this study, chemical and physical properties of cured API adhesive film were studied by using FT-IR and DMA first to confirm the formation of cross-linking structure. Then, the absorption bands of urethane and urea, two main products of NCO reactions, were assigned on FT-NIR spectrum. After that, the chemical structure variation of API adhesive glue-line sandwiched between two adherends was studied by using FT-NIR. In order to obtain a stronger post-cured glue-line, the influences of aging condition and adhesive components on chemical structure as well as physical property were also studied. Finally, to better understand the bonding mechanism of API adhesive to wood component, the product of NCO-cellulose reaction was studied by using FT-IR.

## 2 Post-Curing Process of API Adhesive

### 2.1 Introduction

API adhesive is prepared from water-based resin and cross-linker. After API adhesive was applied onto wood, water permeates into wood and evaporates into ambient environment. In the meanwhile, NCO reactions proceed. This process was called ‘curing’ of adhesive and normally took one day. After water evaporation, adhesive turns into solid state and glue-line finally forms. However, NCO reactions still can continue for several other days, leading to the variations of chemical structure and physical property of glue-line, and this process is called ‘post-curing’. The purpose of this chapter is to confirm NCO reaction in post-curing process and the physical property change of glue-line.

Ordinarily used test methods for chemical structure analysis are NMR and FT-IR spectroscopy. However, as it had been mentioned, molecular structure is highly cross-linked in post-cured API adhesive, contributing to an un-dissolvable block, so the liquid-state NMR test is impossible to be carried out. Solid-state NMR was also considered at first. Nevertheless, the abundance bands were overlapped significantly due to its poor resolution. FT-IR test can be applied on solid-state sample and it has a good resolution, but its sample preparation process needs to be deliberated. As long as the sample amount for FT-IR test is just several mg, adhesive glue-line with adherend is unsuitable to be tested immediately. For this reason, an API thin film prepared from API adhesive was applied.

In this chapter, three materials, PVA, SBR, and pMDI, were used to prepare API adhesive. TGA (thermogravimetric analysis), DSC (differential scanning calorimetry) and DMA (dynamic thermomechanical analysis) were also used to study the physical property of post-cured API adhesive. TGA was applied to observe the thermal degradations of adhesive component that included formed chemical linkages. DMA detects the rheological property of material which is a

material's response to oscillating force, i.e., elastic and viscous behaviors [32]. Besides, the tangent of phase angle can be used to discuss Tg of polymer (glass transition temperature). Previous studies [20, 21] reported that NCO can remain in adhesive block for several days and acutely react under heat treatment.

In this chapter, chemical and physical properties of post-cured API adhesive were evaluated by using FT-IR and DMA test, respectively. In previous study [7, 33], NCO reactions in adhesive film were tracked by using FT-IR spectroscopy, where not only urea and urethane formations but also hydrogen bonds generated from phase mixing were discussed. In addition, several spectra of the same sample corresponding to different ambient environments were collected together and compared with each other to investigate the influence of post-curing conditions, such as humidity and temperature, on NCO reactions. DMA was widely used to test the Tg of polymer material which is one important factor in practical application. For the material that has cross-linking structure, cross-linking density can be calculated from the value of storage module on rubbery plateau [34]. As a preliminary work for the following *in-situ* analysis of bonding structure, this chapter confirm the consumption of NCO, the generation of chemical linkages, and the formation of cross-linking structure.

## **2.2 Experimental**

### **2.2.1 Materials**

Base resin: Two base resins were used in this experiment: one was 15wt% PVA (polyvinyl alcohol) aqueous solution and the other one was SBR (styrene butadiene-rubber) latex. PVA powder product purchased from Wako Pure Chemical industries, Ltd. (Japan) had the degree of saponification of 99.1% and  $M_n$  of  $6.8 \times 10^4$  g/mol. SBR latex supplied by NIPPON A & L Inc. (Japan), used as softener, had the solid content of 51.7% and the styrene/butadiene mass ratio of 7/3.

Cross-linker: pMDI (polymethylene polyphenyl polyisocyanate) (MR-200), supplied by Nippon Polyurethane Industry Co., Ltd. (Japan), had the NCO content of 29.4% (measured by titration).

Plastic container (volume 50 ml), Teflon sheet (thickness 2 mm), and vinyl tape (thickness 0.2 mm) were also utilized.

### 2.2.2 Sample Preparation

15wt% PVA aqueous solution: 7.5 g PVA powder and 42.5 g distilled water were added into a four-neck flask. The mixture was stirred at 80°C for 8h and then stirred at room temperature for one night. Distilled water used for aqueous solution was purified by Elix UV 3/5/10 (Millipore, Japan).

API adhesive: 3 g PVA aqueous solution and 3 g SBR latex were poured into the plastic container, mixed for 1 min and degassed for 30 s by using Hybrid Mixer HM-500 (Keyence, Japan). Thereafter, 1.5 g pMDI was added. The mixture was mixed for 2.5 min and degassed for 30s.

API thin film: API adhesive was used soon after it was prepared. API thin film was made by thinly casting API adhesive onto Teflon sheet and aging in thermostatic chamber (23°C, RH 50%) for one day. API thin film was peeled off from the Teflon sheet after aging and it had the thickness of 0.03 mm (Fig. 2.1).

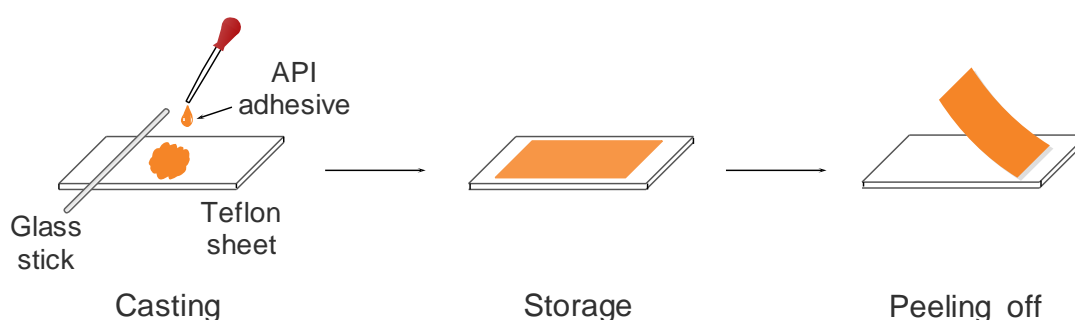


Fig. 2.2.1. Preparation of API thin film.

API film: A mould was made of Teflon sheet and vinyl tape first. Then, API adhesive was casted into the mould, and aged in thermostatic chamber for one day. Then, API film was peeled off. API film had the thickness of 0.2 mm (Fig. 2.2).

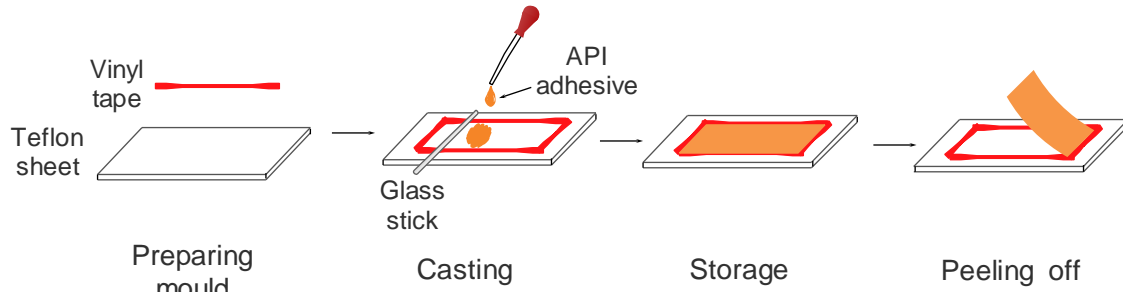


Fig. 2.2.2. Preparation of API film.

API thin film and API film were aged in thermostatic chamber.

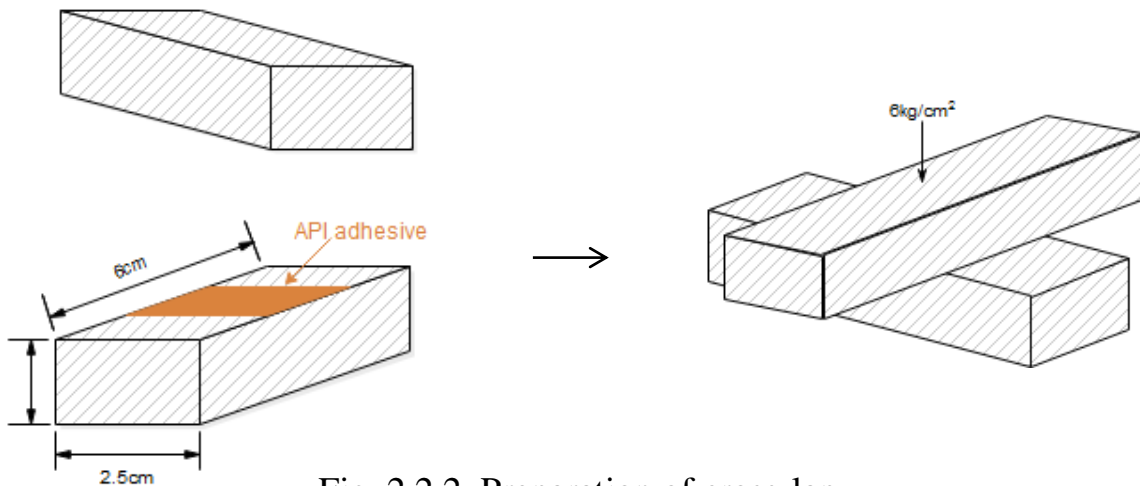


Fig. 2.2.2. Preparation of cross-lap.

Cross-lap: API adhesive was also used to prepare cross-lap samples. Wood pieces in the size of  $1.5\text{cm} \times 2.5\text{cm} \times 6\text{cm}$  were cut from birch. Priority to usage, wood pieces were aged in thermostatic chamber, and it had the density of  $0.7\text{g}/\text{cm}^3$  and the moisture content of 9.58wt%.  $\approx 14\text{mg}/\text{cm}^2$  glue-spread and  $6\text{kg}/\text{cm}^2$  pressure were employed for cross-lap preparation. Cross-laps were 24h pressed and then aged in thermostatic chamber.

### **2.2.3 Characterizations**

As it had been mentioned above, TGA, DSC, DMA and FT-IR were applied to analyze chemical and physical property variations of API adhesive in post-curing process.

TGA: Thermogravimetric analysis was carried out with STA 6000 (PerkinElmer, Japan). 5-8mg sample was used and the temperature was elevated from 30°C to 600°C at 10°C/min in dry nitrogen gas flow of 20ml/min

DSC: The instrument was DSC-8500 (PerkinElmer, Japan). 2-3mg sample was heated at 10°C/min in dry nitrogen gas flow of 20ml/min.

DMA: Rheologic curves were acquired on DVA-200s (ITK, Japan). Sample was cut into the size of 20×5mm<sup>2</sup> (length×width) for tensile mode. Frequency was 10Hz, and temperature range was -50-250°C at 10°C/min in dry nitrogen gas flow of 0.5L/min.

FT-IR: NICOLET-6700 (Thermo Fisher Scientific K.K., Japan) (KBr beam splitter, resolution 4 cm<sup>-1</sup>, 128 scans, 400-4000cm<sup>-1</sup>) was used to test sample in dry air flow.

Bond strength: TENSILON UCT-5T (A&D Co., Ltd, Japan) was used. Crosshead speed was 10mm/min.

## **2.3 Results and Discussion**

### **2.3.1 TGA**

PVA powder was 100°C vacuum dried for over 4 hours. SBR latex was dried at room temperature to make SBR block, and then the SBR block was ground into powder form. Prior to TGA test, SBR powder were 100°C vacuum dried for over 4 hours.

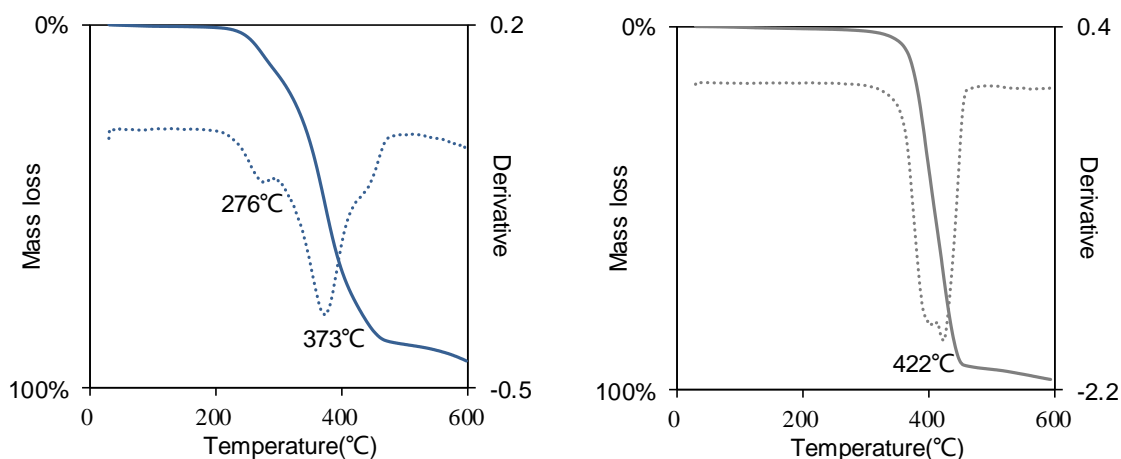


Fig. 2.3.1. Thermal degradations of PVA powder (left) and SBR powder (right).

TGA and DTG curve of PVA powder were displayed in Fig. 2.3.1 (left). The thermal degradation of PVA powder involved two steps, which showed the fastest degradation rates at 276°C and 373°C, respectively. Thermal degradation of PVA generally involves the dissociation of hydroxyl group, the transition between olefinic alcohol and ketene, the formation of alkynyl group terminated compounds. According to the reports of Holland <sup>[35]</sup> and Yoshio <sup>[36]</sup>, the dissociation of hydroxyl group occurs below 300°C, generating water, acetaldehyde, ketone, etc. As thermal degradation carried on, a rapid mass loss arose at 373°C. Acetyl group on PVA molecular chain, due to the uncomplete saponification in manufacture process, could accelerate the degradation process.

TGA and DTG curve of SBR powder were showed in Fig. 2.3.1 (right). The thermal decomposition reaction of SBR started with the breakup of molecule chain generating butadiene, styrene and hydrogen gas. Then, the addition reaction of styrene carried on in gas phase forming benzene derivatives such as xylene, trimethyl benzene and triethyl benzene <sup>[37]</sup>. The fastest degradation rate was detected at 422°C. In this experiment, SBR powder was prepared from SBR latex, thus containing additives such as emulsifier and inorganic acid salt. However, the thermal stability of SBR powder was barely affected, and it corresponded to the literature result of styrene-butadiene rubber.

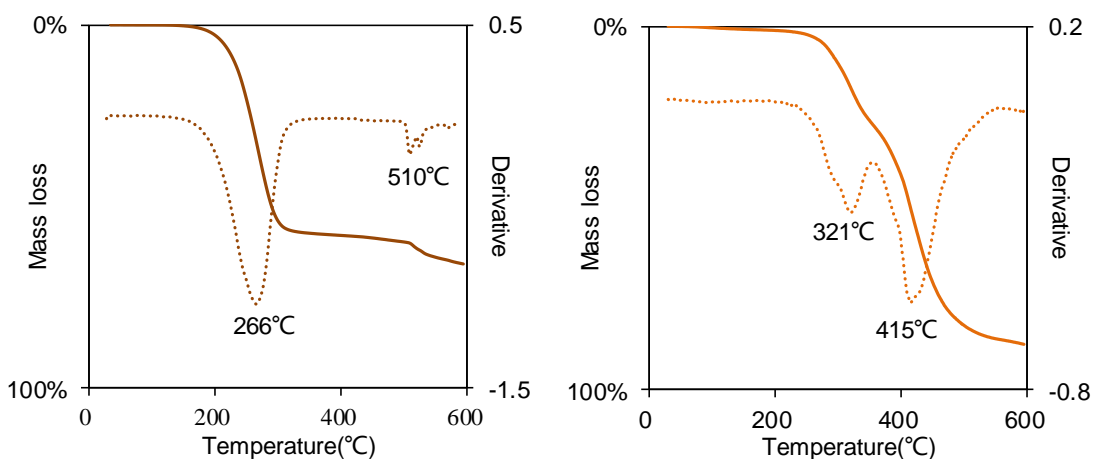
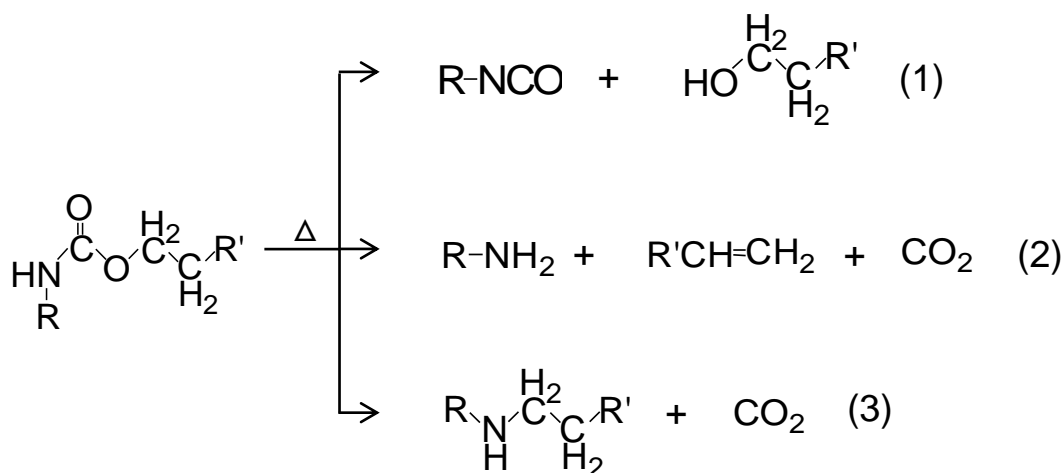


Fig. 2.3.2. Thermal degradations of pMDI (left) and 6 days aged API film (right).

Fig. 2.3.2 (left) demonstrated the result of pMDI. Thermal degradation of pMDI had two steps, at 266 °C and 510 °C. Thermal degradation of pMDI carried on with the formation of carbodiimide, releasing carbon dioxide. Trimerization of isocyanate could also take place and generate thermally stable isocyanurate. The degradation of isocyanurate normally occurs at  $\approx 350$  °C [38]. The second step at 510 °C was attributed to the degradation of char generated in the first step [39]. The finally residual mass at 600 °C was about 34%.

Thermal degradation mechanism of polyurethane product had been studied in other papers. Petrovic et al. [40] reported that the ruptures of urethane linkage (hard segment) occurred at lower temperature, and that of polyol (soft segment) took place at higher temperature. Chattopadhyay et al. [38] suggested that the breakup of urethane linkage took place at  $\approx 200$  °C, followed by the decomposition of urea linkage at  $\approx 250$  °C. The thermal degradation of urethane linkage mainly involves three reactions that were displayed in Scheme 3.2.1, generating isocyanate, polyol, amine, olefin, carbon dioxide and secondary amine (Scheme 2.3.1 b). The generated isocyanate could trimerize, forming isocyanurate [41]. Urea degradation normally forms volatile product and carbonaceous char [42].



Scheme 2.3.1. Thermal degradation reactions of urethane linkage.

Thermal degradation of API film (Fig. 2.3.2 right) had two steps, at 321°C and 415°C. Urethane and urea degradations occurred first during heating but the mass loss in this range was unobvious. The first step, at 321°C, corresponded to the decompositions of PVA hydroxyl and pMDI isocyanate. Carbon-carbon and carbon-nitrogen combinations had better thermal stability, so they degraded at the second step, 415°C.

The thermal degradation temperatures ( $T_{5\%}$ ) of three raw materials and API film were summarized in Table 2.3.1. PVA powder and pMDI had two similar  $T_{5\%}$ s at 231°C and 236°C, respectively. SBR powder showed a higher  $T_{5\%}$  at 357°C. Thus, API film had a  $T_{5\%}$  at 279°C which was between the  $T_{5\%}$ s of raw materials.

Table 2.3.1. Thermal degradation temperatures, corresponding to 5% mass loss.

	PVA film	SBR film	pMDI	API film
$T_{5\%}$	231°C	357°C	214°C	279°C

### 2.3.2 DSC

The samples for differential scanning calorimetry were the same ones that were used in 2.3.1. PVA powder, SBR powder and API film were in solid state, so the DSC tests of them were performed by using aluminum pan (PerkinElmer) as

container. For liquid-state pMDI, the container was stainless steel capsule (PerkinElmer). Furthermore, in order to avoid the over pressure of stainless steel capsule, which could be aroused by the gaseous products generated from thermal degradation reaction, DSC test of pMDI was carried on below 200°C. Before DSC scanning, PVA powder and SBR powder were heated to 200°C and kept for 1min to remove the effect of thermal history. pMDI and API film contained highly reactive NCOs, so there was no pretreatment performed on them.

SBR latex is manufactured by the emulsion polymerization of styrene and butadiene. The  $T_g$  of polystyrene is 100°C, and that of 1,4-tans-polybutadiene is -102°C. SBR latex used in this experiment had the styrene/butadiene mass ratio of 7/3, so  $T_g$  of styrene-butadiene copolymer should be at around 2°C, according to  $T_g$  calculation formula (Equation 2.3.1) [43]. However, SBR latex consists of not only styrene-butadiene copolymer but also additives (such as emulsifier), un-polymerized monomer, etc. Thus, the physical property of SBR powder, prepared from SBR latex, was different from that of styrene-butadiene copolymer.

$$\frac{1}{T_{gc}} = \frac{W_a}{T_{ga}} + \frac{W_b}{T_{gb}}$$

Equation 2.3.1.  $T_g$  calculation formula of copolymer.  $T_{gc}$ ,  $T_{ga}$  and  $T_{gb}$ : Kelvin  $T_g$ s of copolymer, polymer a and polymer b;  $W_a$  and  $W_b$ : mass percentages of polymer a and polymer b.

In Fig. 2.3.3,  $T_g$  of SBR powder was, even though un-obviously, detected at 14°C, which was higher than the estimated value. No  $T_m$  was detected for SBR powder.

PVA powder had both amorphous and semi-crystalline phase, so the DSC curve showed  $T_g$  at 69°C and  $T_m$  at 203°C. The obvious inclination of PVA curve occurred at around 300°C due to thermal degradation.

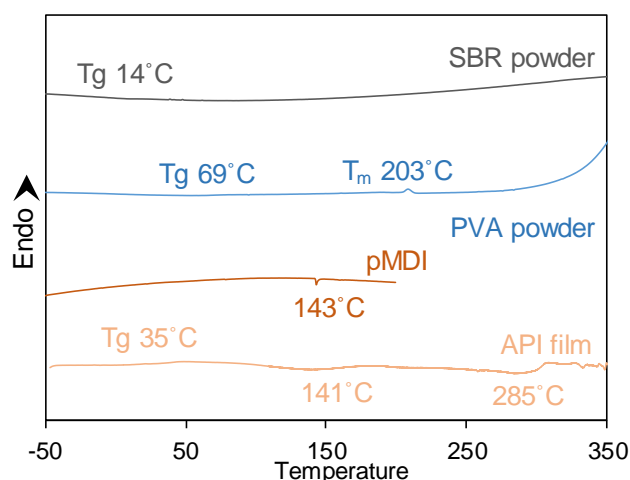


Fig. 2.3.3. DSC thermograms of three materials and API film.

On DSC curve of pMDI, exothermal peak showed up at 143°C, attributing to the self-reactions of isocyanate. Self-reactions of isocyanate generate dimer and trimer, uretdione and isocyanurate (Scheme 1. 2). Watanabe et al. [44] crystallized uretdione from the pyridine solution of phenyl isocyanate at room temperature, and obtained isocyanurate from the pyridine solution of phenyl isocyanate at 100°C by using triethylene diamine as catalyst. 143°C peak was mainly due to uretdione generation, because the formation of dimer occurs more easily than that of trimer.

DSC thermogram API film was performed between -50°C and 350°C. T<sub>g</sub> of un-cross-linked PVA and SBR mixture showed up at 35°C, but unclearly. During post-curing, cross-linking structure was generated significantly due to NCO reactions in API film. Thus, the formed cross-linking structure restricted the movement of molecular and, further, the appearance of T<sub>g</sub> [45]. The unobviousness of T<sub>g</sub> was attributed to the insensitiveness of DSC to molecular chain movement. The broad exothermal peak at 141°C was attributed to the reactions of NCO, forming NCO dimer, etc. There was another exothermal peak occurring at 285°C, which was thought of as due to the complicated thermal degradation reactions of NCO.

### 2.3.3 DMA

DMA (Dynamic Mechanical Analysis), which could also be called as DMTA (Dynamic Mechanical Thermal Analysis), is commonly utilized to analyze the rheological and thermal properties of material. DMA measures the response of sample to an oscillatory force, and this response is separated into one viscos component (loss modulus) and one elastic component (storage modulus) [46]. For DMA test, PVA film (thickness 0.09mm) and SBR film (thickness 0.5mm) was made by casting PVA aqueous solution and SBR latex onto Teflon sheet and aging for one week in thermostatic chamber. It was impossible for liquid-state pMDI to be tested by tensile mode DMA. API film used here was the same as that for previous tests.

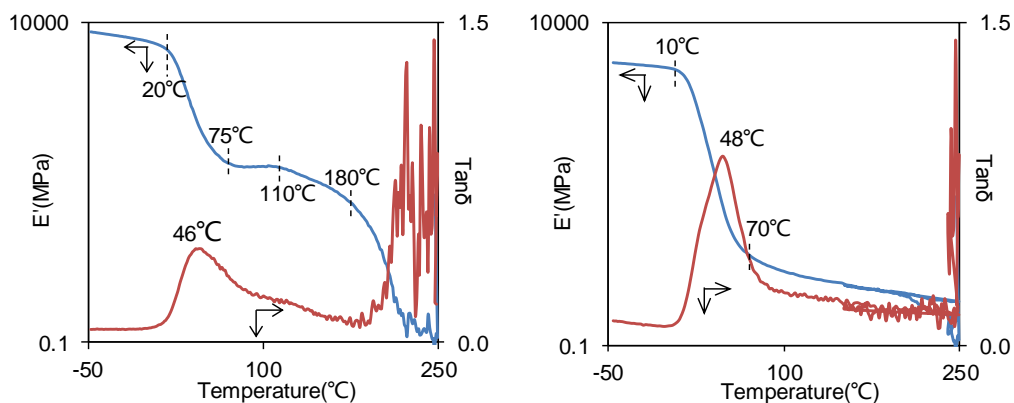


Fig. 2.3.4. DMA thermograms of PVA film (left) and SBR film (right).

The profile of PVA storage modulus (Fig. 2.3.4 left) included several sections: -50-20°C, 20-75°C, 75-110°C, 110-180°C and 180-250°C. -50-20°C: Molecular chains tightly aggregated in this temperature range, but amorphous side chain movement took place and caused a slight descent of modulus. Furthermore, the decreasing modulus in low temperature range could also be associated with water; 20-75°C: Modulus decreased rapidly in this range and  $T_g$  peak showed up at 46°C on  $\tan\delta$  curve, due to the significant movement of PVA amorphous part; 75-110°C: Here, amorphous phase was in flow-state but crystalline phase was still

compacted, contributing to a changeless modulus. 110-180°C: Menard et al. [32] stated that a slippage past each other of semi-crystalline structure occurred in this range. A vague peak appeared on  $\tan\delta$  curve might correspond to their theory. 180-250°C: crystalline structure totally melted and the thermal degradation of molecular chain also occurred, resulting into a rapid decreasing of modulus value.

SBR thermograms were shown in Fig. 2.3.4 right. The side molecular chain motion led to a slight decreasing of storage modulus in -50-10°C; 10-70°C: modulus decreased significantly, and  $T_g$  peak arose at 48°C on  $\tan\delta$  curve.

In Fig. 2.3.5, DMA thermograms of API film aged for 1, 3 and 6 days in thermostatic chamber were demonstrated. There were two position-unchanged peaks occurred at 28°C and 203°C, respectively, in Fig. 2.3.5 left. Peak at 28°C was assigned to the  $T_g$  of API film, related to the mixture of SBR and uncross-linked PVA. From 1 day to 6 days, API film was post-cured in thermostatic chamber (RH 50%, 23 °C), during which time NCO continuously reacted with water and hydroxyl of PVA forming cross-linking. The decreasing of peak intensity at 28°C with aging days implied that the amount of flowable component decreased. During post-curing, cross-linking were formed between the molecular chains of PVA and pMDI. Thus, the generated cross-linking restrained the movements of molecular chains at 28°C.

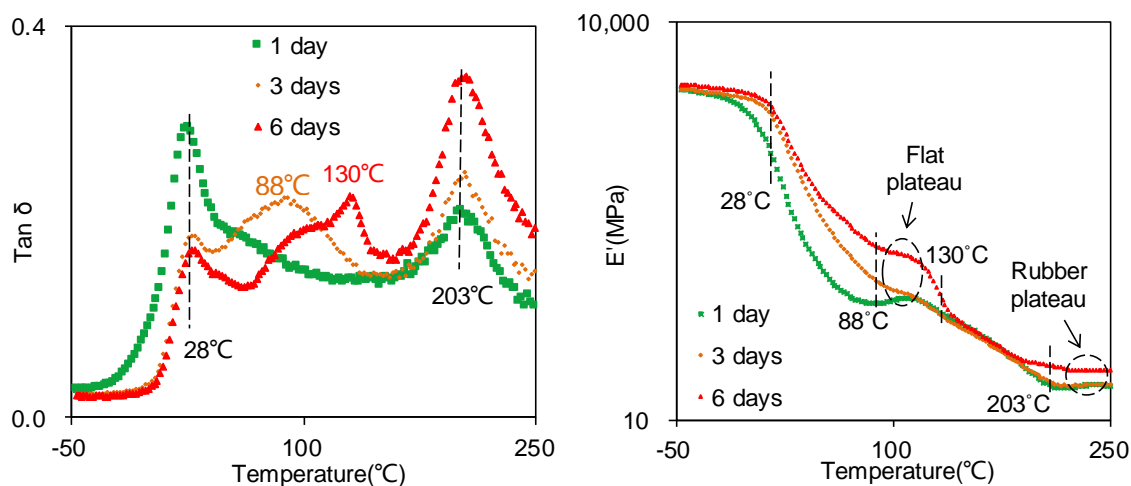


Fig. 2.3.5. DMA thermograms of API film, aged for 1, 3 and 6 days.

Peak at 203°C was relevant to several reasons: (1) The slippage past each other of PVA semi-crystalline structure; (2) Strong interaction between molecular chains, caused by the acute reactions of NCO at high temperature. Menard et al.<sup>[32]</sup> summarized that the  $\tan\delta$  peak originating in acute reactions would shift to higher temperature and the peak intensity would be weaker with post-curing time, since the longer the post-curing process was, the less the reactive group left, and the worse the molecular mobility became. They also demonstrated that  $T_g$  peak on  $\tan\delta$  curve would move to higher temperature with post-curing time increasing, because the scale of molecular chain was increasing in post-curing process. Thus, in this experiment, the slippage of PVA semi-crystal must make a great contribution to the constant peak location, because the melting point of crystal were changeless. Peak intensity increasing at 203°C with post-curing time could be attributed to the ascendant molecular friction promoted by gradual cross-linking formation.

On  $\tan\delta$  curves of 3 days and 6 days films, two peaks showed up at 88°C and 130°C, respectively. These two peaks were regarded as corresponding to the  $T_g$ s of small scale molecular chains generated from pMDI reactions. From 3 days to 6 days, this  $T_g$  shifted to higher temperature, implying that the molecular scale were increasing in post-curing process<sup>[11]</sup>.

The storage modulus curves of API films were showed in Fig. 2.3.5 right. Three films showed almost the same value at low temperature. Then, the molecular chain of 1 day aged film started to flow at about -10°C, resulting in modulus decreasing. The modulus descents of 3 days and 6 days films started at about 5°C. A flat plateau occurred in the area of around 100°C, where modulus decreased just on a small scale, similar to the DMA result of PVA, and longer-time-post-cured film had higher modulus. The result of modulus demonstrated that post-curing process gave rise to a fully cured API film with better resistant ability to impact.

Rubbery plateau showed up at 210-250°C, where modulus was changeless. In this area all amorphous phase was in flow-state, and the crystalline phase of PVA melted. At this moment, cross-linking was the only bonding between molecular chains, resisting oscillatory force. Thus, the modulus in this area could be used to calculate the cross-linking density in API film, based on kinetic theory of rubber elasticity. Here, cross-linking densities at 210°C were calculated by using Equation 2.3.2 [34, 47], and the result was listed in Table 2.3.2. Cross-linking density ascended continuously with post-curing time.

$$E' = 3\nu RT$$

Equation 2.3.2. Calculation of cross-linking density. E': storage modulus;  $\nu$ : cross-linking density; T: the absolute temperature of rubber plateau; R: the gas constant.

Table 2.3.2. The Cross-linking densities of API films.

	1 <sup>st</sup> day	3 <sup>rd</sup> day	6 <sup>th</sup> day
<b>Cross-linking density (mol/cm<sup>3</sup>)</b>	$1.50 \times 10^{-3}$	$1.59 \times 10^{-3}$	$2.15 \times 10^{-3}$

### 2.3.4 FT-IR

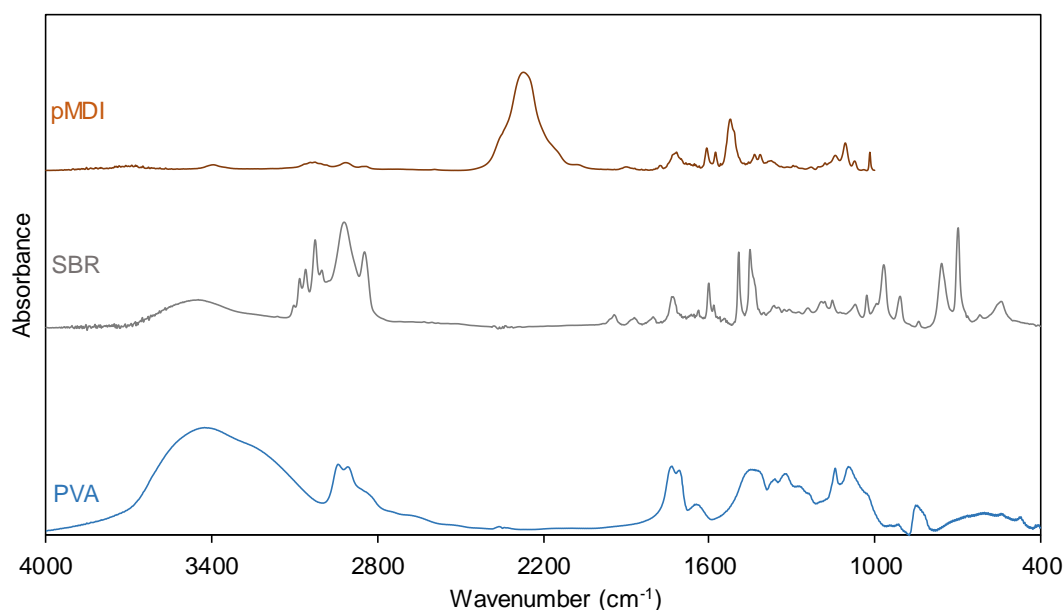


Fig. 2.3.6. FT-IR spectra of pMDI, SBR and PVA.

Table 2.3.3. Band assignment of PVA.

Wavenumber (cm <sup>-1</sup> )	Assignment
3428	O-H str
2944-2910	C-H str
1736-1710	C=O str (free and bonded)
1648	C-H vibration (overtone)
1452	C-H symmetric ben
1367-1328	C-H asymmetric ben
1146-1098	C-O str (rotamers)
854	C-H roc

str: stretching; ben: bending; roc: rocking; bonded: hydrogen bonded; free: non-hydrogen-bonded

Table 2.3.4. Band assignment of SBR powder.

Wavenumber (cm <sup>-1</sup> )	Assignment
3448	O-H str
3032-2847	C-H str
1943-1731	C=C str (alkenyl)
1601-1356	C=C str (phenyl)
1224-1029	C-C and C-H def
968-909	C-H def (trans C=C)
758-609	C-H def (cis C=C)
543	=C-C-C ben

str: stretching; ben: bending; def: deformation

2mg PVA powder was vacuum dried and then mixed with 200mg KBr powder to prepare a disk ( $\Phi$  13mm). Vacuum dried 2mg SBR powder (same as the one used in 2.3.1) and 200mg KBr powder were mixed and made into disk ( $\Phi$  13mm). pMDI was in liquid state at room temperature so it was cast onto CaF<sub>2</sub> disk ( $\delta$  1mm,  $\Phi$  25mm, Pier Optics, Japan). FT-IR tests were performed on these three disks. CaF<sub>2</sub> has significant absorption in the range of below 1000cm<sup>-1</sup>, so only the spectrum of over 1000cm<sup>-1</sup> of pMDI was used. The band assignment of three material were summarized in Table 2.3.3, Table 2.3.4 and Table 2.3.5 [28, 48, 49].

Table 2.3.5. Band assignment of pMDI.

Wavenumber (cm <sup>-1</sup> )	Assignment
3393	N-H str
3026-2915	C-H str
2272	N=C=O asymmetric str
1777-1718	C=O str (NCO oligomer)
1608-1370	C=N str, C=C str (phenyl) and N=C=O symmetric str
1143-1018	C-C def and C-H def

str: stretching; ben: bending; def: deformation

PVA is manufactured by saponifying polyvinyl acetate. PVA powder used in this experiment had the degree of saponification of 99.1%, so there was still 0.9% acetyl group on molecular chain. The C=O stretching band in Table 2.3.3 verified the existence of acetyl. SBR powder was prepared from SBR latex. Thus, the O-H stretching band in Table 2.3.4 was attributed to some additives added in the manufacture process of latex. Even though pMDI was carefully stored, a little bit of NCOs still reacted with water from external forming urea. Self-reaction of NCO could also occur, forming dimer and trimer (Scheme 1.2). Stabilizer was

added in the manufacture process of pMDI. Therefore, N-H stretching and C=O stretching bands were detected on pMDI spectrum.

Table 2.3.6. Band assignment of API thin film.

Wavenumber (cm <sup>-1</sup> )	Assignment
3320	N-H str
3060-2846	C-H str
2272	N=C=O asymmetric str
1779	C=O str (NCO dimer)
1723	C=O str (urethane Amide I, NCO trimer and acetyl)
1639	Urea Amide I
1602-1517	Amide II
1452	C=C str (phenyl)
1413-1234	Amide III (cis and trans)
1106	C-O str
1142 and 1018	C-C def and C-H def
968-563	Out-of-plane def (phenyl)

str: stretching; def: deformation

FT-IR spectroscopy was performed on API thin film prepared in 2.2.2. The FT-IR spectra of API thin films aged for 1 day, 3 days and 6 days were displayed in Fig. 2.3.7 (normalized by using C-H band at 2919cm<sup>-1</sup>), and band assignments were summarized in Table 2.3.6. During post-curing, NCO reactions were carrying on, and two primary reactions generated urea and urethane linkages, as it had been stated in 1.1.4. In the meanwhile, water and PVA hydroxyl were consumed. To study the variation of chemical structure in more detail, 2D correlation spectroscopy (1.2.4) was calculated. The FT-IR spectra of API film from 1 day to 6 days were utilized to obtain 2D correlation spectra, by which resolution was

enhanced and variation trend of band was discussed. Software, 2D shige, used here was made by Morita [50].

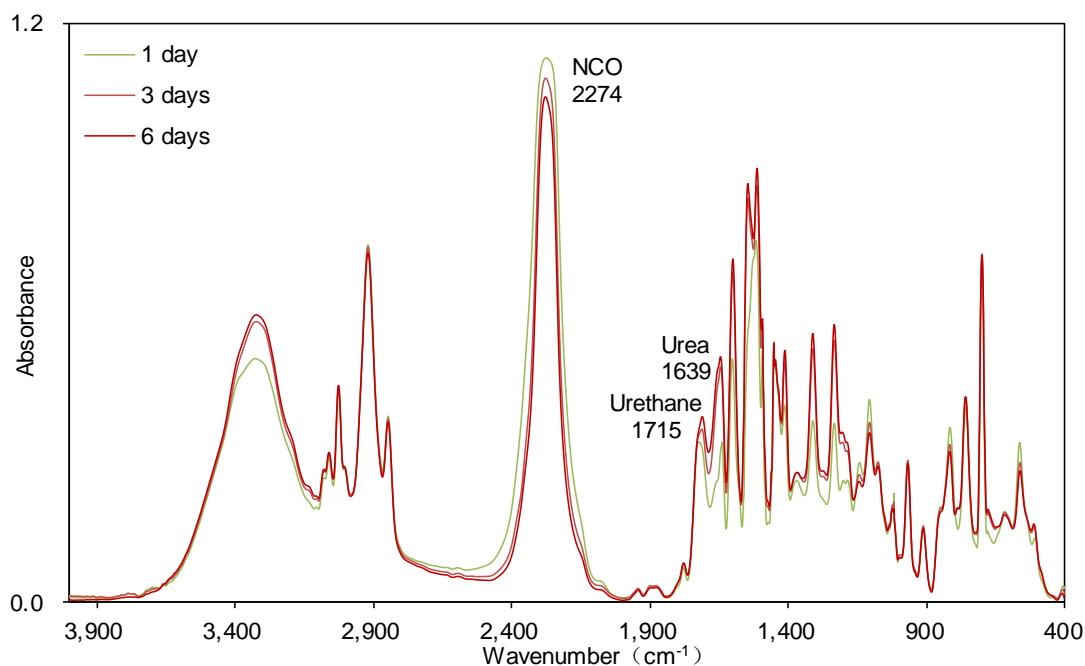


Fig. 2.3.7. FT-IR spectra of API thin film aged for 1 day, 3 days and 6 days.

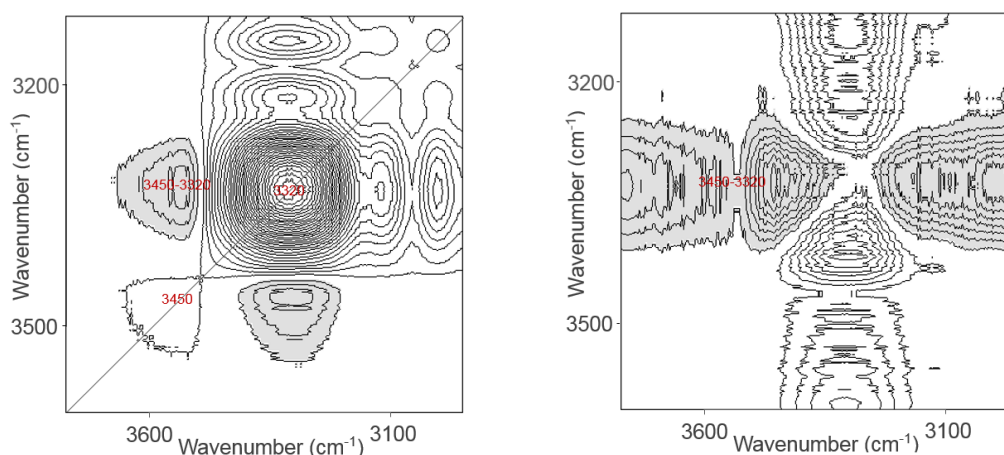


Fig. 2.3.8. Synchronous (left) and asynchronous (right) 2D correlation spectra, generated from Fig. 2.3.7.

On diagonal of synchronous spectrum (Fig. 2.3.8 left) four auto-peaks appeared at 3450 and 3320, implying that the FT-IR bands at these two locations changed on band intensity during post-curing. Moreover, cross-peaks showed up at 3450-3320 on synchronous and asynchronous spectra.

The broad band at  $3320\text{cm}^{-1}$  (Fig. 2.3.7) had increasing band intensity with aging time, so its corresponding auto-peak at 3320 was attributed to N-H stretching vibration. Then, 3450 auto-peak was assigned, based on its relationship with 3320 auto-peak. Negative sign of 3450-3320 synchronous cross-peak suggested that  $3450\text{cm}^{-1}$  FT-IR band had opposite variation trend with  $3320\text{cm}^{-1}$  FT-IR band. Namely, band intensity of  $3320\text{cm}^{-1}$  increased with post-curing time, and that of  $3450\text{cm}^{-1}$  decreased. Thus, 3450 auto-peak was assigned to O-H stretching of hydroxyl. Asynchronous cross-peak at 3450-3320 also had a negative sign, demonstrating that  $3450\text{cm}^{-1}$  band changed faster than  $3320\text{cm}^{-1}$  band. In other words, the break of O-H happened before the formation of N-H.

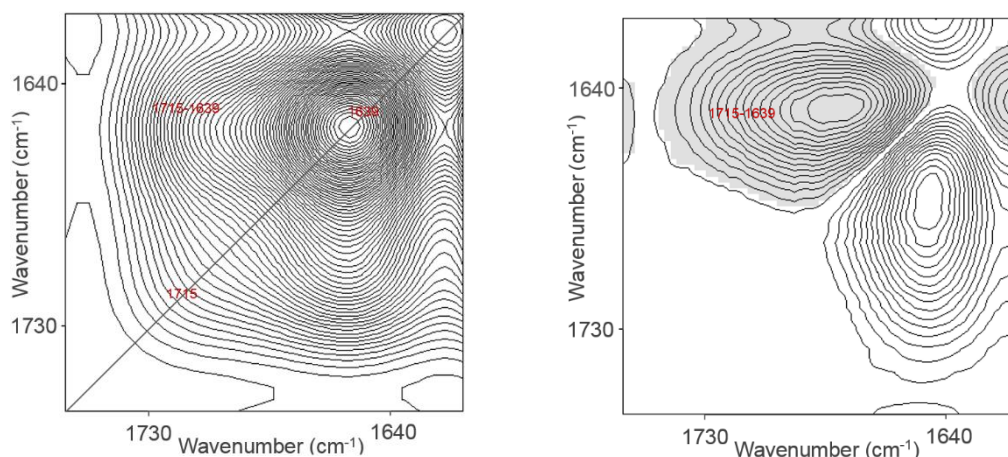


Fig. 2.3.9. Synchronous (left) and asynchronous (right) 2D correlation spectra.

In Fig. 2.3.9 left, two auto-peaks at 1715 and 1639 were detected on diagonal of synchronous spectrum, corresponding to the bands of urethane and urea, respectively. Moreover, positive synchronous cross-peak at 1715-1639 implied the same variation trend of those two band intensities. On the other hand, a negative asynchronous cross-peak occurred at 1715-1639 (Fig. 2.3.9 right). 2D correlation calculation suggested that urethane band and urea band had the same trend, both increasing in post-curing process, but urea band changed faster than urethane band. This might be due to the faster generation rate of urea [12]. It should be noticed that even though the band at  $1715\text{cm}^{-1}$  (Fig. 2.3.7) had a significant

band intensity, it consisted of the absorptions of several chemical compounds, urethane, NCO trimer, acetyl of PVA, etc. But the increasing of band intensity was mainly attributed to urethane generation, since NCO reactions could just generate urethane and NCO trimer, and NCO trimerization barely occurred at ambient temperature.

### 2.3.5 Bond strength

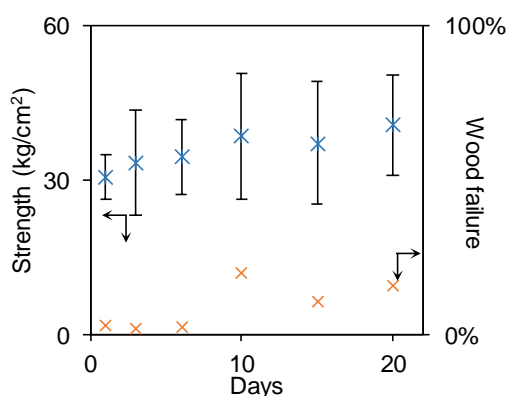


Fig. 2.3.10. Bond strength of cross-laps aged for several days, error bars represent  $\pm 1$  standard deviation,  $n=7$ .

It could be confirmed that bond strength increased with aging time. During aging process, post-curing of glue-line in cross-lap contributed to the increasing of both bond strength and wood failure. This could be due to the gradual generations of urethane and urea linkages inside glue-line and between glue-line and wood.

## 2.4 Conclusions

In this chapter API adhesive was prepared, and the physical and chemical properties of post-cured API film/thin film were characterized by traditional methods, TGA, DSC, DMA and FT-IR. In addition, three raw materials were also characterized to compare with the result of API adhesive.

TGA: In the testing process, PVA powder and pMDI showed  $T_{5\%}$  at around 230 °C. SBR powder had the best stability and showed  $T_{5\%}$  at around 357 °C. As a result,  $T_{5\%}$  of 6 days aged API film appeared at 279 °C. Normally, the thermal

degradations of urethane and urea take place at 200°C and 250°C, respectively. However, the unremarkable mass loss of API film in 200-250°C could not be used to observe urea and urethane degradations.

DSC: T<sub>g</sub> of SBR powder, T<sub>g</sub> and T<sub>m</sub> of PVA powder were detected at 14°C, 69°C and 203°C, respectively. One sharp exothermal peak showed up at 143°C on pMDI curve, which was regarded as related to NCO self-reactions (Scheme 1.2). T<sub>g</sub> appeared on API film curve at around 35°C. Two exothermal peaks at 141°C and 285°C on API film curve were attributed to NCO reactions and NCO thermal degradation reactions.

DMA: By using DMA test, T<sub>g</sub>s of SBR and PVA films were detected at 48°C and 46°C. T<sub>g</sub> at 28°C on API film loss factor curve was assigned to the mixture of SBR and un-reacted PVA, and peak at 203°C was due to the reactions of NCO and the slippage of PVA semi-crystal. Rubbery plateau was observed on storage modulus curve, by which cross-linking density was calculated. Result showed that density of cross-linking increased with post-curing time.

FT-IR: Three materials were tested first, and then the chemical structure variation of API thin film with post-curing time was confirmed: Most of generated amide linkages were hydrogen bonded; C=O stretching bands of urethane and urea appeared at 1715cm<sup>-1</sup> and 1639cm<sup>-1</sup>, and urea band intensity increased faster than urethane band intensity.

Bond strength: API adhesive cross-laps were tested to confirm that urethane and urea generations in post-curing process led to the increasing of bond strength.

In practical application, API adhesive is used to bond two adhesends together and post-cured as glue-line between two adhesends. However, in this chapter only API adhesive film was chemically analyzed and no adherend was involved, which could not be regarded as an actual glue-line. In the following study, FT-

NIR was employed to evaluate the chemical structure of API adhesive sandwiched between two adherends.

### **3 *In-situ* Analysis of API Adhesive glue-line by using FT-NIR**

#### **3.1 Introduction**

The chemical and physical properties of post-cured API adhesive film was studied in chapter 2. However, API adhesive is normally used to bond and cured between two adherends. Thus, the *in-situ* analysis of API adhesive glue-line is very important for practical application. In this chapter, API adhesive was sandwiched by two adherends, and the chemical structure analysis of post-cured API adhesive glue-line was carried on by using FT-NIR (Fourier Transform Near Infrared) spectroscopy.

NIR energy was first discovered by William Herschel in 1880<sup>[27]</sup>. Before World war II, NIR technic was barely used by chemists, because of its narrow region, 800-2500nm (approx. 4000-12000cm<sup>-1</sup>). Furthermore, only overtone and combination tone of fundamental vibrations occur in NIR region. These two tones have lower intensity than fundamental band so they are difficult to be detected and analyzed. In 1960s, Karl Norris found out the intrinsic value of NIR for measuring agriculture products, and the U.S. Department of agriculture applied NIR for rapid measurement. Then, with the increasing of instrument resolution, NIR has been used more and more extensively. Today, NIR spectroscopy is widely used in cosmetic, food and agricultural industries, considering that it is one faster and more simply technic than NMR, GPC, etc. Compared with infrared light, near infrared light has higher energy and less diffracts, which can be performed on untreated samples. In agriculture, NIR can be employed to quantify protein, moisture and oil in soybean; For food products NIR was utilized to qualify wine, cheeses, fruits, etc.; For polymer, NIR can be used to determine the degree of curing without destroying sample.

As it has been mentioned above, NIR spectroscopy collects the overtone and combination tone information of chemical bond vibrations. Therefore, the

assignment for the band in NIR region is not as easy as that for the band in IR region. In this chapter, two model compound were synthesized to assign the particular NIR absorptions of NCO products, amides, first. After that, FT-NIR test was performed on the actual adhesive-bonding-adhered structure. Hydrogen bond plays an important role in both IR and NIR absorption, due to its effect on chemical bond vibration, contributing to the variations of band intensity and band location. In this experiment, temperature dependent FT-IR and FT-NIR was used, since hydrogen bond is very sensitive to temperature.

## **3.2 Experimental**

### **3.2.1 Materials**

Synthesis of model compounds: Phenyl isocyanate (Wako Pure Chemical industries, Ltd., Japan), 2-butanol (Wako Pure Chemical industries, Ltd., Japan), 4, 4'-diphenylmethane diisocyanate (Wako Pure Chemical industries, Ltd., Japan) and distilled water (Elix UV 3/5/10 Millipore, Japan) were used for the preparation of model compounds. N, N-dimethyl formamide (Wako Pure Chemical industries, Ltd., Japan) and n-hexane (Wako Pure Chemical industries, Ltd., Japan) were use as solvent.

Preparation of API adhesive: Raw materials were the same ones as those used in 2.2.1.

Preparations of API paper: filter paper (100% cellulose, thickness 0.2mm, Whatman 6) were used.

### **3.2.2 Sample Preparation**

Synthesis of model compounds: Two model compounds, DPU (1, 3-Diphenylurea) and MUT (Di-2-butyl 4, 4'-diphenylmethane dicarbamate), were synthesized. 1) DPU: 2g phenyl isocyanate was dissolved into 20mL N, N-

dimethyl formamide in 50mL flask, and the solution was stirred at ambient temperature. Then, 3g distilled water was added. The flask was equipped with cold water condenser and heated to 100°C in oil bath. The reaction was carried on for 1h and DPU was precipitated by distilled water. 2) 12 g 2-butanol and 4g 4, 4'-diphenylmethane diisocyanate were added into 50mL flask, and the mixture were stirred at 100°C for 1h with cold water condenser. MUT was precipitated by n-hexane.

Preparation of API adhesive: The process was the same one as 2.2.2.

Preparations of and API paper: Prior to the preparation of API paper, filter paper was cut into small piece (1.5×1.5cm<sup>2</sup>). Prepared API adhesive was soon spreaded on one piece of filter paper (glue-spread ≈12 mg/cm<sup>2</sup>), and another piece of filter paper was overlapped (Fig. 3.2.1). Prepared API paper were aged in thermostatic chamber (23°C, RH 50%).

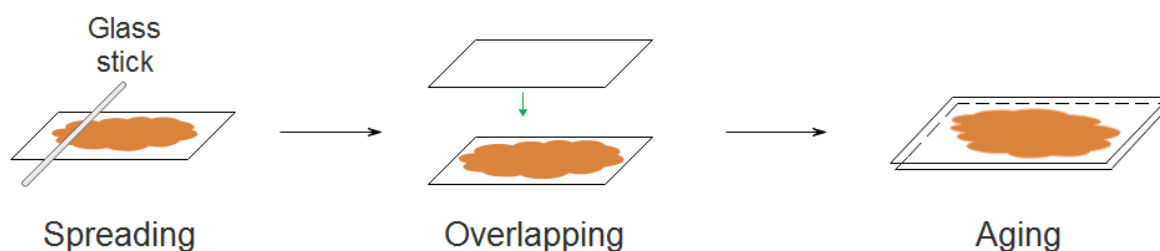


Fig. 3.2.1. Preparation of API paper.

### 3.2.3 Characterizations

DSC: The instrument was DSC-8500 (PerkinElmer, Japan). 2-3mg sample was heated at 10°C/min in dry nitrogen gas flow of 20ml/min.

FT-IR: NICOLET-6700 (Thermo Fisher Scientific K.K., Japan) (KBr beam splitter, resolution 4 cm<sup>-1</sup>, 128 scans, 400-4000cm<sup>-1</sup>) in dry air flow.

FT-NIR: The instrument for FT-NIR spectroscopy was also NICOLET-6700, but beam splitter was changed to CaF<sub>2</sub>. Spectrum was collected in the region of 4000-12000cm<sup>-1</sup> after 512 scans.

Temperature dependent FT-IR and FT-NIR: A temperature controlling accessory, HT-32 Heated Demountable Cell, was used to heat samples during FT-IR and FT-NIR testing.

### 3.3 Results and Discussion

#### 3.3.1 DSC Thermograms of model Compounds

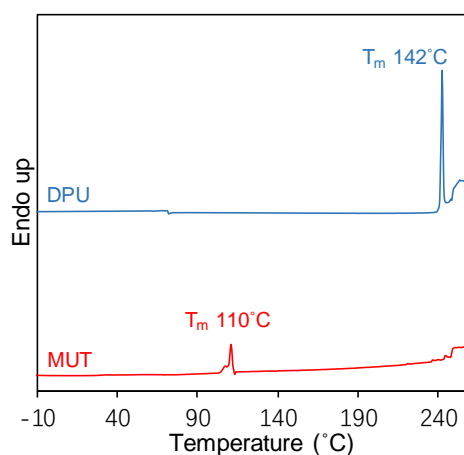


Fig. 3.3.1. DSC thermograms of MUT and DPU.

On DSC thermograms, the T<sub>m</sub> peak of MUT appeared at 110°C. That of DPU appeared at 242°C, soon followed by thermal degradation.

#### 3.3.2 FT-IR Spectra of Model Compounds

During aging process, NCOs in API adhesive mainly reacted with PVA hydroxyl and water, generating urethane and urea linkages. To study urethane and urea, respectively, the synthesized MUT had only urethane linkage on molecular chain,

and DPU just had urea linkage. KBr disk for FT-IR test was made from 2mg DPU or MUT and 200mg 100°C dried KBr powder (Wako Pure Chemical industries, Ltd., Japan). The spectra of MUT and DPU at room temperature were displayed in Fig. 3.3.2.

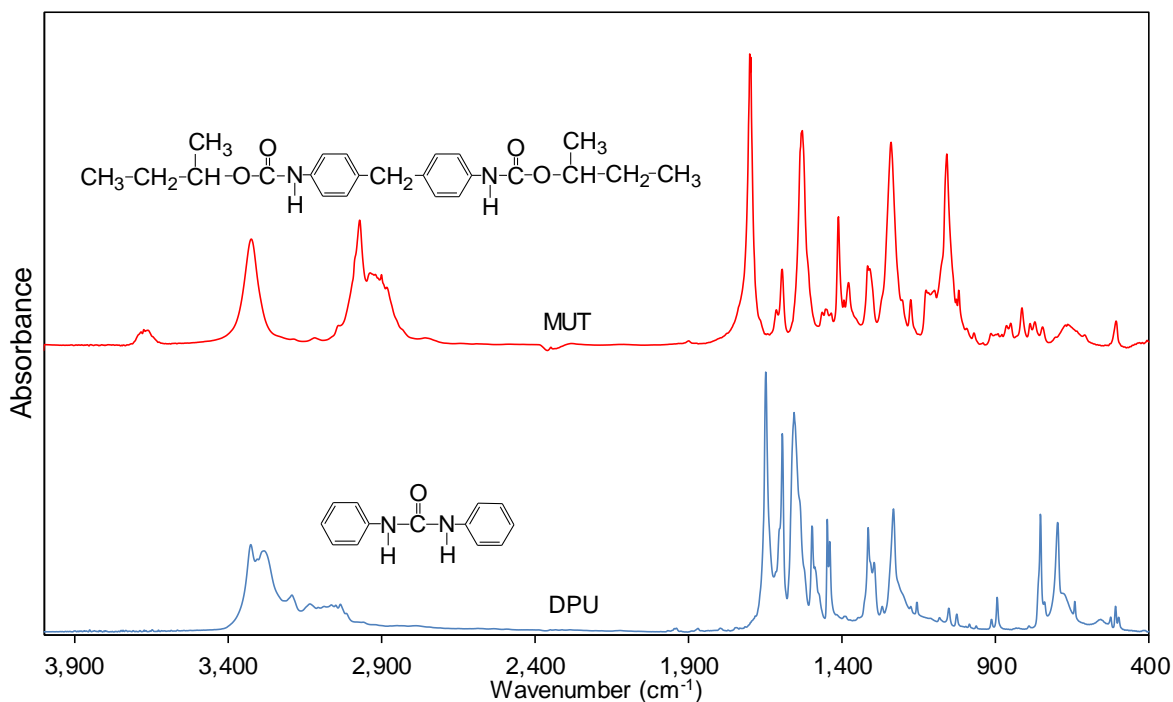


Fig. 3.3.2. FT-IR spectra of MUT and DPU.

Table 3.3.1. FT-IR band assignments of MUT and DPU.

DPU		MUT	
3326 3284	N-H stretching	3325	N-H stretching
1648	Amide I: C=O stretching	1700	Amide I: C=O stretching
1597 1556	Amide II: C-N stretching + N-H bending	1595 1529	Amide II: C-N stretching + N-H bending
1448	N-H bending	1412	N-H bending
1314 1232	Amide III: C-N stretching +N-H bending	1316 1240	Amide III: C-N stretching +N-H bending
		1058	C-O stretching

Amide II consists of more N-H bending; Amide III consists of more C-N stretching.

Band assignments corresponding to urethane and urea linkages of MUT and DPU were listed in Table 3.3.1. In addition, the strong C-H stretching bands of MUT methyl and methylene showed up in the region of 2800-3000 $\text{cm}^{-1}$ , and the weak C-H stretching bands of DPU aromatic ring showed up in the region of 3000-3100 $\text{cm}^{-1}$ . As it has been demonstrated in Table 3.3.1, almost all band locations of urethane and urea were quite close to each other, but two amide I bands, at 1700 $\text{cm}^{-1}$  and 1648 $\text{cm}^{-1}$ , had 52 $\text{cm}^{-1}$  distance. So, amide I bands were used to distinguish between urethane and urea.

At room temperature, H of N-H was easily hydrogen bonded to O of C=O in both API adhesive and model compounds. During FT-IR test, hydrogen bond has the same effect as increasing the mass of H atom. Based on Scheme. 1.4, the increasing of atom mass can lead to a low-wavenumber shift of stretching vibration absorption and a high-wavenumber shift of bending vibration absorption. Namely, on FT-IR spectrum, the band of hydrogen bonded stretching vibration occur at a lower wavenumber than that of non-hydrogen bonded stretching vibration<sup>[27]</sup>, and the band of hydrogen bonded bending vibration occur at a higher wavenumber than that of non-hydrogen bonded one.

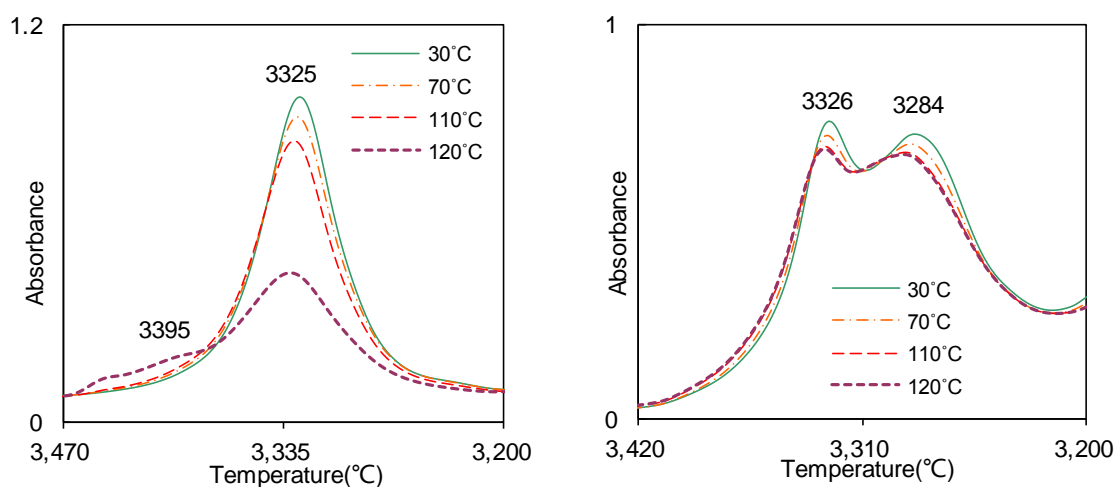


Fig. 3.3.3. Temperature dependent FT-IR spectra of MUT (left) and DPU (right).

Fig. 3.3.3 left and right showed the temperature dependent spectra of MUT and DPU in the region of above  $3200\text{cm}^{-1}$ . The hydrogen bonded N-H stretching band of MUT showed a sharp peak at  $3325\text{cm}^{-1}$  at  $30^\circ\text{C}$ . Band intensity at  $3325\text{cm}^{-1}$  descended with elevated temperature, demonstrating that increasing temperature led to a gradual breakup of hydrogen bands and, as a result, a decreasing of band intensity. At  $120^\circ\text{C}$ , a band appeared at  $3395\text{cm}^{-1}$ , which was attributed to non-hydrogen-banded N-H stretching vibration. On DPU spectra, two bands showed up at  $3284\text{cm}^{-1}$  and  $3326\text{cm}^{-1}$ , respectively. These two bands were considered to be due to the hydrogen bonded N-H stretching vibrations of cis- and trans-conformation amide. The band intensities of  $3284\text{cm}^{-1}$  and  $3326\text{cm}^{-1}$  decreased with temperature, and band peaks shifted slightly to high wavenumber, indicating the dissociation of hydrogen bands. However, there was no separate non-hydrogen-banded N-H stretching band occurred at a higher wavenumber.

In addition, C-H stretching bands at around  $2900\text{ cm}^{-1}$  also had variations on band intensities but no wavenumber shift. Based on the studies of Han S at al.<sup>[51]</sup> and Macphail RA et al.<sup>[52]</sup>, these band variations came from the conformational changes of methyl and methylene.

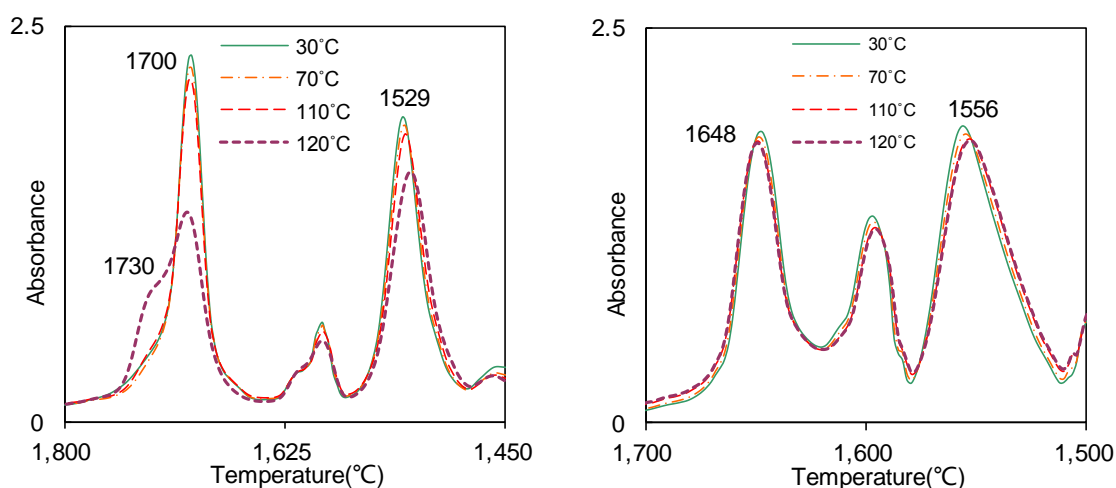


Fig. 3.3.4. Temperature dependent FT-IR spectra of MUT (left) and DPU (right).

Hydrogen bonded C=O stretching bands of urethane and urea were detected at  $1700\text{cm}^{-1}$  and  $1648\text{cm}^{-1}$  at  $30^\circ\text{C}$  in Fig. 3.3.4. The band intensity of urethane C=O

stretching decreased gradually with temperature, attributed to hydrogen bond dissociation. One obvious shoulder peak arose at  $1730\text{cm}^{-1}$ , corresponding to non-hydrogen-bonded C=O stretching of urethane. Urea C=O stretching band at  $1648\text{cm}^{-1}$  also showed a decreasing on band intensity, but no separate non-hydrogen-banded C=O stretching was detected.

Bands at  $1529\text{cm}^{-1}$  and  $1556\text{cm}^{-1}$  were attributed to amide IIs of urethane and urea. Amide II consists of both C-N stretching and N-H bending vibration, but N-H bending occupies more proportion than the other one<sup>[28]</sup>. The band of hydrogen bonded bending vibration normally appears at a higher wavenumber than that of non-hydrogen bonded one. Those two bands showed decreasing band intensity and shifted to lower wavenumber with elevated temperature, which verified their origins.

### 3.3.2 FT-NIR Spectra of Model Compounds

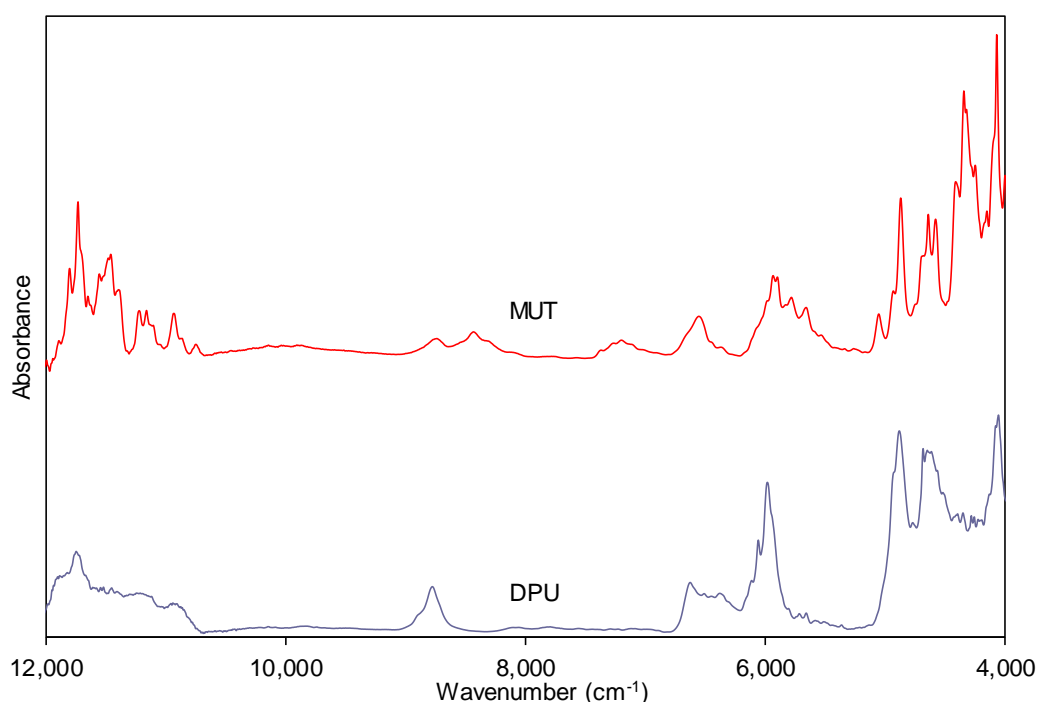


Fig. 3.3.5. FT-NIR spectra of MUT and DPU.

Stretching and bending vibration are the two primary vibration models of chemical bond in molecule. The former one arises along the axis of bond, and the

latter occurs on the molecule with more than three atoms. The fundamental absorption of stretching vibration occurs in the region of  $1000-5000\text{cm}^{-1}$ , and that of bending vibration occurs in  $400-1000\text{cm}^{-1}$ . Overtone can be calculated by using Scheme 1.5. However, anharmonicity constant of chemical bond is an extremely small value that has little effect on overtone wavenumber, so the wavenumber of first overtone is approximately double of fundamental wavenumber, and the wavenumber of second overtone is approximate triple. Therefore, the calculated first overtone of stretching vibration is mainly in the region of  $2000-10000\text{cm}^{-1}$  <sup>[53]</sup>, the first overtone of bending vibration is in  $800-2000\text{cm}^{-1}$ , and the second overtone of bending vibration is in  $1200-3000\text{cm}^{-1}$ . The band intensity of the first overtone is one order of magnitude less than that of fundamental absorption, and the band intensity of the second overtone is two order of magnitude less. Combination tone is the overlapping of two fundamental absorption bands. For example, the combination tone of one stretching and one bending vibration should occur in  $1400-6000\text{cm}^{-1}$ .

Table 3.3.2. FT-NIR band assignments of MUT.

Wavenumber (cm <sup>-1</sup> )	Vibration	Structure
8735	C-H sec	Aromatic
8431	C-H sec	CH <sub>2</sub>
7198	C-H com	CH <sub>2</sub>
6552	N-H str fir	Amide
5932 5896	C-H str fir	Aromatic
5730 5657	C-H str fir	CH <sub>2</sub>
5050	Asym N-H str/amide II com	Amide
4866	Sym N-H str/amide I com	Amide
4636	C-H str/C-H def com	Aromatic
4576	N-H ben sec	Amide
4339	C-H ben sec	CH <sub>2</sub>
4064	C-H com or	CH <sub>2</sub> or
	Sym C-N-C str fir	Amide

fir: first overtone; sec: second overtone; com: combination tone; str: stretching; def: deformation; ben: bending.

Near infrared spectroscopy detects overtone and combination tone of chemical bond vibrations (overtone: multiple of fundamental vibration; combination tone: sum of two fundamental vibration). Overtone and combination tone have much lower probabilities of occurrence than fundamental vibration. Thus, much more sample mass is needed for FT-NIR. Samples for FT-NIR test were pure MUT and DPU disks (100°C vacuum dried), each with the mass of 100mg. FT-NIR spectra of MUT and DPU were displayed in Fig. 3.3.5, and the approximate band assignments were summarized in Table 3.3.2 and Table 3.3.3. Normally, it is difficult to assign NIR band precisely because of significant band overlapping in

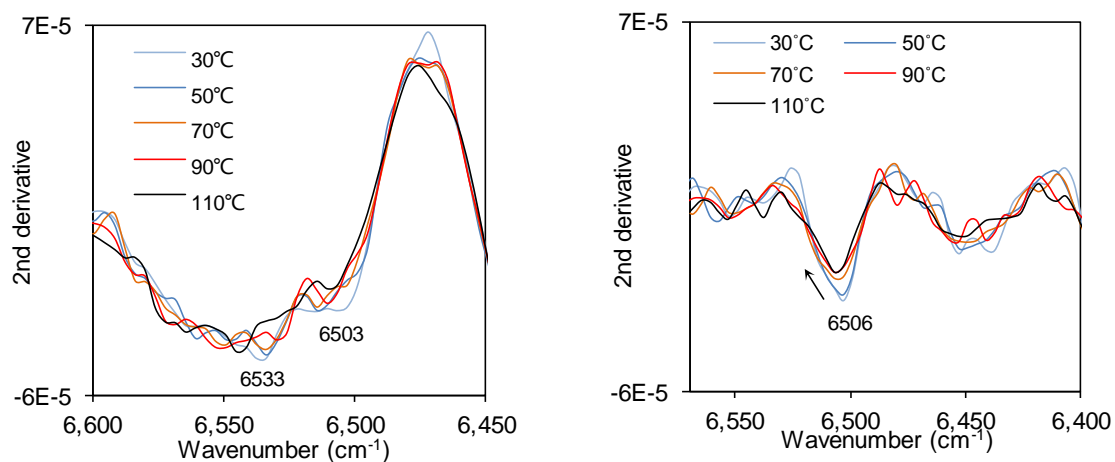
the region, so urethane and urea band were confirmed again by using temperature dependent FT-NIR.

Table 3.3.3. FT-NIR band assignments of MUT.

Wavenumber (cm <sup>-1</sup> )	Vibration	Structure
8776	C-H sec	Aromatic
6623 6377	N-H str fir	Amide
5932 5896	C-H str fir	Aromatic
6054 5980	C-H str first	Aromatic
4778	N-H def ove	Amide
4644	C-H str/C-H def com	Aromatic
4346	C-H ben sec	CH <sub>2</sub>
4050	C-H com or	CH <sub>2</sub> or
	Sym C-N-C str fir	Amide

fir: first overtone; sec: second overtone; com: combination tone; str: stretching; def: deformation.

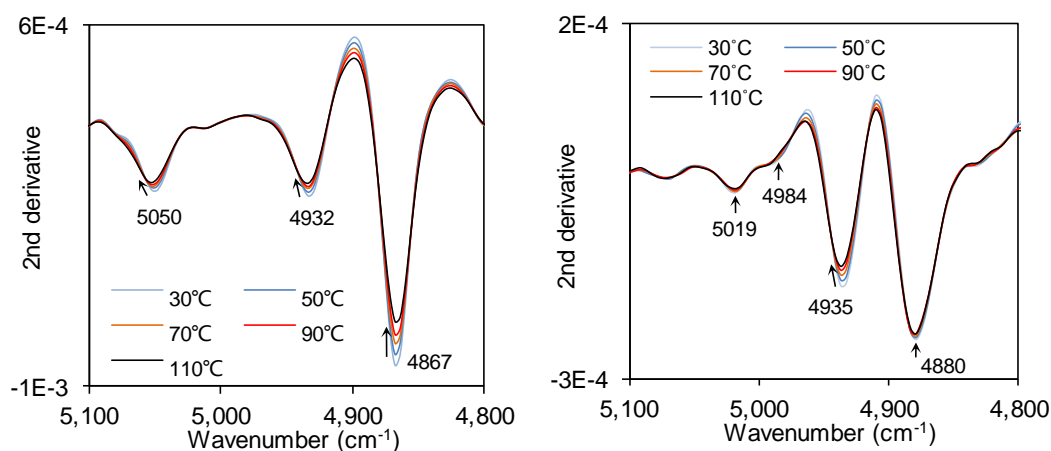
Pure DPU disk melted at above 110°C, so the temperature dependent FT-NIR of DPU was collected below T<sub>g</sub>. The test temperature for DPU was also below 110°C in accordance with MUT. Based on Table 3.3.2 and 3.3.3, amide bands mainly occurred at round 6500cm<sup>-1</sup> and 5000cm<sup>-1</sup>, so these two regions were discussed. Furthermore, 2<sup>nd</sup> derivative calculation was performed on FT-NIR spectrum to enhance resolution and separate overlapping bands. 2<sup>nd</sup> derivative spectrum demonstrated the variation of gradient of raw FT-NIR spectrum. On the obtained 2<sup>nd</sup> derivative spectra, absorption band of chemical bond occurs as downward peak. In addition, the variation of band intensity on raw FT-NIR spectrum could also be estimated by using 2<sup>nd</sup> derivative spectrum as it had been stated in 1.2.3.



For vertical axis value, aE-b was equal to  $a \times 10^{-b}$ .

Fig. 3.3.6. 2<sup>nd</sup> derivative spectra of MUT (left) and DPU (right).

Fig. 3.3.6 showed the 2<sup>nd</sup> derivative spectra of MUT and DPU in the region of around  $6500\text{cm}^{-1}$ . According to the study of Wheeler et al. [53], this region was assigned to the first overtone of N-H stretching vibration. In Fig. 3.3.6 left, a peak at  $6533\text{cm}^{-1}$  occurred, and a peak at  $6503\text{cm}^{-1}$  occurred as a shoulder. However, some unknown noises affected this region, causing a lot of fluctuating peaks, so the peak variation was difficult to confirm. In Fig. 3.3.6 right, the N-H stretching first overtone caused a clear peak at  $6506\text{cm}^{-1}$ . This peak showed decreasing peak intensity and high-wavenumber shift, which was attributed to the dissociation of hydrogen bond under elevated temperature.



For vertical axis value, aE-b was equal to  $a \times 10^{-b}$ .

Fig. 3.3.6. 2<sup>nd</sup> derivative spectra of MUT (left) and DPU (right).

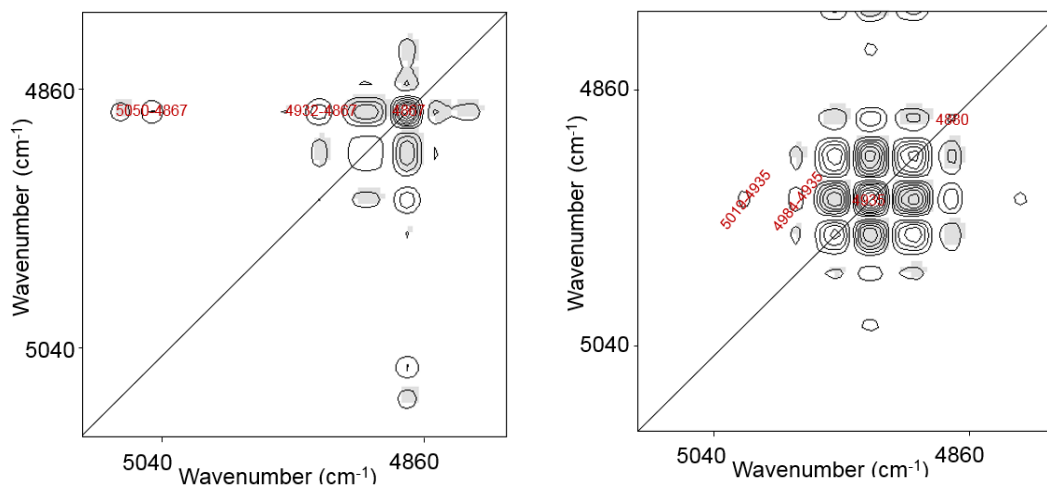


Fig. 3.3.7. Synchronous 2D correlation spectra of MUT (left) and DPU (right), generated from Fig. 3.3.6.

The other main absorption band of amide is at around  $5000\text{cm}^{-1}$ . Burns DA et al. [27] summarized that the combination tone of asymmetric N-H stretching/amide II occurs at  $5050\text{cm}^{-1}$ , the combination tone of N-H stretching/N-H bending occurs at  $5025\text{cm}^{-1}$ , the second overtone of C=O stretching occurs at  $4926\text{cm}^{-1}$ , the combination tone of N-H/amide II occurs at  $4878\text{cm}^{-1}$ , and the combination tone of symmetric N-H stretching/amide I occurs at  $4866\text{cm}^{-1}$ . Thus, in Fig. 3.3.6 left (MUT), the peak at  $5050\text{cm}^{-1}$  was assigned to N-H stretching/amide II combination tone, the peak at  $4932\text{cm}^{-1}$  was attributed to C=O stretching second over tone, and the peak at  $4867\text{cm}^{-1}$  was assigned to N-H stretching/amide I combination tone. Hydrogen bonds was broken up gradually by elevated temperature, which led to three decreasing peak intensities. In addition,  $5050\text{cm}^{-1}$  and  $4932\text{cm}^{-1}$  peak shifted a little to high wavenumber, the same behavior as FT-IR bands did (in Fig. 3.3.4). However, the peak of non-hydrogen-bonded chemical bond did not occur. On synchronous 2D correlation spectrum of MUT (Fig. 3.3.7), auto-peak appeared significantly at  $4867$ . Even though no auto-peak at  $5050$  or  $4932$  occurred, the positive cross-peaks at  $5050-4867$  and  $4932-4867$  were detected, suggesting that  $5050\text{cm}^{-1}$  and  $4932\text{cm}^{-1}$  peak also varied as  $4867\text{cm}^{-1}$  peak did.

In Fig. 3.3.6 right (DPU),  $5019\text{cm}^{-1}$ ,  $4984\text{cm}^{-1}$ ,  $4935\text{cm}^{-1}$  and  $4880\text{cm}^{-1}$  peaks decreased on peak intensity with elevated temperature.  $5019\text{cm}^{-1}$  and  $4984\text{cm}^{-1}$  were assigned to N-H stretching/amide II combination tone or N-H stretching/N-H bending combination tone.  $4935\text{cm}^{-1}$  peak was assigned to C=O stretching second overtone, and  $4880\text{cm}^{-1}$  was due to N-H stretching/amide I combination tone. On synchronous 2D correlation spectrum, 4935 and 4880 auto-peaks and 5019-4935 and 4984-4935 cross-peaks occurred, due to the peak intensity variations of them.

### 3.3.3 FT-NIR Spectra of API paper

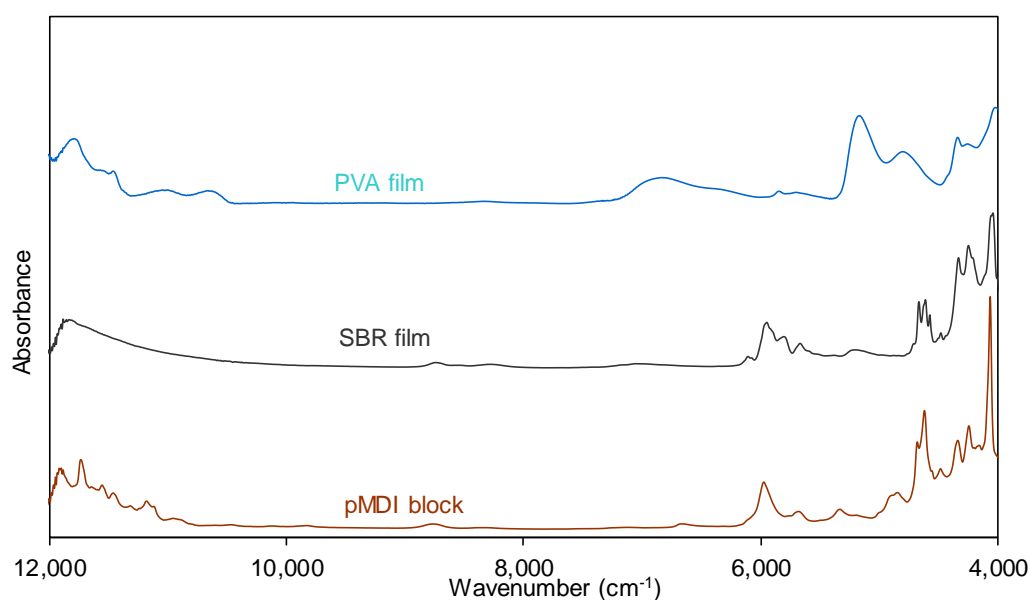


Fig. 3.3.8. FT-NIR spectra of three raw materials.

Prior to API paper, FT-NIR spectroscopy was performed on three raw materials. PVA film and SBR film were prepared by casting 15wt% PVA aqueous solution and SBR latex on Teflon sheet and aging in thermostatic chamber for 1 week. pMDI block was prepared by casting pMDI on Teflon sheet and aging in thermostatic chamber for 1 month.

Table 3.3.4. FT-NIR band assignments of PVA film.

Wavenumber (cm <sup>-1</sup> )	Vibration	Structure
6833	O-H str fir	Hydroxyl and H <sub>2</sub> O
5844 5700	C-H str fir	CH <sub>2</sub>
5166	O-H ben sec	H <sub>2</sub> O
4801	O-H com	Hydroxyl
5355 4923	C=O sec	Acetyl
4336 4254	C-H ben sec	CH <sub>2</sub>
4018	C-H str/C-C str com	CH <sub>2</sub>

fir: first overtone; sec: second overtone; com: combination tone; str: stretching; def: deformation; ben: bending.

Table 3.3.5. FT-NIR band assignments of SBR film.

Wavenumber (cm <sup>-1</sup> )	Vibration	Structure
7051	C-H com	Aromatic
6107	C-H str fir	=CH
5948	C-H str fir	Aromatic
5803	C-H str fir	CH <sub>2</sub>
5667	C-H str fir	CH <sub>2</sub>
5202	O-H ben sec	H <sub>2</sub> O
4663 4609 4571	C-H str/C-H def com	CH=CH
4329	C-H ben sec	CH <sub>2</sub>
4245	CH <sub>2</sub> ben sec	CH <sub>2</sub>
4039	C-H com	CH <sub>2</sub>

fir: first overtone; sec: second overtone; com: combination tone; str: stretching; def: deformation; ben: bending.

Table 3.3.6. FT-NIR band assignments of pMDI block.

Wavenumber (cm <sup>-1</sup> )	Vibration	Structure
5973	C-H str fir	Aromatic
5681	C-H str fir	CH <sub>2</sub>
5333	C=O str sec	C=O
4900	N-H/amide II com or N-H/amide III com	Urea
4847	N-H ben sec or N-H ben/N-H str com	Urea
4677 4617	C-H def com	CH <sub>2</sub>
4481	C-H str/CH <sub>2</sub> def com	CH=CH
4335	C-H ben sec	CH <sub>2</sub>
4241	CH <sub>2</sub> ben sec	CH <sub>2</sub>
4061	C-H com	CH <sub>2</sub>

fir: first overtone; sec: second overtone; com: combination tone; str: stretching; def: deformation; ben: bending.

API paper was prepared by sandwiching API adhesive between two pieces of filter paper, and the *in-situ* chemical structure analysis of API adhesive glue-line was carried out by using FT-NIR (Fig. 3.3.9). Background for API paper was overlapped two pieces of filter paper, by which the NIR absorption of filter paper was deducted automatically when API paper was tested. Actually, liquid-state NMR is a more precise method for chemical analysis, but API paper used in this experiment could not be dissolved in any solvent. API paper could also be grinded into powder form, for FT-IR spectrum testing. However, the grind process destroyed API paper and was considered to accelerate NCO reactions since NCO is highly reactive. FT-NIR test is one damage-less method, so after FT-NIR test

it was possible to age API paper continuously in thermostatic chamber. FT-NIR spectra of API paper were collected, 1 day, 3 days, 6 days, 10 days, 15 days and 20 days after API paper was prepared. Spectrum of 20 days aged API paper was showed in Fig. 3.3.10. Band assignments were summarized in Table 3.3.7.

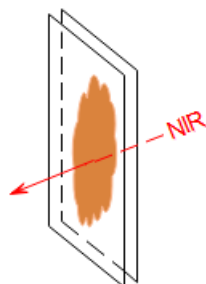


Fig. 3.3.9. FT-NIR test for API paper.

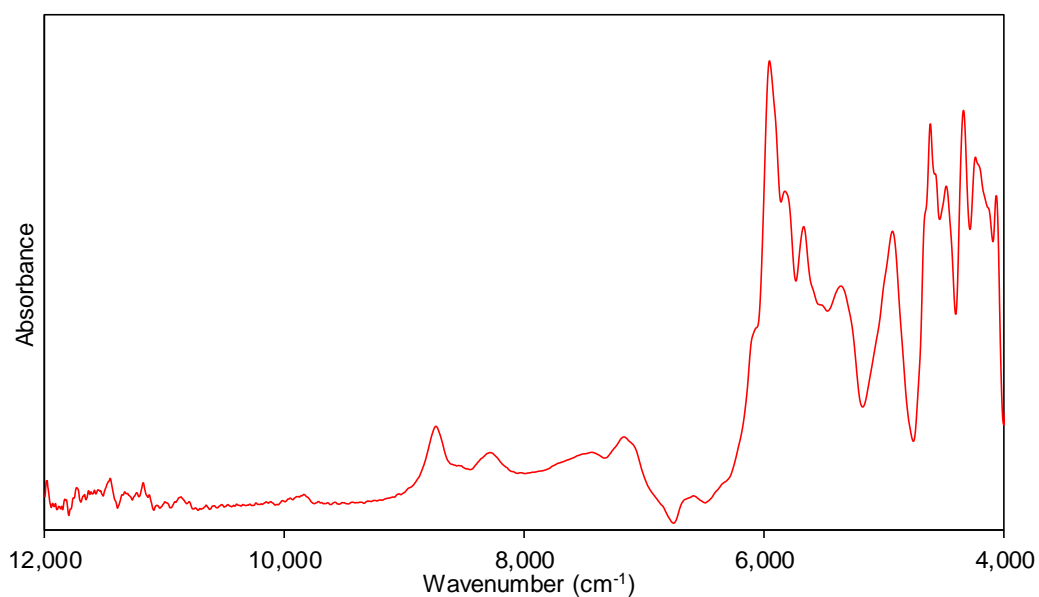


Fig. 3.3.10. FT-NIR spectrum of 20 days aged API paper.

Table 3.3.7. FT-NIR band assignments of API paper.

Wavenumber (cm <sup>-1</sup> )	Vibration	Structure
8734	C-H sec	Aromatic
8283	C-H sec	CH <sub>2</sub>
7434	C-H com	CH <sub>3</sub>
7164	C-H com	CH <sub>2</sub>
5953	C-H str fir	Aromatic
5814	C-H str fir	CH <sub>2</sub>
5664	C-H str fir	Aromatic
4923	C=O sec	Amide
4615	Asym C-H str/C-H def com	HC=CH
4480	O-H str/C-O str com	Hydroxyl
4333	C-H ben sec	CH <sub>2</sub>
4063	C-H com or Sym C-N-C str fir	CH <sub>2</sub> or Amide

fir: first overtone; sec: second overtone; com: combination tone; str: stretching; def: deformation.

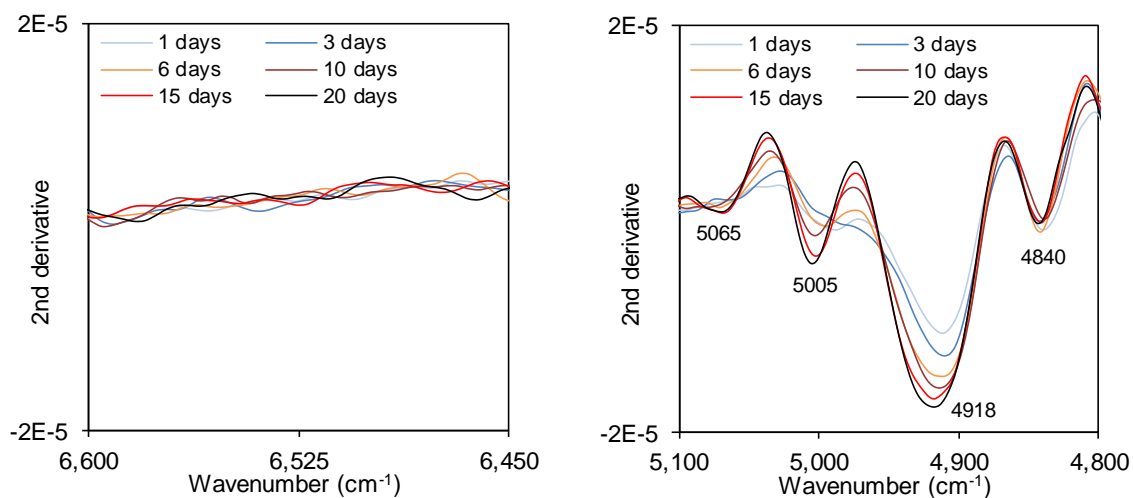


Fig. 3.3.11. 2<sup>nd</sup> derivative spectra of API paper.

After NIR spectra were collected, 2<sup>nd</sup> derivative calculation was applied to enhance resolution (Fig. 3.3.11). All 2<sup>nd</sup> derivative spectra were normalized by using C-H stretching first overtone peak as a standard. However, in Fig. 3.3.11 (left), no obvious peak was detected in the range of N-H stretching first overtone, which might be related to noise and sample condition. In the region of 4800-5100cm<sup>-1</sup>, four peaks appeared at 5065cm<sup>-1</sup>, 5005cm<sup>-1</sup>, 4918cm<sup>-1</sup> and 4840 cm<sup>-1</sup>. According to model compounds results, 5065cm<sup>-1</sup> and 5005cm<sup>-1</sup> were attributed to the N-H stretching/amide II combination tones of urethane and urea, respectively. 4918cm<sup>-1</sup> was attributed C=O stretching overtone, consisting of the information of both urethane and urea. Those three peak intensities increased gradually with aging time, implying the generations of urethane and urea. On the other hand, 4840cm<sup>-1</sup> peak did not have variation on peak intensity.

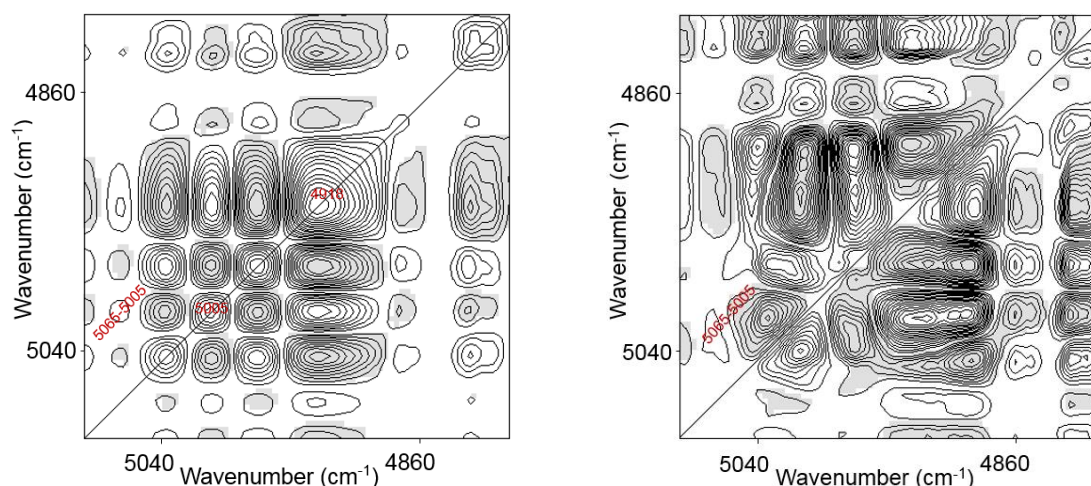
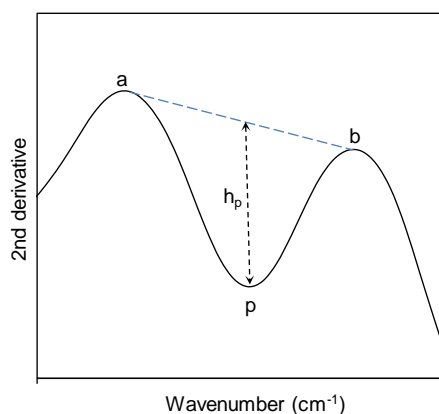


Fig. 3.3.12. Synchronous (left) and asynchronous (right) spectra, generated from Fig. 3.3.11 (right).

On synchronous spectrum, 5005 auto-peak and 4918 auto-peak occurred obviously. 5065 auto-peak did not show up but a positive cross-peak appeared at 5065-5005. The negative asynchronous peak at 5065-5005 in Fig. 3.3.12 (right) suggested that 5005cm<sup>-1</sup> peak (urea) varied faster than 5065cm<sup>-1</sup> peak (urethane). 4840 cm<sup>-1</sup> peak did not increase on peak intensity as other peaks did, and neither auto-peak nor cross-peak at 4840 was detected in Fig. 3.3.12. Based on model compounds results, 4840 cm<sup>-1</sup> peak might be due to N-H stretching/amide II

combination tone. Burns DA et al. [27] also reported that O-H combination absorption shows up in this region, which could be PVA hydroxyl in this experiment, so the assignment of  $4840\text{cm}^{-1}$  peak was still unclear.



$$h_p = [y_a + \frac{w_a - w_p}{w_a - w_b} (y_b - y_a)] - y_p$$

Scheme 3.3.1. calculations of peak intensities.

Fig. 3.3.13. Diagram of peak intensities.

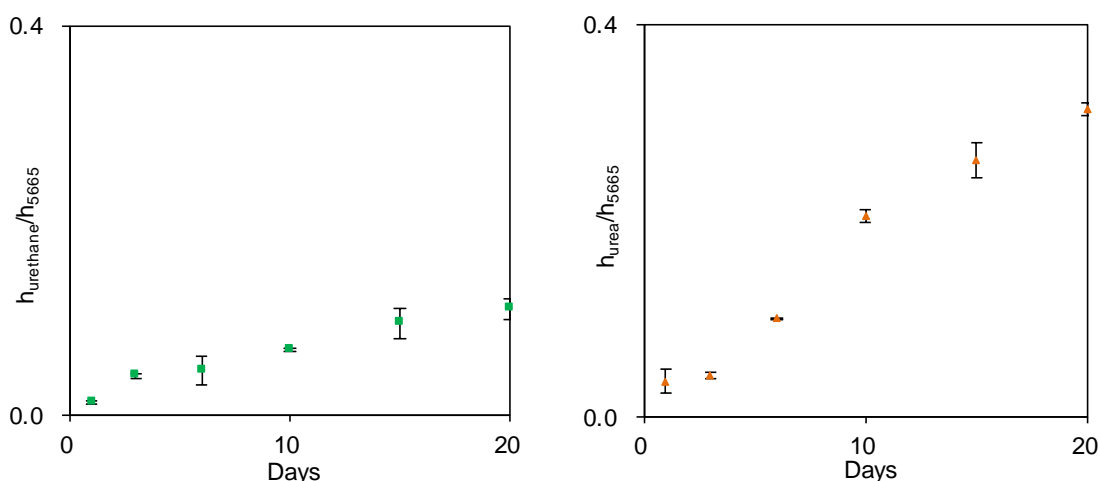


Fig. 3.3.14. Generations of urethane (left) and urea (right) in API paper, error bars represent  $\pm 1$  standard deviation,  $n=3$ .

Further, peak intensity on 2<sup>nd</sup> derivative was calculated to track the formations of urethane and urea [54, 55]. As it was demonstrated in Fig. 3.3.13, downward peak of chemical bond, p, was clamped by two upward peaks, a and b. Thus, peak intensity,  $h_p$ , was calculated based on those three peak locations. Calculation formulas were displayed in Scheme 3.3.1, where w was wavenumber and y corresponded to vertical axis value of each peak. Urethane and urea peak

intensities were obtained first and then divided by the peak intensity at  $5665\text{cm}^{-1}$  (C-H first overtone of methylene) for normalization.

Generations of urea and urethane in API paper during post-curing process were showed in Fig. 3.3.14, calculated from 2<sup>nd</sup> derivative spectra in Fig. 3.3.11. In this experiment API papers were prepared in triplicate, and average value and  $\pm 1$  standard deviation were employed. It seemed like that urea had more generation amount than urethane. Hori et al. [12] already reported that urea generates much faster than urethane, so the difference between urethane and urea generation amounts in Fig. 3.3.14 could be attributed to the discrepant reactivities of between PVA hydroxyl and water.

### 3.4 Conclusions

In this chapter, the chemical structure of API glue-line sandwiched between two pieces of filter paper was analyzed by using FT-NIR spectroscopy. Prior to the FT-NIR test on API paper, two model compounds (MUT and DPU) were synthesized to assign the NIR absorption locations of urethane and urea, two primary products of NCO reactions. Temperature dependent FT-IR and FT-NIR spectroscopy were employed for band assignment, since hydrogen bonded amide is sensitive to temperature. Band assignments of amides in model compounds and API paper were listed below.

MUT:  $3325\text{cm}^{-1}$ : N-H stretching;  $1700\text{cm}^{-1}$ : C=O stretching (amide I);  $1529\text{cm}^{-1}$ : C-N stretching+N-H bending (amide II);  $6533\text{cm}^{-1}$ ,  $6503\text{cm}^{-1}$ : N-H stretching first overtone;  $5050\text{cm}^{-1}$ : N-H stretching/amide II combination tone;  $4932\text{cm}^{-1}$ : C=O stretching second overtone;  $4867\text{cm}^{-1}$ : N-H stretching/amide I combination tone.

DPU:  $3326\text{cm}^{-1}$ ,  $3284\text{cm}^{-1}$ : N-H stretching;  $1648\text{cm}^{-1}$ : C=O stretching (amide I);  $1556\text{cm}^{-1}$ : C-N stretching+N-H bending (amide II);  $6506\text{cm}^{-1}$ : N-H stretching first overtone;  $5019\text{cm}^{-1}$ ,  $4984\text{cm}^{-1}$ : N-H stretching/amide II combination tone or N-H

stretching/N-H bending combination tone;  $4935\text{cm}^{-1}$ : C=O stretching second overtone;  $4880\text{cm}^{-1}$ : N-H stretching/amide I combination tone.

API thin film:  $3320\text{cm}^{-1}$ : N-H stretching;  $1723\text{cm}^{-1}$ : C=O stretching (urethane);  $1639\text{cm}^{-1}$ : C=O stretching (urea).

API paper:  $5065\text{cm}^{-1}$ : N-H stretching/amide II combination tone of urethane;  $5005\text{cm}^{-1}$ : N-H stretching/amide II combination tone of urea;  $4918\text{cm}^{-1}$ : C=O stretching overtone;  $4840\text{cm}^{-1}$ : N-H stretching/amide II combination tone or O-H combination tone.

After band assignment, the generations of urethane and urea in API paper during post-curing were tracked by using FT-NIR spectroscopy. From 1 day to 20 days, urethane and urea was generated continuously.

## **4 Influence of Adhesive Components and Aging Conditions on The Chemical Structure of API Adhesive Glue-Line**

### **4.1 Introduction**

During aging time, urethane linkages were generated from the reactions of between NCOs and hydroxyls (Scheme 1.2). In API paper, there could be two types of formed urethanes, one from NCO and PVA hydroxyl and the other one from NCO and cellulose hydroxyl. Thus, urethane formations contributed to the ascents of both cohesion strength (due to the reaction of between NCO and PVA hydroxyl) and adhesion strength (due to the reaction of between NCO and cellulose hydroxyl). In the meanwhile, urea was generated from NCO-H<sub>2</sub>O reaction, leading to the formation of cross-linking and the increasing of bond strength. Even though there are several factors that affect the bonding strength of API adhesive, such as viscosity, penetration and surface roughness, chemical bond is regarded as a quite important one.

The research on chemical structure of API adhesive, instead of just on bond strength, was started by Taki et al. They confirmed the reaction of between isocyanate cross-linker and polyvinyl alcohol by FT-IR spectroscopy and water solubility test <sup>[56]</sup>. Then, the emission amount of carbon dioxide, due to NCO reaction with water, was measured, and the effect of NCO-H<sub>2</sub>O reaction products on the storage modulus of adhesive film was studied <sup>[57]</sup>. They also investigated the reactions of NCOs with cellulose and wood by using DSC <sup>[58]</sup>. However, the chemical structure analysis of API glue-line was not carried out, because a suitable analysis method was difficult to find.

Chemical structure of API glue-line in API paper was analyzed by using FT-NIR spectroscopy in chapter 3. In this chapter, FT-NIR was further used to investigate

the influences of adhesive components and aging conditions on urethane and urea generations. PVA: Yamada et al. [59, 60] reported that acetoacetylated PVA and pMDI produced a higher cross-linking density than normal PVA and pMDI. Thereby, the influence of PVA on NCO reactions was investigated by using different PVAs as base resin; Mass ratio of SBR latex: The copolymer of styrene and butadiene does not react at all with NCO. However, SBR micelle in latex has hydroxyls on surface, which could participate in NCO reactions. In addition, SBR micelle has both hydrophilicity and hydrophobicity so that it could accelerate the mixing of PVA and pMDI; Aging humidity: During post-curing process, API glue-line could absorb moisture from ambience. Urea was generated from NCO-H<sub>2</sub>O reaction so the aging humidity was considered to have influence on it; Heat treatment: High temperature could accelerate chemical reaction, so the effect of heat treatment on glue-line chemical structure was studied.

## **4.2 Experimental**

### **4.2.1 Materials**

SBR latex, pMDI and filter paper were the same ones as those used in 3.2.1. Three types of 15wt% PVA aqueous solutions were used.

### **4.2.2 Adhesive Preparation**

API adhesives were prepared in the same process as 2.2.2 described. In addition, three different PVAs (Table 4.2.1, Wako Pure Chemical industries, Ltd., Japan) were used to prepare API adhesives, and the mass ratio of SBR latex was also changed. Prepared API adhesives were showed in Table 4.2.2, corresponding to different PVAs and SBR latex mass ratios.

Table 4.2.1. PVAs.

	PVA I	PVA II	PVA III
DS (%)	98	95	86-90
$M_n$ ( $\times 10^4$ )	14.6	5.8	14.2
$\eta$ (Pa·s)	5.7	0.85	2.5

DS: degree of saponification

$M_n$ : g/mol; measured by GPC; 20mmol/L LiCl/DMAC flow; PEO standard

$\eta$ : measured by HAAKE Rheostress 600; 100 (1/s); 25 °C

Table 4.2.2. API adhesives.

	SBR 2g	SBR 3g	SBR 4g
PVA I	×	API I-3	×
PVA II	API II-2	API II-3	API II-4
PVA III	×	API III-3	×

Table 4.2.3. API papers aged in three conditions.

	Dry	Moist	Thermostatic chamber
API paper	API II-3-dry paper	API II-3-moist paper	API II-3-paper

### 4.2.3 Sample Preparation

API adhesives were used to prepare API papers in the same process as 3.2.2. After preparation, API papers were aged in thermostatic chamber (23°C, RH50%). API adhesives were also used to prepare API films in the process of 2.2.2. Cross-laps for bonding test was prepare in the process of 2.2.2.

#### 4.2.4 Aging Humidity

Some of API II-3 papers were also aged in dry and moist conditions. Dry (23°C, RH 0%): a desiccator with P<sub>2</sub>O<sub>5</sub>; Moist (23°C, RH 98%): a desiccator with saturated K<sub>2</sub>SO<sub>4</sub> aqueous solution. (Table 4.2.3)

#### 4.3.5 Heat Treatment

API paper, API film and cross-laps prepared from API II-3 adhesive were aged in thermostatic chamber for 4 days and then heated at 80°C for 2h, 4h and 6h. After that, all samples were continually aged in thermostatic chamber.

#### 4.2.6 Characterizations

FT-NIR spectroscopy was the same process as 3.2.3 described. FT-NIR spectra of 1 day, 3 days, 6 days, 10 days, 15 days and 20 days aged API paper were collected.

DMA and cross-lap test were carried out as 2.2.3 described.

### 4.3 Results and Discussion

#### 4.3.1 Different PVAs

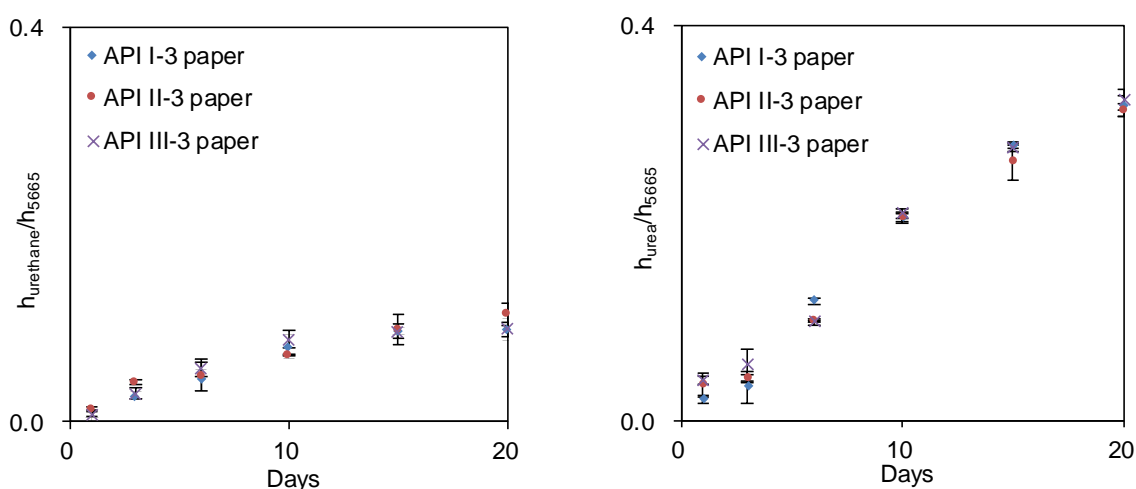


Fig. 4.3.1. Generations of urethane (left) and urea (right) in API papers prepared from three PVAs, error bars represent  $\pm 1$  standard deviation,  $n=3$ .

Three PVAs were employed to prepare adhesives, API I-3, API II-3 and API III-3. High DS (degree of saponification) PVA had more hydroxyl groups on molecular chain, due to which the reaction of between NCO and hydroxyl could take place more in chemical stoichiometry. However, low DS PVA carried more hydrophobic acetyl groups that could lead to a better mixing of PVA and pMDI. Besides, Yamada et al. already found out that acetoacetylated PVA reacted better with pMDI than ordinary PVA in either water emulsion or organic solution [59]. Urethane and urea generating results of different API papers were illustrated in Fig. 4.3.1. Three urethane generations showed almost the same amount, but API II-3 paper seemed like having a bit more amount than the other two on 20 days. For urea, three API papers also had similar amounts.

The storage modulus of API II-3 and API III-3 films (Fig. 4.3.2) increased obviously after 200°C, due to NCO reactions caused by elevated temperature, but that of API I-3 film decreased. The storage modulus decreasing of API I-3 film could be explained as that high DS PVA was not miscible with other two components, so the effect of phase separation surpassed the effect of NCO reactions at over 200°C. Tan  $\delta$  curves of API II-3 and API III-3 films both had three peaks: 28°C,  $T_g$  of the mixture of SBR and uncross-linked PVA; 117°C,  $T_g$  of small scale molecular chain generated from NCO reactions; 205°C, due to NCO reactions and the slippage of PVA semi-crystal. 28°C and 205°C peaks of API I-3 film curve were attributed to the same reasons as it was stated above. Different from API II-3 and API III-3 film, API I-3 film did not show 117°C peak but had 99°C and 155°C peaks. This phenomenon might correspond to two different scale molecules that were generated separately in the uneven phase of API I-3 film.

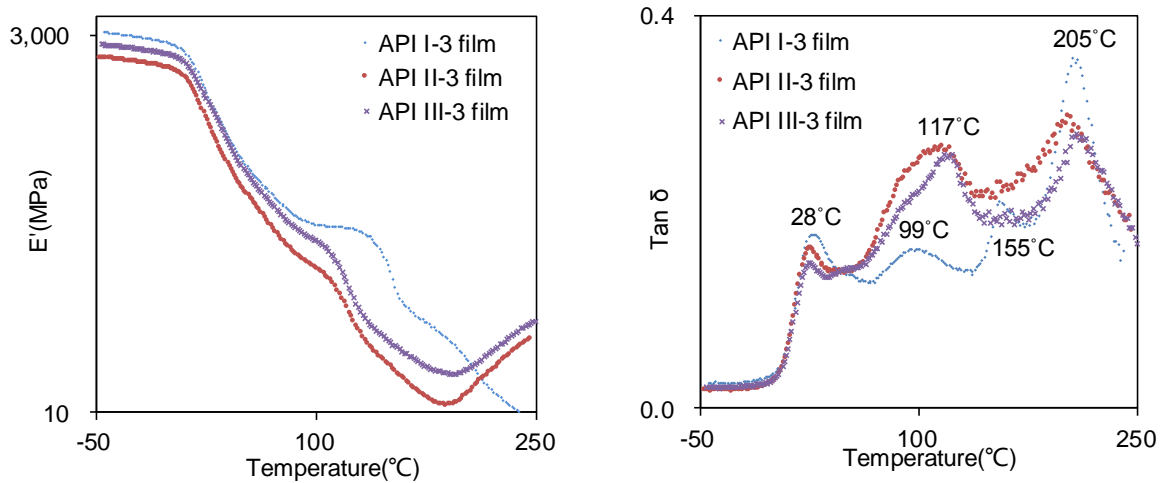


Fig. 4.3.2. DMA thermograms of API films prepared from three PVAs and aged for 6 days.

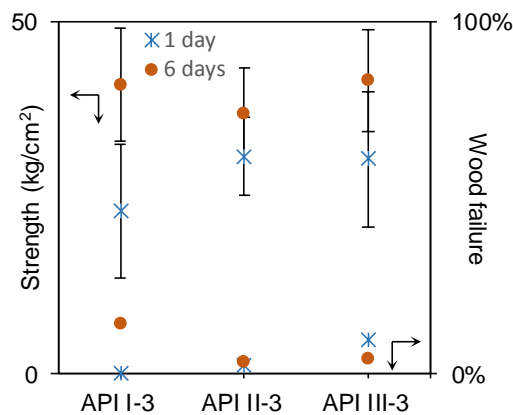


Fig. 4.3.3. Bond strength of cross-laps prepared from API adhesives with different PVAs, error bars represent  $\pm 1$  standard deviation,  $n=7$ .

Cross-lap results of API I-3, API II-3 and API III-3 were demonstrated in Fig. 4.3.3. Significant difference in urethane and urea generation among three adhesives were not found by FT-NIR result. DMA curves indicated that high DS PVA I was not mixed well in adhesive. API I-3 cross-laps aged 1 day showed lower strength than other two adhesive, which might be due to the uneven phase in API I-3 glue-line. However, 6 days aged cross-laps indicated that the adhesives prepared from PVA I and III had higher bond strength than the adhesive from PVA II. This was attributed to the much higher molecular weights of PVA I and III (Table 4.2.1) [61]. In addition, 6 days aged API III-3 cross-laps had a little bit

stronger bond strength than API I-3 cross-laps, which could be attributed to the better dispersion of low DS PVA in adhesive, but the effect was not remarkable.

### 4.3.2 Different SBR latex Mass Ratios

In previous study, 2<sup>nd</sup> derivative FT-NIR spectra were normalized by using C-H first overtone band of methylene bonded to benzene ring at 5665cm<sup>-1</sup>. This band involved the information of both SBR latex and pMDI. However, SBR latex mass ratio of API adhesive was changed in the section, which contributed to a fluctuating ratio of pMDI to SBR latex. Thus, instead of 5665cm<sup>-1</sup> band, the band at 5786cm<sup>-1</sup> due to C-H first overtone of HC=CH was used as standard. Furthermore, calculated urethane and urea generations (as 3.3.3) were multiplied by the mass ratio of SBR block (dried SBR latex) (Table 4.2.4) in API glue-line to normalize the results of three API papers.

Table 4.2.4. Component mass ratios in three API glue-lines.

	API II-2 paper	API II-3 paper	API II-4 paper
SBR block (wt%)	34.7	44.3	51.5
pMDI (wt%)	50.3	42.8	37.3
PVA (wt%)	15	12.9	11.2

API II-2 glue-line: 3g×15% PVA, 2g×51.7% SBR block and 1.5g pMDI;  
 API II-3 glue-line: 3g×15% PVA, 3g×51.7% SBR block and 1.5g pMDI;  
 API II-4 glue-line: 3g×15% PVA, 4g×51.7% SBR block and 1.5g pMDI.

Urethane and urea generations in API II-2, API II-3 and API II-4 paper were summarized in Fig. 4.3.4. It was quite obvious that API II-2 paper generated more urethane and urea than other two API papers, because API II-2 glue-line had higher pMDI ratio. The difference between urethane and urea was observed on 1 day, when three urethanes showed similar but three ureas showed dissimilar amount. Moisture contents in prepared API adhesives increased in the order of API II-4 paper (52.7wt%), API II-3 paper (53.3wt%) API II-2 paper (54.1wt%).

Hence, API II-2 adhesive with higher moisture content produced more urea. On the other hand, urethane generations on 1 day was very little due to the low reaction rate of between PVA and pMDI.

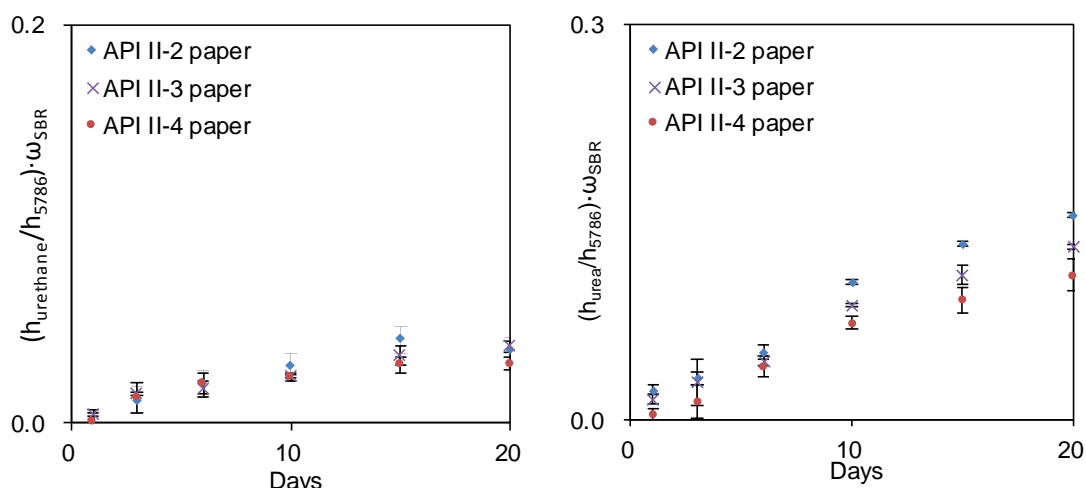


Fig. 4.3.4. Generations of urethane (left) and urea (right) in API papers with different SBR latex ratios, error bars represent  $\pm 1$  standard deviation,  $n=3$ .

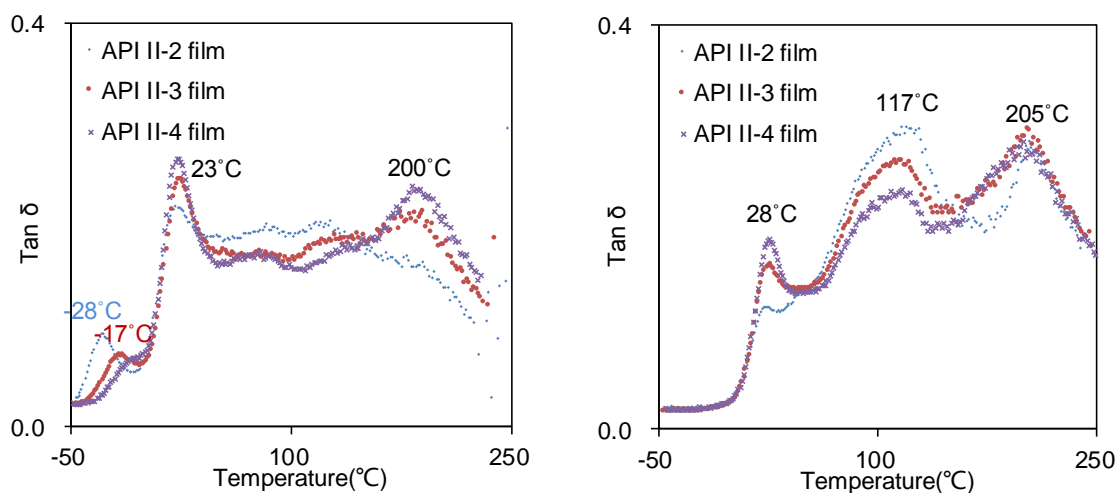


Fig. 4.3.5. Loss factor curves of API films with different SBR latex mass ratios aged for 1 day (left) and 6 days (right).

Loss factor curves of 1 day aged API films were displayed in Fig. 4.3.5 (left).  $T_g$  of the mixture of SBR and un-cross-linked PVA was detected at  $23^\circ\text{C}$ . Two small peaks related to un-reacted pMDI appeared at  $-28^\circ\text{C}$  and  $-17^\circ\text{C}$  of API II-2 and API II-3 film, but that of API II-4 film only occurred as a shoulder peak. This was due to more pMDI contents in API II-2 and API II-3 film. In addition, API II-3 and API II-4 film had a peak at  $200^\circ\text{C}$ , but API II-2 film did not show this peak.

200°C peak was attributed to acute NCO reactions at higher temperature. Increasing of loss factor before 200°C was attributed to ascendant phase friction arose by the interactions of between NCO and other chemical groups (NCO and/or PVA hydroxyl). After 200°C, reactions of NCO were gradually accomplished and chemical linkages between molecules were abundantly bridged, so the molecular stiffness overwhelmed the effect of phase friction, which led to a loss factor decreasing. Loss modulus on 1 day was displayed in Fig. 4.3.6, where all three films showed ascent from 200°C. Thus, the disappearance of 200°C peak of 1 day aged API II-2 film was explained that there was more un-cross-linked pMDI in adhesive film, phase separating effect overcame phase friction effect at 200°C, and therefore loss factor peak did not occur.

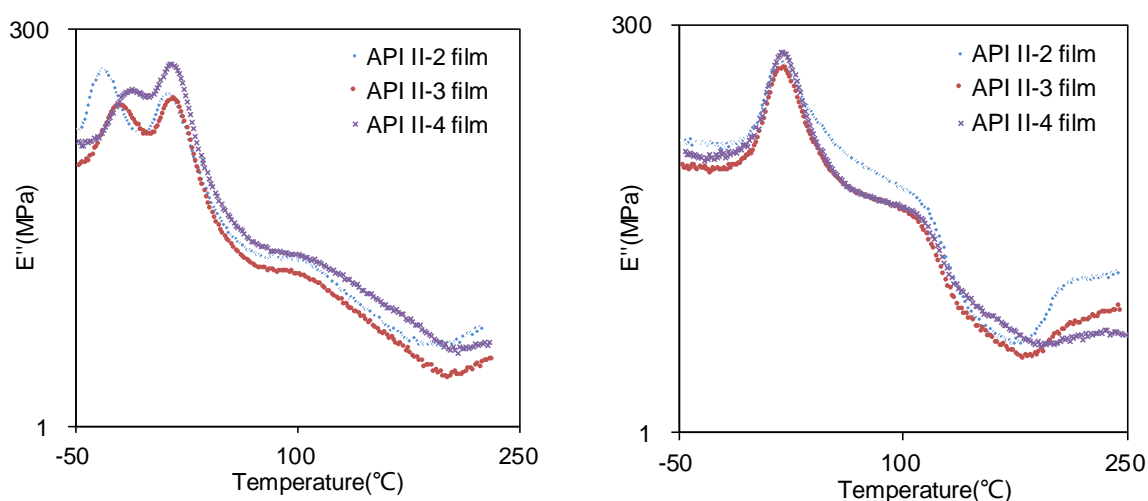


Fig. 4.3.6. Loss modulus curves of API films with different SBR latex mass ratios, aged for 1 day (left) and 6 days (right).

Loss factor curves of 6 days aged API films were demonstrated in Fig. 4.3.5 (right). The large peak at 117°C was  $T_g$  of small scale molecule generated in post-curing period. Differing from 1 day loss factor curve, 6 days aged API II-2 film also had a peak at 205°C as other two films did. In Fig. 4.3.6 (right), loss modulus of three film increased significantly from about 180°C. After 6 days post-curing, more pMDI reacted and formed a large amount of cross-linking structure in

adhesive films. As a result, cross-linking network intensified molecular friction, contributing to an obvious loss factor peak.

Bond strength result of cross-laps was concluded in Fig. 4.3.7. Cross-linking structure was not fully formed after 1 day aging. On the other hand, water evaporation contributed to dense aggregation of SBR particles, and emulsifier and inorganic salt aqueous solution in the gap between SBR particles led to strong bond strength<sup>[5]</sup>. After 6 days aging, too much water evaporation reduced SBR particle adsorption, but cross-linking was significantly formed. API adhesive was prepared from PVA aqueous solution and SBR latex so contained more than 50wt% water. In the glue-line of 1 day aged cross-lap, there was still same moisture left in glue-line. Thereby, high SBR latex mass ratio contributed to a high initial bond strength. In 1 day aged glue-line, pMDI did not form enough cross-linking structure but acted as a phase lubricant. Low bond strength of API II-2 cross-laps on 1 day were due to too much unreacted pMDI. NCOs of pMDI fully reacted after 6 days and generated enough cross-linking network in glue-line. On the other hand, fully dried SBR block produced a brittle structure. The bond strength increasing of API II-2 and API II-3 cross-laps with aging time were attributed to the formation of cross-linking structure. For API II-4 cross-laps, the decreasing of bond strength was relevant to the brittle SBR block.

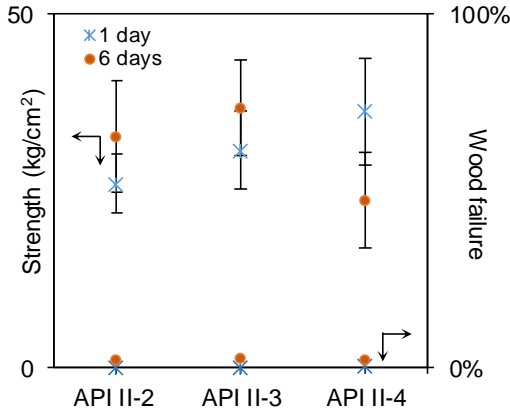


Fig. 4.3.7. Bond strength of cross-laps prepared from API adhesives with different SBR latex mass ratios, error bars represent  $\pm 1$  standard deviation,  $n=7$ .

### 4.3.3 Different Humidity conditions

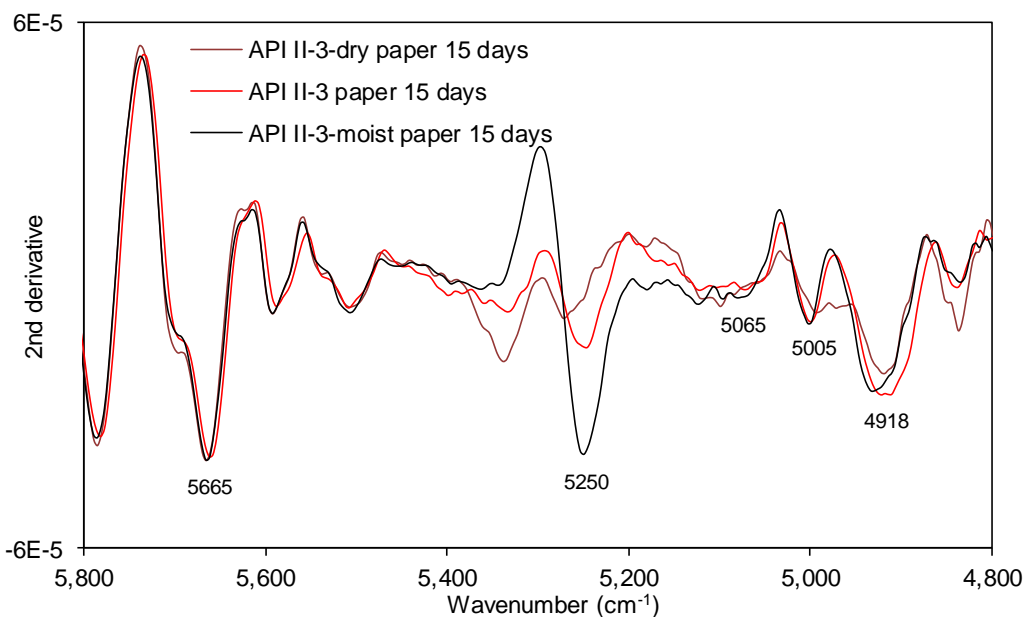


Fig. 4.3.8. 2<sup>nd</sup> derivative spectra of API papers aged for 15 days in three humidity conditions.

API papers prepared from API II-3 were aged in three humidity conditions, dry, normal (thermostatic chamber) and moist. During aging period, adhesive glue-line could absorb moisture from ambience [62, 63, 64]. 2<sup>nd</sup> derivative spectra of API papers were shown in Fig. 4.3.8. Three 2<sup>nd</sup> derivative spectra were normalized by using aromatic C-H stretching first overtone peak at 5665cm<sup>-1</sup> as standard. Burns et al. [27] reported that O-H stretching first overtone of hydroxyl occurred at 5241cm<sup>-1</sup> and O-H bending second overtone of H<sub>2</sub>O occurred at 5154cm<sup>-1</sup>. Hence, the peak at 5250 cm<sup>-1</sup> in Fig. 4.3.8 consisted of the chemical bond information of both hydroxyl and H<sub>2</sub>O. From dry to moist spectrum, peak intensity at 5250cm<sup>-1</sup> increased significantly, implying that moisture content in API glue-line increased with ambient humidity. Furthermore, the difference in peak intensity at 5065cm<sup>-1</sup> (urethane), 5005cm<sup>-1</sup> (urea) and 4918cm<sup>-1</sup> (urethane and urea) could also be observed. Peak intensities at 5065cm<sup>-1</sup> and 5005cm<sup>-1</sup> of all spectra were calculated to confirm the generations of urethane and urea in more detail.

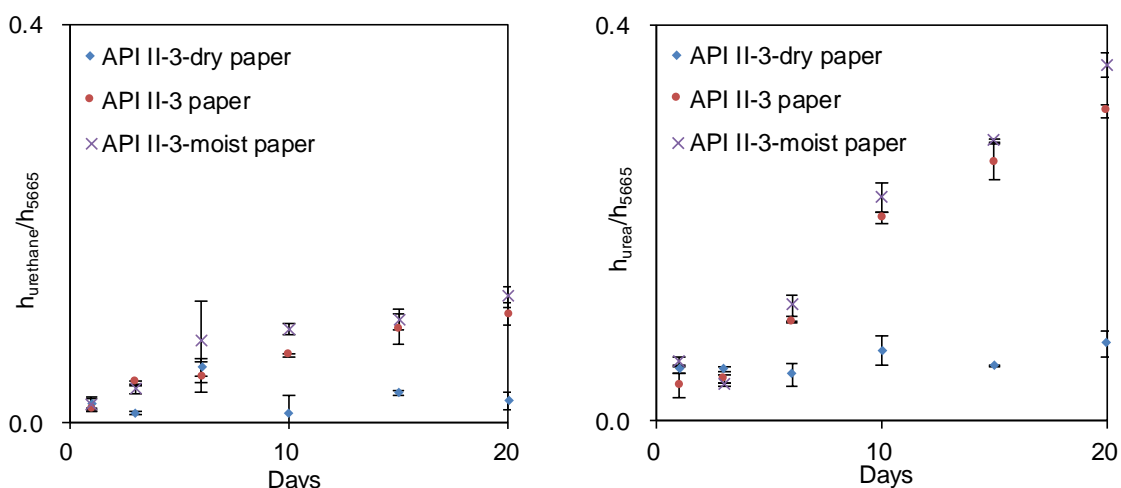


Fig. 4.3.9. Generations of urethane (left) and urea (right) in API papers aged in three humidity conditions, error bars represent  $\pm 1$  standard deviation,  $n=3$ .

Urea was generated from the reaction of NCO with water, so it was affected obviously by humidity (Fig. 4.3.9 right). API II-3-dry paper was still aged in RH 0% desiccator and just taken out every time for FT-NIR test. Thus, almost all urea in API II-3-dry paper was generated before 1 day, during the 24h after API paper was prepared, and the amount barely changed from 1 day to 20days due to the lack of moisture. Normal (RH 50%) and moist (RH 98%) conditions aged API II-3 and API II-3-moist papers had much more urea generation amounts than API II-3-dry paper, and API II-3-moist paper showed the most. The result of urea indicated that high humidity accelerated urea generation during post-curing process. Even though the generating reaction of urethane was not related immediately to  $H_2O$ , urethane result was also affected by humidity (Fig. 4.3.9 left). Urethane in API II-3-dry paper had extremely limited amount, and, on the other hand, API II-3-moist paper generated much more urethane, even than API II-3 paper. This phenomenon could be explained as that the molecular chain in moist condition aged glue-line was more bendable, so both urethane and urea generating reaction carried out smoothly [65].

DMA results of 6 days aged API films were demonstrated in Fig. 4.3.10.  $\tan \delta$  peaks at  $28^\circ C$  were attributed to  $T_g$  of adhesive, and  $205^\circ C$  peak was attributed to

NCO reactions and the slippage of PVA semi-crystal, (2.3.3). The peak at  $-17^{\circ}\text{C}$  on  $\tan \delta$  curve was related to the large amount of uncross-linked pMDI in API II-3-dry film, but this peak was not detected for API II-3 film and API II-3-moist film. It was quite obvious that API II-3-dry film was broken by DMA clamps at  $85^{\circ}\text{C}$  but the other two films were still stiff. The break of API II-3-dry film at  $85^{\circ}\text{C}$  could be credited with less cross-linking structure and brittleness caused by low moisture content. In a word, DMA result implied that dry condition limited NCO reactions remarkably, which verified the results of FT-NIR above.

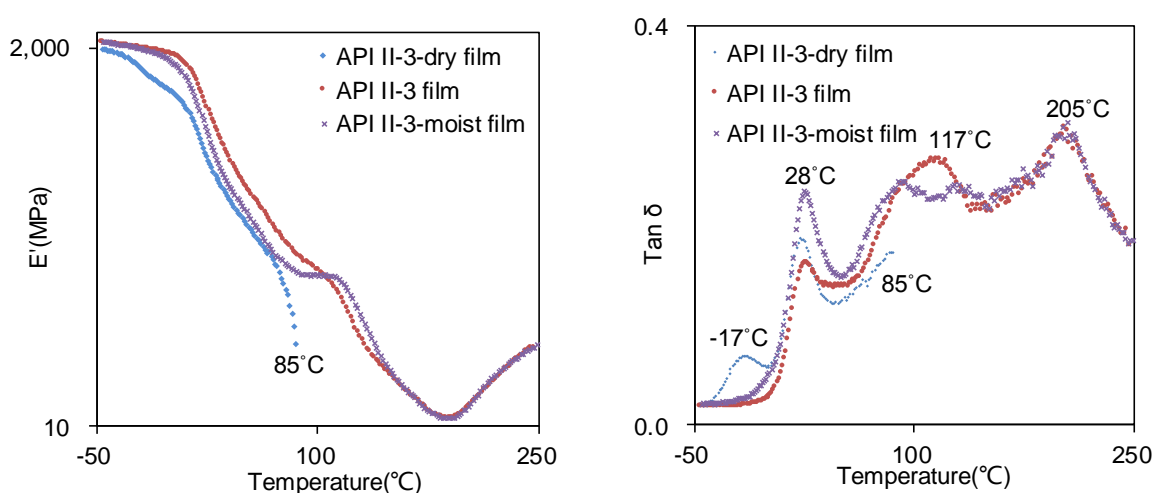


Fig. 4.3.10. DMA thermograms of API films aged in three humidity conditions for 6 days.

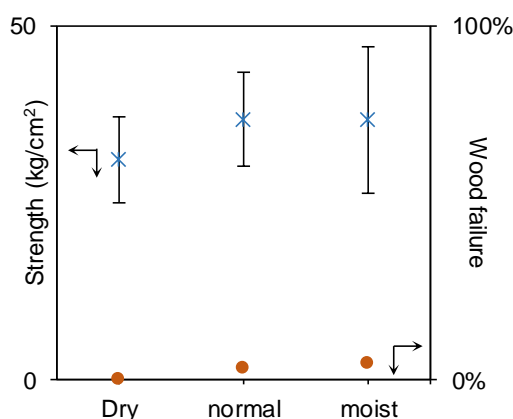


Fig. 4.3.11. Bond strength of cross-laps aged in three humidity conditions for 6 days, error bars represent  $\pm 1$  standard deviation,  $n=7$ .

Bond strength of cross-laps were showed in Fig. 4.3.11. Cross-laps prepared from API II-3 adhesive were 24h pressed in thermostatic chamber (23°C, 0RH%), and then aged in dry (23°C, 0RH%), normal (23°C, 50RH%) and moist (23°C, 98RH%) conditions. It was very clear that the bond strength and wood failure of dry cross-laps were lower than those of normal and moist cross-laps. FT-NIR result already proved that urethane and urea generations in API II-3-dry paper were very much restricted. DMA result indicated that API II-3-dry film contained more un-cross-linked pMDI than other two films and it was more brittle at high temperature. The result of bond strength was in accordance with the former two results. All cross-laps were prepared in the same process so there was no difference in adhesive penetration. Thus, low damage rate of dry cross-laps was attributed to the weak interaction between wood and adhesive.

#### **4.3.4 Heat Treatment**

Heat treatment was applied to accelerate NCO cross-linking reactions, and the improvement of bond strength was also respected. Prepared API paper, API film and cross-laps were first aged in thermostatic chamber (23°C, RH50%) for 4 days. Then, samples were heat treated at 80°C for 2h, 4h and 6h. After that, sample were taken back into thermostatic chamber and aged continuously. The used temperature, 80°C, was lower than water boiling point that permitted moisture to leave in glue-line and react. Wood thermal degradation normally occurs at over 100°C, so no degradation was arose by heat treatment.

Urethane and urea generations in API paper, before and after heat treatment, were showed in Fig. 4.3.12. Heat treatment promoted NCO reactions significantly. However, urea and urethane generation rates decreased after treatment, and the longer treatment was, the more rate decreased. On 35 days, urethane and urea amounts of four API papers became almost the same. Namely, heat treatment accelerated NCO reactions temporarily, but this effect could be offsetted by time.

During post-curing, the more NCOs reacted, the more imprisoned molecule was, and then the slower NCO reactions became. Heat treatment speeded up NCO reaction and, at the same time, reduced molecular mobility. Thus, the longest treatment time resulted in the lowest possibility for NCO to further react.

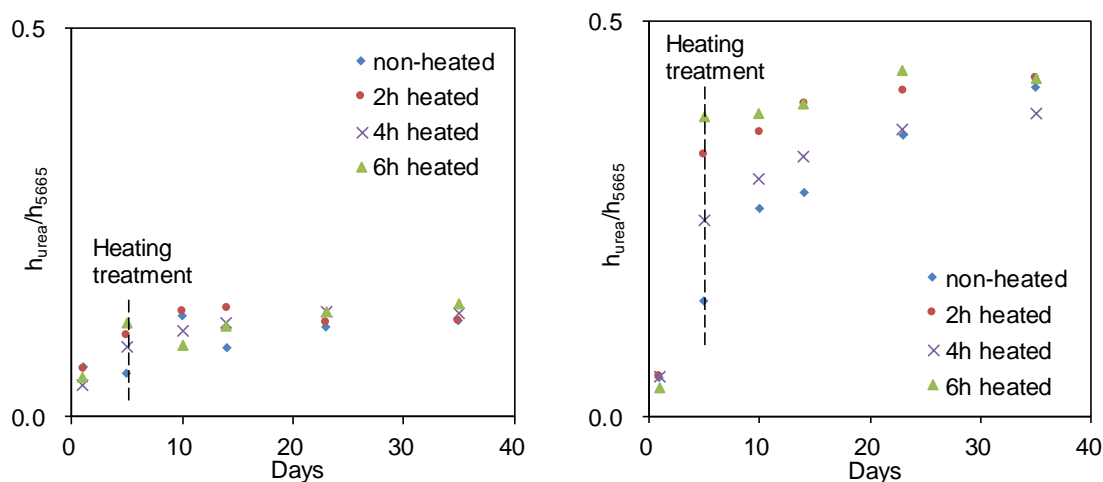


Fig. 4.3.12. Generations of urethane (left) and urea (right) in API papers, before and after heating treatment, error bars represent  $\pm 1$  standard deviation,  $n=3$ .

API films heated for different time were DMA tested. All storage modulus curves (Fig. 4.3.13 left) showed increasing from 180 to 210°C, due to acute reactions of residual NCO at high temperature. Cross-linking restricted molecular movement in glue-line and limited the accelerating effect of heat treatment. Therefore, a lot of NCO groups still remained in API film. 24°C and 185°C peak occurred on loss factor curve (Fig. 4.3.13 right), due to  $T_g$  and NCO reactions. Differing from heat treated API films, API film without heat treatment had another peak at 124°C that was from  $T_g$  of small scale molecule formed during post-curing. After heat treatment, chemical groups (NCO and hydroxyl) on small scale molecule further reacted and formed cross-linking. Thus,  $T_g$  at 124°C disappeared.

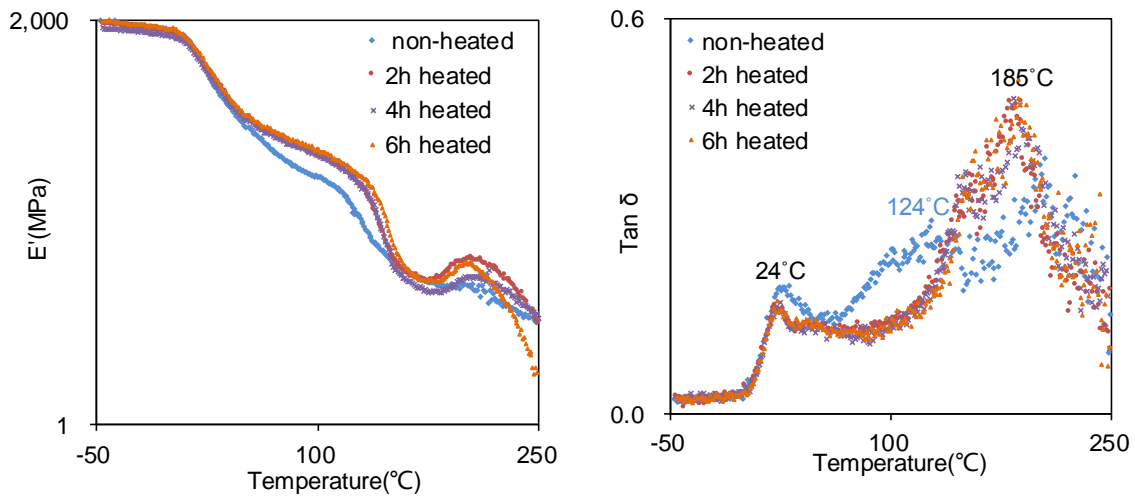


Fig. 4.3.13. DMA thermograms of API films 80°C heated for different hours and aged for 6 days.

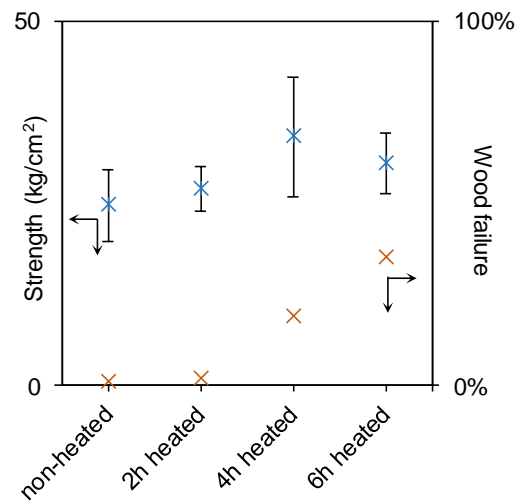


Fig. 4.3.14. Bond strength of cross-laps 80°C heated for different hours and aged for 6 days, error bars represent  $\pm 1$  standard deviation,  $n=7$ .

Bond strength of cross-laps were tested (Fig. 4.3.14). Those cross laps were aged in thermostatic chamber for 4 days first before heating treatment. After heating treatment cross-laps were aged in thermostatic chamber for 2 days. During heating, moisture content in wood was reduced, contributing to a strength decreasing of wood interior. The purpose of continuous aging in thermostatic chamber was to reinstate moisture content of wood. From non-heated to 4h heated cross-laps, both bond strength and damage rate increased. Heating treatment accelerated NCO reactions and generated more cross-linking structure in glue-line. However, 6h treated cross-laps showed lower bond strength but higher wood failure than 4h

treated cross-laps. 6h treated cross-laps lost more moisture content and this loss could not be compensated by 2 days aging, which led to a brittle bonding structure.

#### 4.4 Conclusions

NIR absorption bands of urethane and urea in API adhesive glue-line were assigned in chapter 3. In this chapter, in order to investigate the practicability of FT-NIR test on glue-line, FT-NIR was used to study the influences of adhesive components and aging conditions on urethane and urea generating reactions. In addition, DMA and bonding test were used as supplementary explanations for FT-NIR result.

Three PVAs were employed separately to prepare API adhesives. At first, PVA with low DS (degree of saponification) was expected to mix and react better with pMDI. However, there was almost no disparity on glue-line chemical structures of three adhesives. DMA result indicated that adhesive prepared from high DS PVA might generate uneven phase in glue-line. High bond strength was obtained on the adhesive with high molecular weight PVA.

SBR latex mass ratio in adhesive was also adjusted. Since the application amounts of adhesive for all tests was the same, the higher SBR latex mass ratio it was, the lower PVA and pMDI mass ratios they would be. FT-NIR result demonstrated that the adhesive with less SBR latex produced more urethane and urea, due to high pMDI and PVA contents. DMA showed that after 1 day aging, the API film with low SBR latex content had more unreacted pMDI. Cross-laps with higher SBR latex content showed higher bond strength after 1 day aging. After 6 days, cross-laps with more pMDI had been fully post-cured and thus displayed high bond strength. On the other hand, cross-laps with high SRB latex content had a lower bond strength after fully aging.

Aging humidity was found out to have significant influence on both chemical structure and physical property of glue-line. API paper aged in dry condition had

much less urethane and urea generating amounts than those aged in other conditions. Dry condition aged API film was broken at 85°C during DMA test, due to less cross-linking structure and brittleness. Similar to the former two results, dry condition aged cross-laps had worse bonding performance.

Heat treatment was applied to speed up urethane and urea generations. After heating, two linkages generating amounts were increased but just temporary. The effect of heat treatment became more and more unobvious after long time aging, because the mobility of molecule in glue-line dominated NCO reactions. DMA result showed that heat treatment speeded up the formation of cross-structure. Cross-lap test proved that heat treatment increased bond strength. However, too long time heating generated strength decreasing, due to embrittlement of wood interior.

## 5 Further Studies on NCO self-reactions and Urethane Generating Reactions

### 5.1 Introduction

At room temperature, the main reactions of NCO in API adhesive generated urethane and urea linkages, which were discussed in previous chapters. At room temperature, aromatic isocyanate can slowly dimerize and generate uretdione due to its high reactivity. Trimerizations of most of isocyanate compounds can occur in the presence of catalyst (Scheme 1.2)<sup>[66]</sup>. Therefore, there was a possibility that uretdione and isocyanurate could form, even though in a small amount, in API adhesive. In industry, uretdione is used as blocked isocyanate, because it can decompose to isocyanate monomer and then react with other components<sup>[67]</sup>. Similarly, uretdione in API adhesive might decompose, react during post-curing process and further affect urethane and urea generating reactions. Watanabe et al. synthesized uretdione and isocyanurate, and found that out that these two compounds had different reactivities with amines<sup>[68]</sup>. In this chapter, in order to study uretdione and isocyanurate in API adhesive, phenyl isocyanate was used to synthesize dimer and trimer model compounds first. Then, the specific and FT-IR bands of uretdione and isocyanurate were assigned. At last, uretdiones and isocyanurates in pMDI and API adhesive were confirmed.

One advantage of API adhesive is that NCO may react with hydroxyls of wood component, forming urethane linkage between glue-line and wood. In the meanwhile, the reaction of between NCO and PVA hydroxyl inside API glue-line generates another type of urethane linkage. Namely, there are two types of urethanes formed in API adhesive-bonding-wood structure. The urethane linkage between glue-line and wood surface contributes to adhesion bond strength, and the urethane linkage inside glue-line contributes to cohesion bond strength (Fig. 1.1). In chapter 2, the urethane generated from NCO-PVA reaction was confirmed

by using FT-IR spectra of API thin film (Fig. 2.3.7). In chapter 3 and 4, urethane generation in API paper was detected by using FT-NIR spectroscopy. Actually, the urethane band on FT-NIR spectrum involved the information of both PVA urethane and cellulose urethane, but it had not been carried out to analyze these two types of urethanes, respectively. Wood consists of several components, cellulose, hemi-cellulose, lignin, etc., and the most one is cellulose ( $\approx 40\text{wt}\%$ ), so the reaction of NCO with cellulose hydroxyl, were also studied in this chapter.

## **5.2 Experimental**

### **5.2.1 Materials**

Phenyl isocyanate (Wako Pure Chemical industries, Ltd., Japan), pMDI (Nippon Polyurethane, Japan), hydrated pyridine (Wako Pure Chemical industries, Ltd., Japan) and hydrated DMF (N, N-dimethylformamide) (Wako Pure Chemical industries, Ltd., Japan) were used for synthesizing uretdione and isocyanurate. 2-butanol (Wako Pure Chemical industries, Ltd., Japan) was used to block NCO of pMDI. Phenyl isocyanate (Wako Pure Chemical industries, Ltd., Japan), PVA (degrees of saponification 99.1%,  $M_w$   $6.8 \times 10^4 \text{g/mol}$ , Wako Pure Chemical industries, Ltd., Japan), fibrous cellulose powder (CF-1, Whatman), hydrated DMSO (dimethyl sulphoxide) (Wako Pure Chemical industries, Ltd., Japan) and acetone (Wako Pure Chemical industries, Ltd., Japan) were used for synthesizing PVA-carbamate and cellulose-carbamate. Dehydrated DMAC (N, N-dimethylacetamide, Wako Pure Chemical industries, Ltd., Japan) was also used.

### **5.2.2 Synthesis**

ph-uretdione: 1g phenyl isocyanate was dissolved into 10ml hydrated pyridine and settled for 4 days at room temperature. Then, the white ph-uretdione crystal precipitation was vacuum dried.

ph-isocyanurate: 1g phenyl isocyanate and 1ml hydrated DMF were dissolved into 10ml pyridine and settled at 100°C for 15h. Then, the organic solvent was evaporated to obtain ph-isocyanurate.

pMDI-uretdione: 1g pMDI was dissolved into 10 ml hydrated pyridine and settled at room temperature for 4days. After that the solvent was evaporated to obtain pMDI-uretdione.

pMDI-isocyanurate: 1g pMDI and 1ml hydrated DMF were dissolved into 10 ml hydrated pyridine and settled at 100°C for 15h. pMDI-isocyanurate was collected by evaporating solvent.

PVA-carbamate: 300mg PVA were dissolved into 20ml hydrated DMSO at 80°C. Then, 1500mg phenyl isocyanate was added. The reaction was carried out at 80°C for 15h. Ph-carbamate was precipitated out by using water and washed by using methanol.

Cellulose-carbamate: 1500mg phenyl isocyanate was dissolved into 20ml hydrated DMSO. Then, 300mg cellulose powder was added in and stirred at 80°C for 2 days. Cellulose-carbamate was precipitated out by using water and washed by using methanol.

PVA-pMDI: 300mg PVA was put into 15ml dehydrated DMAC and dissolved at 90°C. 1g pMDI was dissolved into 5ml dehydrated DMAC. Then, pMDI/DMAC solution was added into PVA/DMAC solution at 90°C. 5min later, PVA-pMDI gel was obtained. The gel was vacuumed dried and ground into powder. Finally, PVA-pMDI was washed by using acetone.

Cellulose-pMDI: 900mg cellulose powder and 2g pMDI was put into 20ml hydrated DMSO and reacted for two weeks. Then, cellulose-pMDI was filtered out and washed by using acetone.

pMDI-PVA-cellulose film: 3g 15wt% PVA aqueous solution, 1.5g pMDI and 450mg cellulose were mixed for 5min and degassed for 30s. Then, this mixture

was cast onto Teflon sheet to make pMDI-PVA-cellulose film (thickness  $\approx 0.02\text{mm}$ ). The obtained film was aged in thermostatic chamber.

pMDI-PVA film: 3g 15wt% PVA aqueous solution and 1.5g pMDI were stirred for 5min and degassed for 30s. A thin film (thickness  $\approx 0.02\text{mm}$ ) was obtained by casting the mixture on Teflon sheet. pMDI-PVA film was aged in thermostatic chamber.

pMDI-cellulose mixture: 100mg pMDI and 100mg cellulose powder were mixed and aged in thermostatic chamber.

### **5.2.3 Characterizations**

$^1\text{H-NMR}$ : Nuclear magnetic resonance spectrum was obtained by using JEOL JNM-A 500 FT-NMR (500MHz). Solvent was  $\text{D}_6\text{-DMSO}$ , and tetramethylsilane (TMS) was used as internal standard. Solution concentration was approximately 10mg/ml.

TGA and FT-IR were the same instruments as 2.2.2 and 2.2.3 described.

## **5.3 Results and Discussion**

### **5.3.1 Uretdione and Isocyanurate**

The FT-IR spectra of phenyl isocyanate and synthesized ph-uretdione and ph-isocyanurate were demonstrated in Fig. 5.3.1. For FT-IR test, ph-uretdione disk and ph-isocyanurate disk were prepared by mixing 2mg sample with 200mg KBr powder and pressing for 5min. Phenyl isocyanate liquid was casted onto  $\text{CaF}_2$  board and then FT-IR spectrum was collected, so the region was just  $1000\text{-}4000\text{cm}^{-1}$ . Specific absorption bands of phenyl isocyanate, ph-uretdione and ph-isocyanurate appeared at  $2270\text{cm}^{-1}$  ( $\text{N}=\text{C}=\text{O}$  asymmetric stretching),  $1775\text{cm}^{-1}$

(C=O stretching) and  $1720\text{cm}^{-1}$  (C=O stretching). In addition, two slight bands of uretdione and isocyanurate were also detected at  $1775\text{cm}^{-1}$  and  $1720\text{cm}^{-1}$  on phenyl isocyanate spectrum, suggesting that phenyl isocyanate was easy to dimerize and trimerize at room temperature. The solubility of phenyl isocyanate, ph-uretdione, ph-isocyanurate and DPU (diphenyl urea, Table 3.3.1) in organic solvents were checked and summarized in Table 5.3.1.

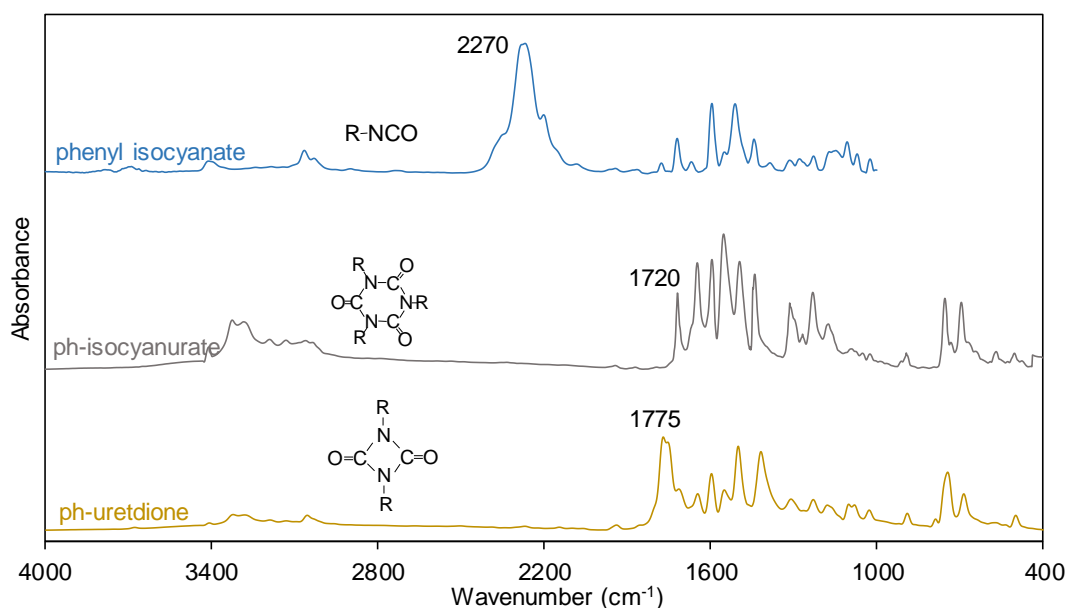


Fig. 5.3.1. FT-IR spectra of phenyl isocyanate, ph-uretdione and ph-isocyanurate, R: phenyl.

pMDI, cross-linker for API adhesive, was also utilized to synthesize uretdione and isocyanurate (Fig. 5.3.2). Uretdione band (C=O stretching) of pMDI-uretdione was also showed up at  $1775\text{cm}^{-1}$ , the same position as ph-uretdione. However, isocyanurate band (C=O stretching) of pMDI-isocyanurate appeared at  $1705\text{cm}^{-1}$ , which was  $15\text{cm}^{-1}$  lower than ph-isocyanurate. This difference in wavenumber was attributed to the disparity of molecular structures. pMDI had more than two NCO groups on molecular chain, so cross-linking structure was easily formed during synthesizing process. Generated cross-linking linkage restricted the movement of molecular chains and NCO reactions. Thus, a significant amount of NCO remained in pMDI-uretdione and pMDI-isocyanurate, and urea linkage was generated during sample preparation. Synthesized pMDI-

uretdione and pMDI-isocyanurate were insoluble in any organic solvent, because of the existence of cross-linking. Besides, pMDI also showed two bands at  $1778\text{cm}^{-1}$  and  $1721\text{cm}^{-1}$ .  $1778\text{cm}^{-1}$  was attributed to uretdione [45] generated in manufacture and storage processes of pMDI.  $1721\text{cm}^{-1}$  was considered as from isocyanurate.

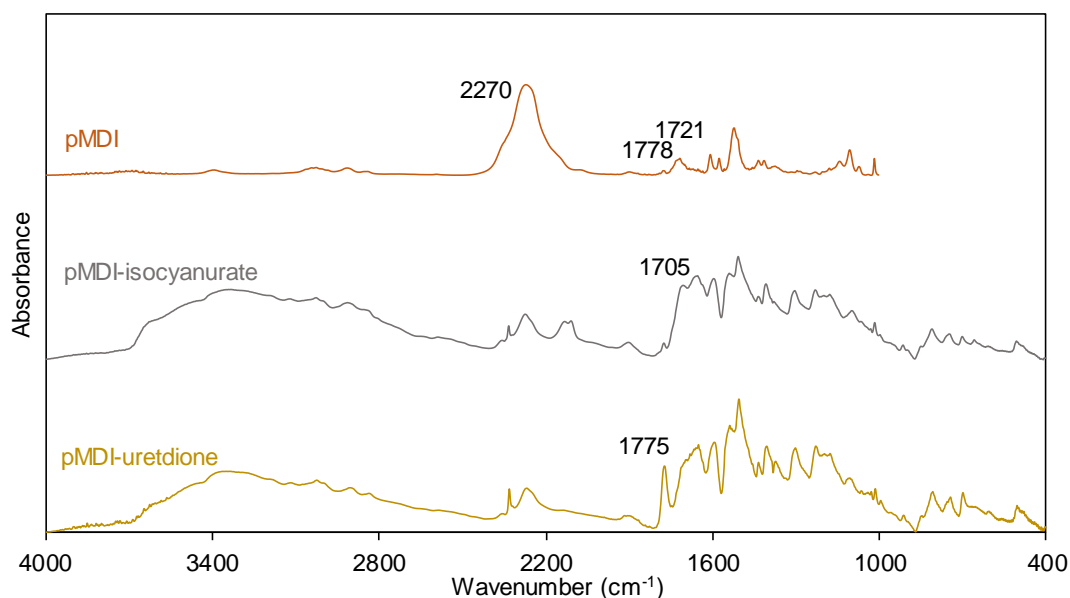


Fig. 5.3.2. FT-IR spectra of pMDI, pMDI-uretdione and pMDI-isocyanurate.

### 5.3.2 Difference on Band Location Between Urethane and Isocyanurate

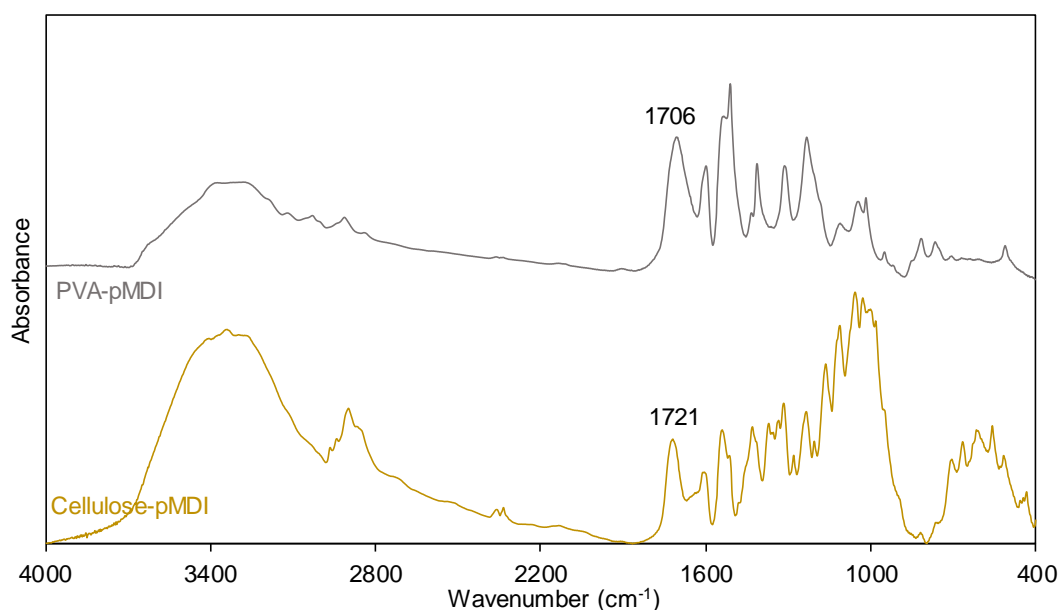


Fig. 5.3.3. FT-IR spectra of PVA-pMDI and cellulose-pMDI.

FT-IR absorption bands of urethane and isocyanurate are very close to each other (all at 1710-1730 $\text{cm}^{-1}$ ), so it is difficult to separate them on FT-IR spectrum. API adhesive cross-linker, pMDI, was also used to react with PVA and cellulose in organic solvent. FT-IR test was performed on KBr disk with 2mg sample and 200mg KBr. FT-IR spectra of synthesized PVA-pMDI and cellulose-pMDI were displayed in Fig. 5.3.3. Urethane N-H stretching bands showed up at 3377 $\text{cm}^{-1}$  and 3344 $\text{cm}^{-1}$ , and 1705 $\text{cm}^{-1}$  and 1721 $\text{cm}^{-1}$  band consisted of urethane C=O stretching absorption. To enhance resolution, 2<sup>nd</sup> derivative calculation was employed. 2<sup>nd</sup> derivative spectrum of pMDI (Fig. 5.3.4) was calculated from the spectrum in Fig. 5.3.2. Downward peaks of uretdione and isocyanurate occurred at 1779 $\text{cm}^{-1}$  and 1721 $\text{cm}^{-1}$ . 1666 $\text{cm}^{-1}$  was attributed to non-hydrogen-bonded urea, and 1639 $\text{cm}^{-1}$  was attributed to hydrogen bonded urea. In Fig. 5.3.5, 1784 $\text{cm}^{-1}$  and 1781 $\text{cm}^{-1}$  peaks were assigned to uretdione. Peaks at 1661 $\text{cm}^{-1}$ , 1658 $\text{cm}^{-1}$  and 1641 $\text{cm}^{-1}$  were assigned to urea, since NCO was easy to react with water. In organic solvent, NCO reacted with PVA and cellulose hydroxyls, forming urethane linkages. Thus, 1712 $\text{cm}^{-1}$  and 1706 $\text{cm}^{-1}$  peaks were due to hydrogen bonded urethane, and 1731 $\text{cm}^{-1}$  and 1732 $\text{cm}^{-1}$  peaks were due to non-hydrogen-bonded urethane. Of course, 1721 $\text{cm}^{-1}$  peak may also exist on the 2<sup>nd</sup> derivative spectra in Fig. 5.3.5, but it was covered by urethane absorption. So, the absorption wavenumbers of urethane and isocyanurate were in the order of non-hydrogen-bonded urethane ( $\approx 1730\text{cm}^{-1}$ ) > isocyanurate ( $\approx 1720\text{cm}^{-1}$ ) > hydrogen bonded urethane( $\approx 1710\text{cm}^{-1}$ ).

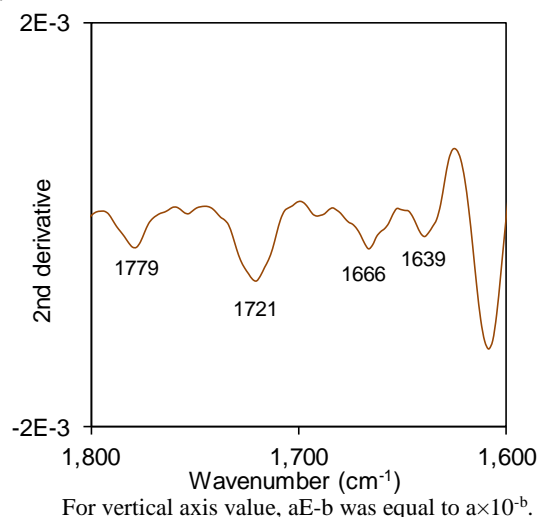


Fig. 5.3.4. 2<sup>nd</sup> derivative spectrum of pMDI.

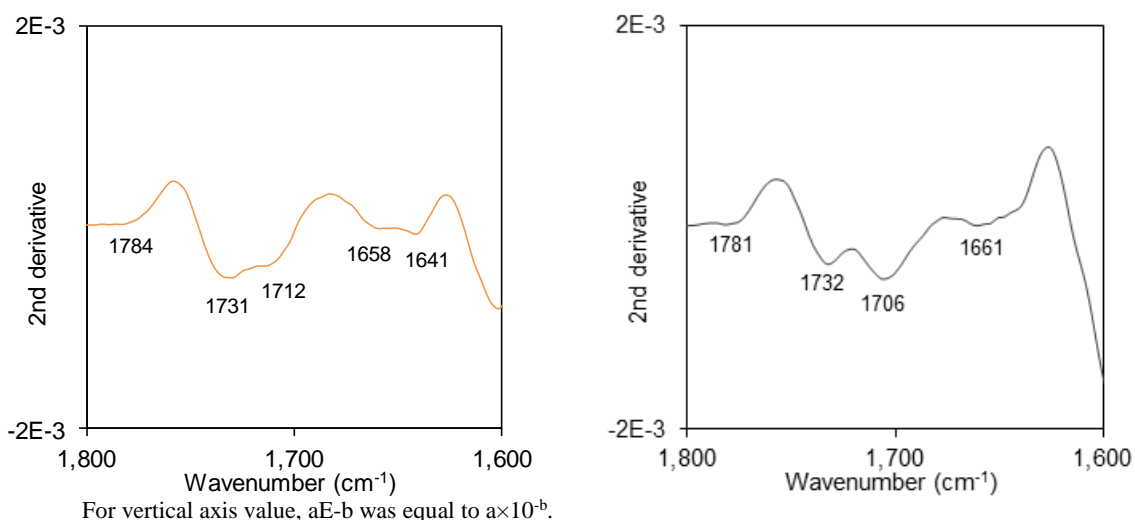


Fig. 5.3.5. 2<sup>nd</sup> derivative spectra of cellulose-pMDI (left) and PVA-pMDI (right).

### 5.3.3 Uretdione and Isocyanurate in API thin Film

During aging in thermostatic chamber, post-curing reactions of NCO occurred. The generations of urethane and urea had been particularly discussed in previous chapter. Here, the self-reactions of NCO in API adhesive were studied. In Fig. 2.3.7, generated uretdione in API thin film was detected at  $1779\text{cm}^{-1}$ , and the strong band detected at  $1715\text{cm}^{-1}$  was attributed to overlapping urethane (C=O stretching) and isocyanurate absorption. The API thin film used for Fig. 2.3.7 was further aged until 20 days, and 2D correlation spectra were calculated in Fig 5.3.6. Auto-peak at 2274 represented NCO consumption during post-curing. A broad auto-peaks at from 1600 to 1740, corresponding to overlapping urethane, isocyanurate and urea peaks. On synchronous spectrum, a mall negative cross-peak appeared at 2274-1776, suggesting that uretdione band had an opposite variation direction to NCO band. Namely, uretdione was gradually generated, but the amount was very limited. Cross-peaks of NCO-urethane, NCO-isocyanurate and NCO-urea overlapped into a broad negative cross-peaks, so it was difficult to distinguish isocyanurate band individually. On asynchronous spectrum, peak overlapping also occurred significantly.

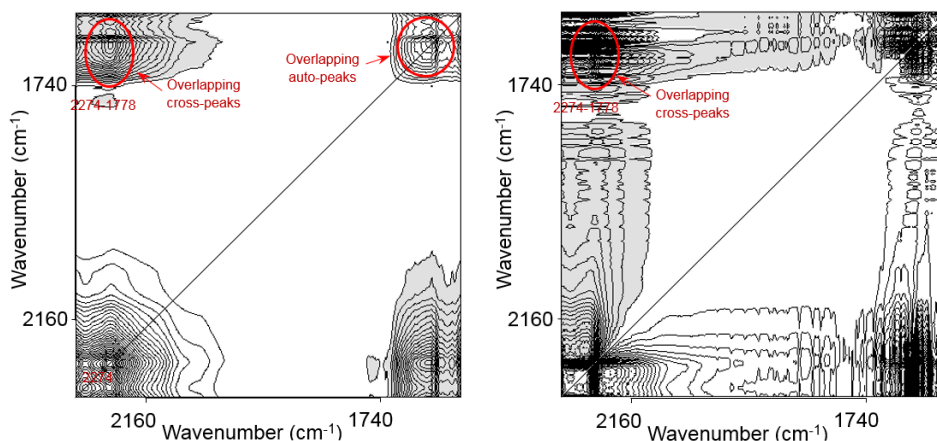


Fig. 5.3.6. Synchronous (left) and asynchronous (right) 2D correlation spectrum of API thin film, generated from 1 day-20 days FT-IR spectra.

### 5.3.4 Thermal degradation of urethane

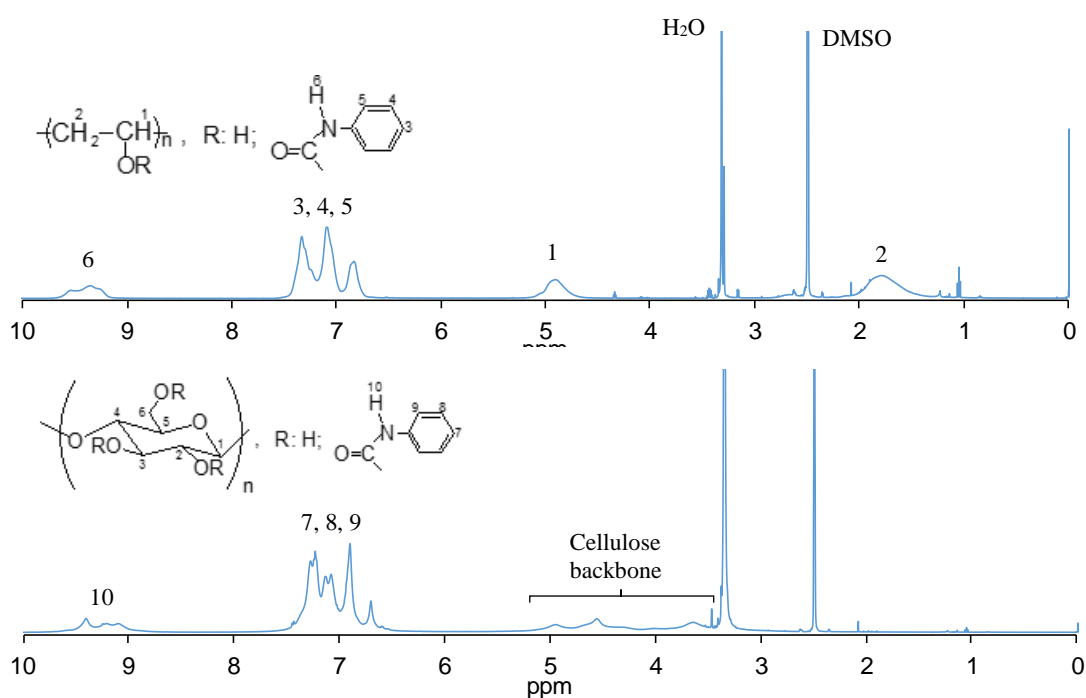


Fig. 5.3.7.  $^1\text{H-NMR}$  spectra of PVA-carbamate (upper) and cellulose-carbamate (lower).

Phenyl isocyanate reacted with polyvinyl alcohol and cellulose in organic solvent, forming PVA-carbamate and cellulose-carbamate. During synthesis process, little amount of DPU, uretdione and isocyanurate were also generated, but these by-products were removed by using methanol<sup>[69]</sup>. To confirm the degree of substitution of hydroxyl on PVA and cellulose chain,  $^1\text{H-NMR}$  test was carried

out (Fig. 5.3.7). Degree of substitution was calculated, based on the integral area ratio of aromatic resonance to cellulose backbone resonance. Result indicated that PVA hydroxyls were 100% substituted and cellulose hydroxyls were 97% substituted.

FT-IR spectra of PVA-carbamate and cellulose-carbamate were also collected (Fig. 5.3.8). 27mg cellulose-carbamate (or PVA-carbamate) was dissolved into 1ml acetone. After that, one drop of the acetone solution was cast onto CaF<sub>2</sub> disk ( $\delta$  1mm,  $\Phi$  25mm, Pier Optics, Japan) and acetone was evaporated. Urethane bond (C=O stretching) of PVA-carbamate appeared at 1720cm<sup>-1</sup> and that of cellulose-carbamate appeared at 1715cm<sup>-1</sup>. Other bands, such as N-H stretching, Amide II and Amide II, were almost detected at the same wavenumbers for these two carbamates.

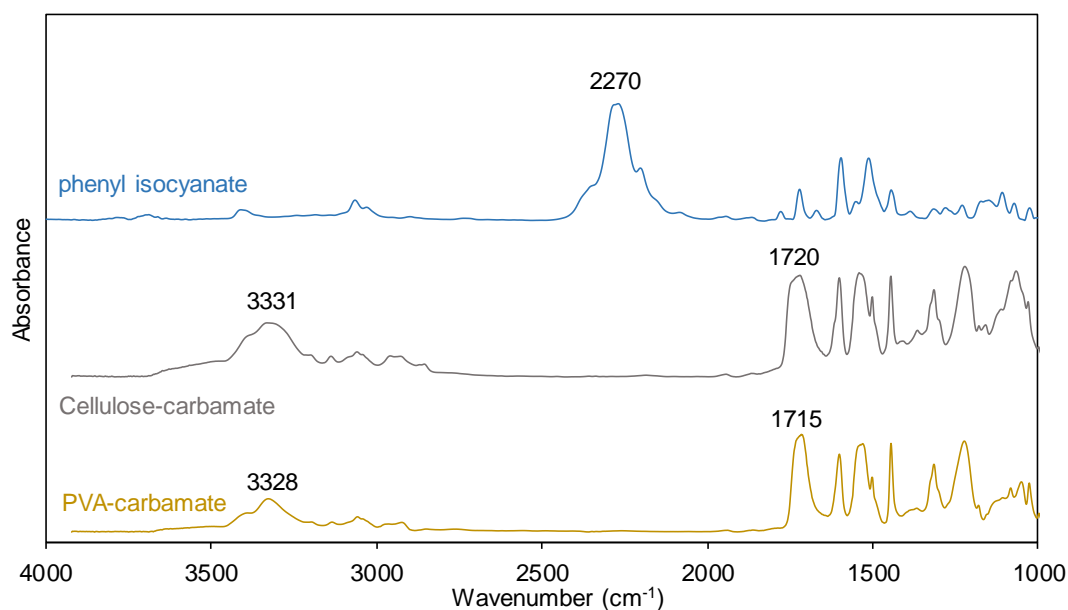


Fig. 5.3.8. FT-IR spectra of phenyl isocyanate and carbamates.

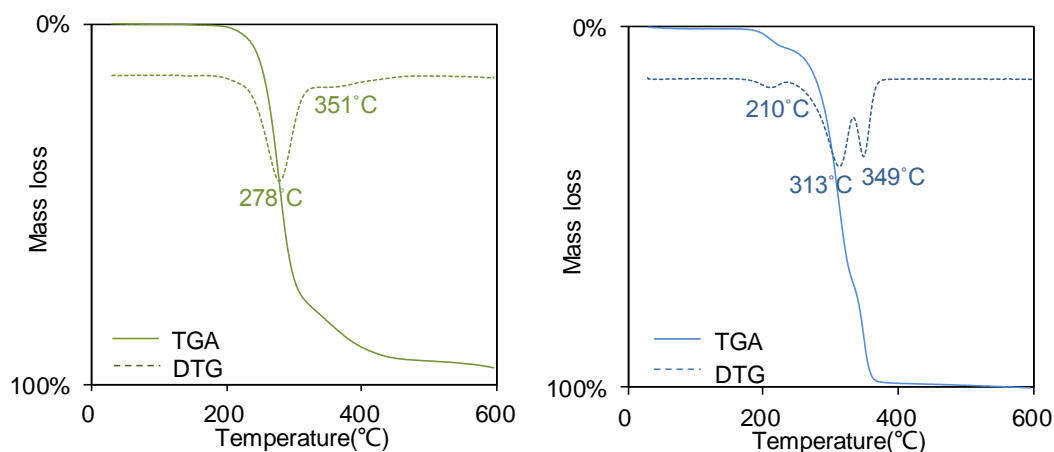


Fig. 5.3.9. Thermal degradation curves of PVA-carbamate (left) and cellulose-carbamate (right).

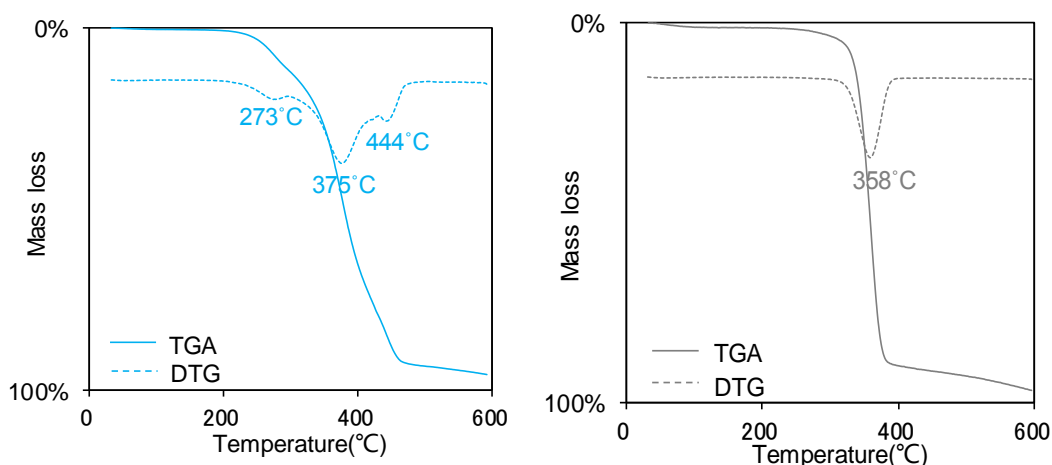
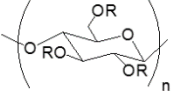
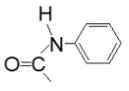


Fig. 5.3.10. Thermal degradation curves of PVA (left) and cellulose (right).

TGA and DTG curves of carbamates were showed in Fig. 5.3.9. Thermal degradation of PVA-carbamate separated into two steps, at 278°C and 351°C, and that of cellulose-carbamate had three steps, at 210°C, 313°C and 349°C. For comparison, thermal degradation curves of PVA and cellulose were demonstrated in Fig. 5.3.10. Beginning, end and mass loss of each DTG peak were summarized in Fig. 5.3.11. Thermal degradation of urethane was reported to have three routes (Scheme 2.3.1) <sup>[38]</sup>. Products of carbamate degradation were studied by using TGA and temperature dependent FT-IR spectroscopy.

Table. 5.3.1. Mass ratios of substituent in carbamates.

	PVA-carbamate	Cellulose-carbamate
Structure unit	$(\text{CH}_2-\text{CH})_n$ OR 163g/mol	 519g/mol
Substituent (R)	 120g/mol	
Mass ratio of substituent	73.62%	69.63%

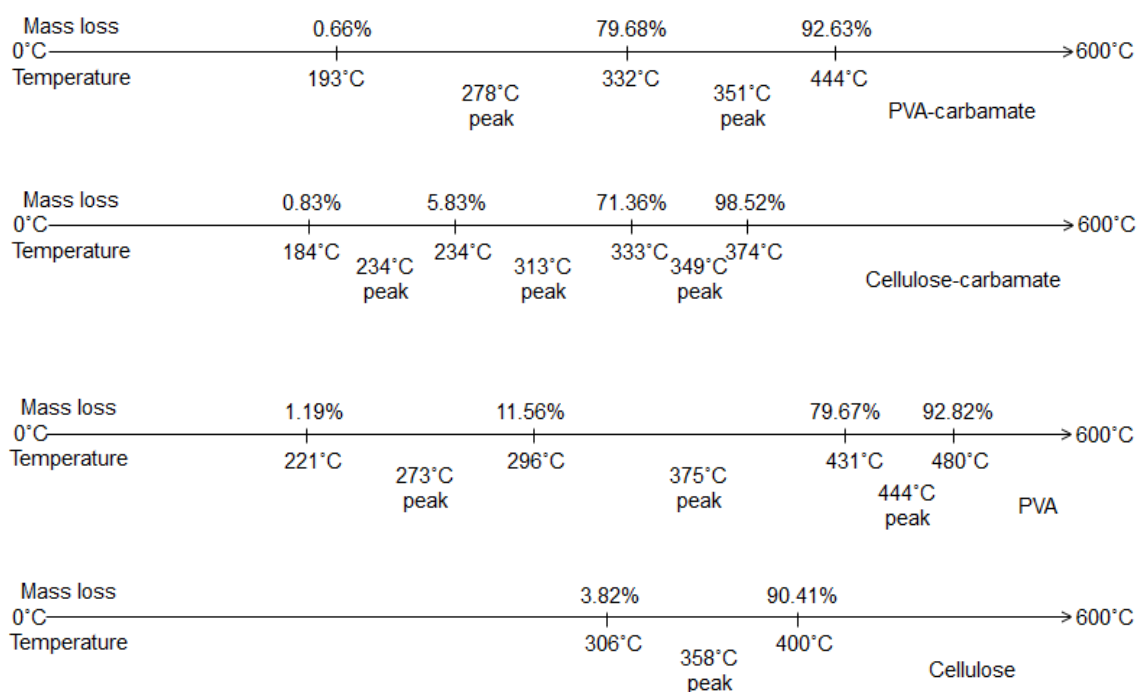


Fig. 5.3.11. Beginning, end and mass loss of each DTG peak.

Mass ratios of substituent on carbamate molecular chains, 73.62% and 69.63%, were listed in Table 5.3.1. PVA-carbamate had 79.68% mass loss at the end of first step, and cellulose-carbamate showed 71.36% mass loss at the end of second step. Thus, it was considered that the thermal degradations of two carbamates mainly advanced in the first and second route of Scheme 2.3.1. FT-IR spectra at 290°C were shown in Fig. 5.3.12. Even though there were still some urethane linkages left, the bands at 3475 $\text{cm}^{-1}$  and 3503 $\text{cm}^{-1}$  (containing O-H stretching absorption) implied that urethane degradations formed hydroxyls and phenyl

isocyanate (evaporated). The weak bands at  $1650\text{cm}^{-1}$  suggested that a little bit of alkene was generated due to hydroxyl degradation.

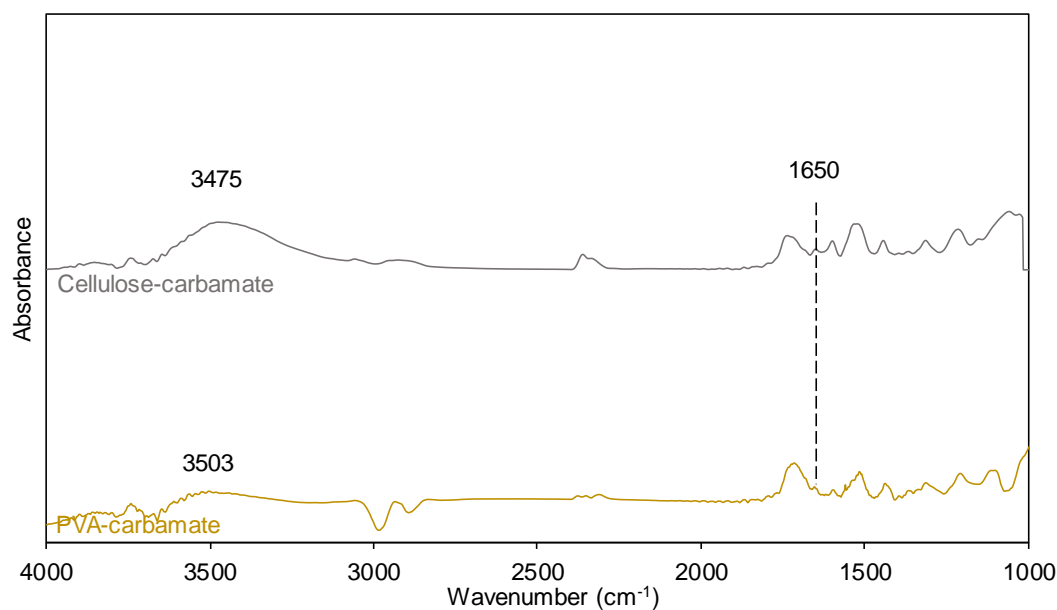


Fig. 5.3.12. FT-IR spectra of carbamates at  $290^\circ\text{C}$ .

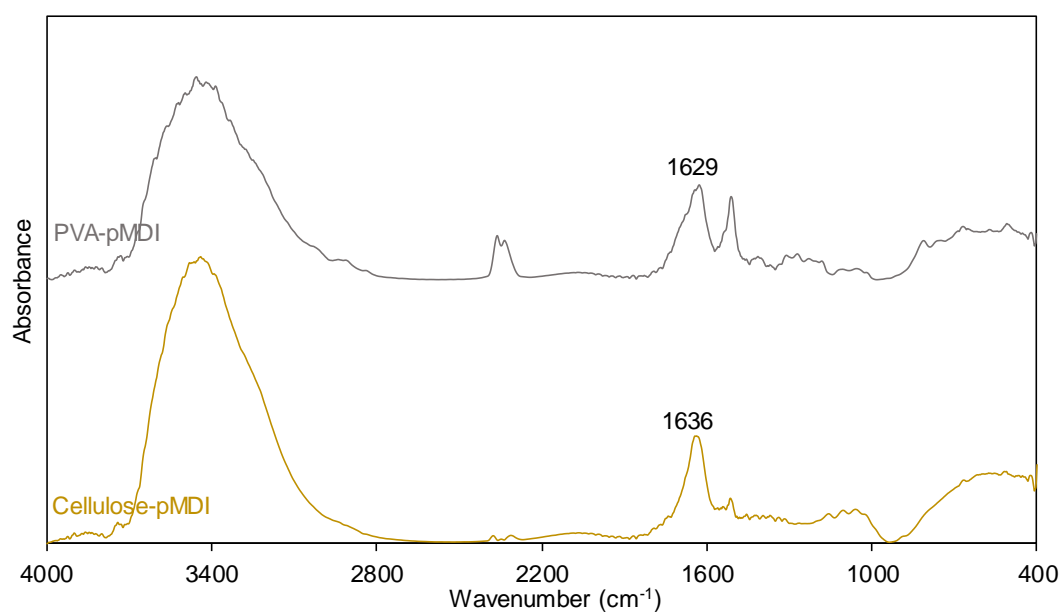
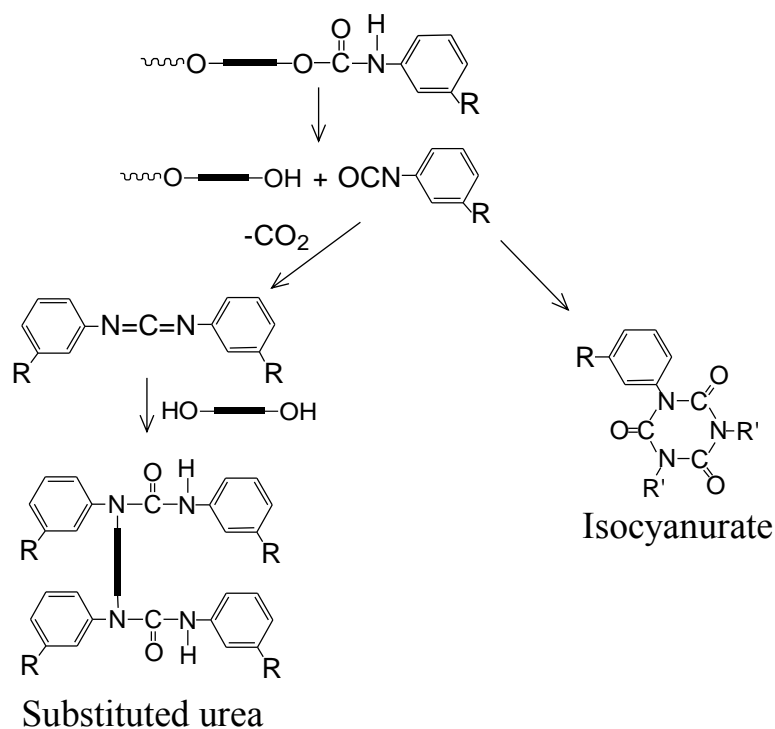


Fig. 5.3.13. FT-IR spectra of PVA-pMDI and cellulose-pMDI at  $290^\circ\text{C}$ .

KBr disks of PVA-pMDI and cellulose-pMDI were heated to  $290^\circ\text{C}$  (Fig. 5.3.13). Most of urethane linkages degraded at  $290^\circ\text{C}$ . It had been verified that urethane degradation mainly formed NCO and hydroxyl. Formed phenyl isocyanate soon evaporated, but formed pMDI here could not volatilize so further decomposed.

Two NCOs generated carbodiimide first at high temperature and then carbodiimide reacted with hydroxyl forming substituted urea (Scheme 5.3.1). Therefore,  $1629\text{cm}^{-1}$  and  $1636\text{cm}^{-1}$  bands were attributed to urea and substituted urea [38, 70].



Scheme 5.3.1. Thermal decomposition of urethane.

### 5.3.5 Urethane formation in ambient condition

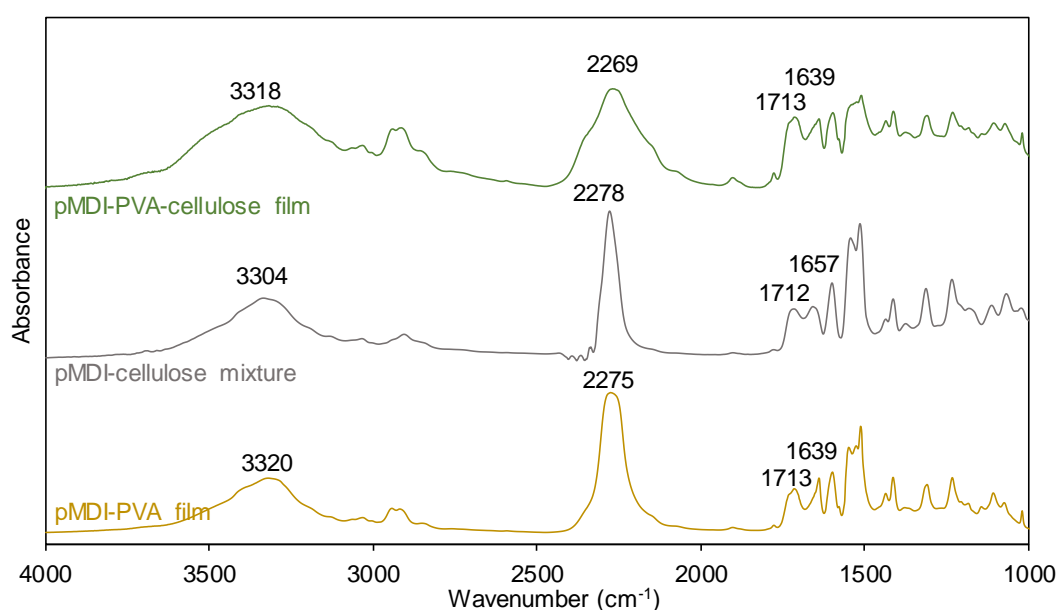


Fig. 5.3.14. FT-IR spectra of pMDI products.

pMDI-PVA-cellulose film, pMDI-cellulose mixture and pMDI-PVA film were prepared and aged in ambient condition. Thus, NCO reactions in those three samples were quite similar with the reactions in API adhesive glue-line. FT-IR test was performed on pMDI-PVA-cellulose film, pMDI-PVA film and pMDI-cellulose mixture disk (made of 2mg sample and 200mg KBr powder). FT-IR spectra at room temperature were summarized in Fig. 5.3.14. O-H stretching and N-H stretching overlapped at  $3318\text{cm}^{-1}$ ,  $3304\text{cm}^{-1}$  and  $3320\text{cm}^{-1}$ .  $2269\text{cm}^{-1}$ ,  $2278\text{cm}^{-1}$  and  $2275\text{cm}^{-1}$  bands were attributed to N=C=O asymmetric stretching of residual NCO, and  $1639\text{cm}^{-1}$  and  $1657\text{cm}^{-1}$  bands were attributed to urea. As it had been discussed above,  $1713\text{cm}^{-1}$  and  $1712\text{cm}^{-1}$  bands consisted of the absorptions of urethane, isocyanurate and/or additives.

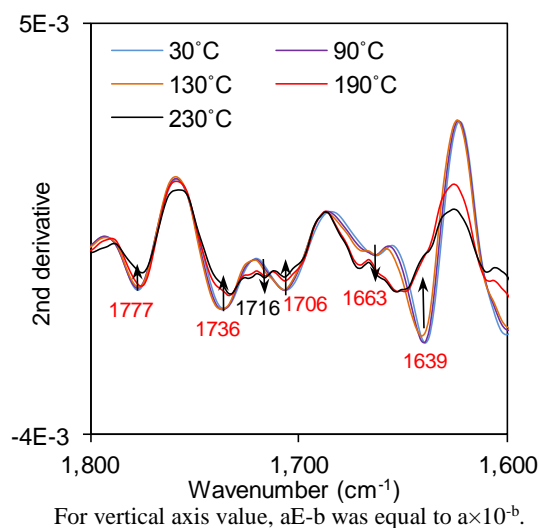


Fig. 5.3.15. Temperature dependent 2<sup>nd</sup> derivative spectra of pMDI-PVA-cellulose film.

To separate overlapped bands, temperature dependent FT-IR spectra were collected and 2<sup>nd</sup> derivative calculation was performed. Result of pMDI-PVA-cellulose film was showed in Fig. 5.3.15. During heating, hydrogen band dissociated, so the bands of hydrogen bonded urethane and urea at  $1706\text{cm}^{-1}$  and  $1639\text{cm}^{-1}$  decreased. Non-hydrogen-bonded urethane band at  $1736\text{cm}^{-1}$  also descended, because of urethane thermal degradation. Non-hydrogen-bonded urea as well as isocyanurate band increased with temperature, because substituted urea and trimer were generated during urethane thermal decomposition (Scheme.

5.3.1). Uretidione decomposition led to band intensity descent at  $1777\text{cm}^{-1}$ . Here, urethane formed in NCO-hydroxyl reaction in ambient condition was confirmed. Nevertheless, it was impossible to distinguish between the urethane from PVA and the urethane form cellulose.

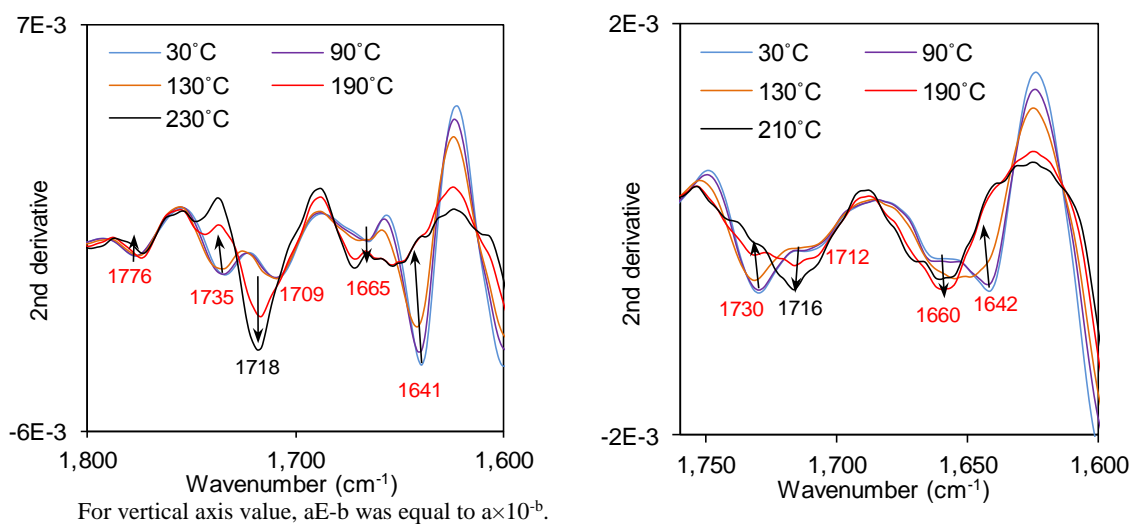


Fig. 5.3.16. Temperature dependent 2<sup>nd</sup> derivative spectra of pMDI-PVA film (left) and pMDI-cellulose (right).

Temperature dependent 2<sup>nd</sup> derivative spectra of pMDI-PVA film and pMDI-cellulose mixture were shown in Fig. 3.5.16. At  $30^\circ\text{C}$ ,  $1641\text{cm}^{-1}$  and  $1642\text{cm}^{-1}$  were assigned to hydrogen bonded C=O stretching bands of urea, and non-hydrogen-bonded C=O stretching bands of urea appeared at  $1661\text{cm}^{-1}$  and  $1660\text{cm}^{-1}$ . Based on the results of Fig. 5.3.4 and Fig. 5.3.5,  $1735\text{cm}^{-1}$  and  $1730\text{cm}^{-1}$  were attributed to non-hydrogen-bonded C=O stretching absorption bands of urethane, and  $1709\text{cm}^{-1}$  and  $1712\text{cm}^{-1}$  were assigned to hydrogen bonded urethane C=O stretching. Isocyanurate C=O stretching bands at  $\approx 1720\text{cm}^{-1}$  were covered by urethane bands. Uretidione band appeared at  $1776\text{cm}^{-1}$ . After heating, thermal degradation of urethane contributed obvious band decreasing at  $1735\text{cm}^{-1}$  and  $1730\text{cm}^{-1}$ . Band decreasing at  $1641\text{cm}^{-1}$  and  $1642\text{cm}^{-1}$  was attributed to hydrogen bond dissociation of urea. Bands decreasing at  $1776\text{cm}^{-1}$  was related to uretidione decomposition. On the other hand, band increasing at  $1665\text{cm}^{-1}$  and  $1660\text{cm}^{-1}$  was due to the generations of non-hydrogen-bonded urea and substituted urea.

Isocyanurate bands at  $1709\text{cm}^{-1}$  and  $1712\text{cm}^{-1}$  had increasing, attributed to NCO trimerization at high temperature. In this part, urethane from NCO-PVA reaction and urethane from NCO-cellulose reaction were confirmed, respectively. However, those two types of urethanes had quite similar FT-IR absorptions, so it was difficult to distinguish between them.

#### **5.4 conclusions**

Dimerization and trimerization of NCO, even though limited, could not be ignored, especially for aromatic isocyanate which has high reactivity. Dimer and trimer of NCO, uretdione and isocyanurate, were synthesized first to assign their specific absorption bands. Then, the generated uretdione in API thin film were confirmed. Result indicated that self-reaction of NCO carried on slowly in API thin film during aging period.

Several carbamates were synthesized to study PVA-NCO reaction and cellulose-NCO reaction, respectively. TGA results of the carbamates synthesized from phenyl isocyanate implied that thermal degradation of urethane linkage mainly formed NCO and hydroxyl. FT-IR results of the carbamates synthesized from pMDI suggested that NCO decomposition formed substituted urea. At last, temperature dependent FT-IR was performed on pMDI-PVA film and pMDI-cellulose mixture to confirm NCO reactions with PVA hydroxyl and cellulose hydroxyl in ambient condition.

## 6 Summary

In this research, chemical structure as well as physical property of cured glue-line of aqueous vinyl polymer-isocyanate adhesive for wood were studied. In order to *in-situ* detect the chemical structure of glue-line sandwiched between two adherends, Fourier transform near infrared spectroscopy, which has high penetration ability, was utilized. In addition, dynamic thermomechanical analysis and cross-lap bonding test were employed to analyze the physical properties of glue-line.

In chapter 2, the variations of chemical structure and physical property of API films during post-curing were studied.  $T_{5\%}$  of 6 days aged API film occurred at 279°C, but the thermal degradations of urethane and urea linkage could not be observed on TGA curve.  $T_g$  peak did not show up clearly on DSC curve due to the restricting effect of cross-linking on molecular movement. Two exothermal peaks at 141°C and 285°C on DSC curve were attributed to NCO self-reactions and NCO thermal degradation reactions, respectively.  $T_g$  of API film at 28°C was confirmed by DMA test. PVA semi-crystal slippage as well as acute NCO reactions contributed to a significant peak at 203°C on loss factor curve. Rubbery plateau was observed on storage modulus curve, by which cross-linking density was calculated. Chemical structure variation of API thin film during post-curing was confirmed by FT-IR spectroscopy. C=O stretching bands of urethane and urea appeared at 1715 $\text{cm}^{-1}$  and 1639 $\text{cm}^{-1}$ , respectively, and urea band intensity increased faster than urethane band intensity. Cross-laps test indicated that urethane and urea generation in post-curing process led to an increasing of bond strength.

In chapter 3, two model compounds (MUT and DPU) were synthesized first to assign the NIR absorptions of urethane and urea, two primary products of NCO reactions. Temperature dependent FT-IR and FT-NIR spectroscopy were

employed for band assignment, since hydrogen bonded amide is sensitive to temperature. By using model compounds, the specific NIR absorptions of urethane were detected at  $6533\text{cm}^{-1}$ ,  $6503\text{cm}^{-1}$  (N-H stretching first overtone),  $5050\text{cm}^{-1}$  (N-H stretching/amide II combination tone),  $4932\text{cm}^{-1}$  (C=O stretching second overtone) and  $4867\text{cm}^{-1}$  (N-H stretching/amide I combination tone), and the specific bands of urea were detected at  $6506\text{cm}^{-1}$  (N-H stretching first overtone),  $5019\text{cm}^{-1}$ ,  $4984\text{cm}^{-1}$  (N-H stretching/amide II combination tone or N-H stretching/N-H bending combination tone),  $4935\text{cm}^{-1}$  (C=O stretching second overtone) and  $4880\text{cm}^{-1}$  (N-H stretching/amide I combination tone).

Then, the chemical structure of API glue-line sandwiched between two pieces of filter papers was analyzed by using FT-NIR spectroscopy. NIR absorption bands of API paper occurred at  $5065\text{cm}^{-1}$  (N-H stretching/amide II combination tone of urethane),  $5005\text{cm}^{-1}$  (N-H stretching/amide II combination tone of urea),  $4918\text{cm}^{-1}$  (C=O stretching overtone) and  $4840\text{cm}^{-1}$  (N-H stretching/amide II combination tone or O-H combination tone). After that, the generations of urethane and urea in API paper during post-curing were tracked. From 1 day to 20 days, urethane and urea generated continuously.

In chapter 4, in order to investigate the practicability of FT-NIR test on glue-line, FT-NIR was used to study the influences of adhesive components and aging conditions on chemical structure. PVA with low DS (degree of saponification) was expected to mix and react better with pMDI. However, there was almost no disparity in glue-line chemical structures based on different PVAs. High bond strength was obtained on the adhesive with high molecular weight PVA. FT-NIR result demonstrated that the adhesive with less SBR latex produced more urethane and urea, due to high pMDI and PVA content. DMA showed that after 1 day aging the API film with low SBR latex content had more unreacted pMDI. Cross-laps with high SBR latex content showed high initial bond strength, and its strength

decreased after 6 days aging. Cross-laps with more pMDI had been fully post-cured after 6 days aging and thus displayed increasing bond strength.

Dry aging condition contributed to much less urethane and urea generation amount than other humidity conditions. Dry condition aged API film was broken at 85°C during DMA test, due to brittleness and less cross-linking structure. Dry condition also led to worse bonding performance of cross-lap. The accelerating effect of heating treatment was just temporary and it became more and more unobvious with aging time, because the mobility of molecule in glue-line dominated NCO reactions. DMA test verified that heating treatment speed up the formation of cross-linking. Bond strength was also promoted by heating.

In chapter 5, uretdione and isocyanurate, dimer and trimer of NCO, in API thin film were confirmed. Self-reactions of NCO carried on slowly in API thin film during aging period. The difference between two urethanes, one from PVA-NCO reaction and the other one from cellulose-NCO reaction, was studied. TGA and FT-IR result implied that thermal degradation of urethane linkage mainly generated NCO and hydroxyl. FT-IR result suggested that NCO decomposition of pMDI formed substituted urea. Finally, NCO-PVA and NCO-cellulose reactions in ambient condition were confirmed by temperature dependent FT-IR spectroscopy.

Conclusions: Residual NCO in cured API adhesive glue-line still can react with hydroxyls, forming chemical linkages and contributing to bond strength increasing. In the experiment, FT-NIR spectroscopy was employed for the *in-situ* chemical structure analyzing of glue-line. Further, the relationship between chemical structure and physical property of glue-line was studied. For better understanding the bonding mechanism of API adhesive to wood, the reaction between cross-linker and cellulose (one wood component) were confirmed.

## References

- [1] JIS K 6806 (2003) (Japanese Industrial Standard)
- [2] Grøstad K, Pedersen A. Emulsion polymer isocyanates as wood adhesive: a Review. *J Adhes Sci Technol* 2010; 24: 1357-81.
- [3] Hori N, Asai K, Takemura A. Effect of the ethylene/vinyl acetate ratio of ethylene–vinyl acetate emulsion on the curing behavior of an emulsion polymer isocyanate adhesive for wood. *J Wood Sci* 2008; 54: 294-9.
- [4] SPSJ (Compiled by). 高性能液状ポリマー材料 [High Performance Liquid Polymeric Materials]. Tokyo: Maruzen Publishing Co., Ltd.; 1990.
- [5] Ling N. 水性高分子-イソシアネート系接着剤の硬化メカニズムに関する研究 [Research on API adhesive's curing mechanism] (Doctor thesis). Tokyo: The University of Tokyo; 2008. Japanese.
- [6] Kayano Y. 充填剤 [Fillers]. *ADHESION TECHNOLOGY, JAPAN* 2001; 21: 34-40.
- [7] Chattopadhyay DK, Sreedhar B, Raju KVS. The phase mixing studies on moisture cured polyurethane-ureas during cure. *Polym* 2006; 47: 3814-25.
- [8] Daniel da Silva AL, Martín-Martínez JM, Moura Bordado JC. Influence of the storage of reactive urethane quasi-prepolymers in their composition and adhesion properties. *Int J Adhes Adhes* 2007; 28: 29-37
- [9] Taki K. 水性高分子-イソシアネート系接着剤 [Aqueous Vinyl Polymer-Isocyanate Adhesive for Wood]. In: Tomida B, editor. 木材の接着・接着剤 [Adhesion and Adhesive for Wood], Tokyo: Wood Technological Association of Japan; 1996. p. 130-43. Japanese.

- [10] Taki K. 水性ビニルウレタン系接着剤に関する研究 [The Research on Aqueous Vinyl Polymer-Isocyanate Adhesive for Wood]. JWRS Journal 1985; 31: 573-578. Japanese.
- [11] Taki K, Tomita B, Mizumachi H. 水性ビニルウレタン系接着剤に関する研究 (第3報) イソシアネート基の反応メカニズムについて [Studies on Aqueous Vinyl Polymer-Isocyanate Adhesives III. Reaction mechanism of the isocyanate group]. JWRS Journal 1983; 29: 145-52.
- [12] Hori N. 水性高分子-イソシアネート系木材接着剤の化学構造 [Chemical structure of API adhesive]. Wood Industry 2006; 61: 190-4. Japanese.
- [13] Yamada M, Taki K, Shibutani M. 水および有機溶媒中でのイソシアネート化合物とアセトアセチル化 PVA の架橋反応 [Crosslinking Reactions Between Isocyanate Compounds and Acetoacetylated PVA in Water and in Organic solvent systems]. JWRS Journal 2008; 54: 191-8.
- [14] Maehara A. API 接着剤の硬化初期における動的粘弾性挙動 [Rheological behavior of initially cured API adhesive] (Bachelor Thesis). Tokyo: The University of Tokyo; 2006. Japanese.
- [15] Clauß S, Dijkstra DJ, Gabriel J, Karbach A, Matner, M, Meckel W, Niemz P. Influence of the Filler Material on the Thermal Stability of One-Component Moisture-Curing Polyurethane Adhesives. J Appl Polym Sci 2012, 124, 3641-9.
- [16] Donate-Robles J, Martín-Martínez J. Addition of precipitated calcium carbonate filler to thermoplastic polyurethane adhesives. Int J Adhes Adhes 2011; 31: 795-804.

- [17] Taki K, Yamada M, Tomiya S, Yoshida M. 水性高分子-イソシアネート系接着剤とそれを用いた合板からのMDI放散挙動 [API adhesive and MDI releasing of plywood]. *Wood Industry* 2006; 61: 305-9. Japanese.
- [18] Taki K, Tomita B, Mizumachi H. 水性ビニルウレタン系接着剤に関する研究 [Studies on Aqueous Vinyl Polymer-Isocyanate Adhesive III]. *JWRS Journal* 1983; 29: 145-52. Japanese.
- [19] Yamada M, Taki K, Shibutani M. アセトアセチル化PVAとイソシアネート化合物との反応 [The Reaction between Acetoacetylated PVA and isocyanate compound]. *J Adh Sco Jpn* 2006; 42: 309-14. Japanese.
- [20] Ling N, Hori N, Takemura A. Effect of postcure conditions on the dynamic mechanical behavior of water-based polymer-isocyanate adhesive for wood. *J Wood Sci* 2008; 54: 377-82.
- [21] Ling N, Hori N, Takemura A. 熱処理したAPI接着剤の動的粘弾性分析 [Effect of Postcure Conditions on The Dynamic Behavior of Water-Based Polymer-Isocyanate Adhesive for Wood]. *JWRS Journal* 2009; 55: 293-8. Japanese.
- [22] He G, Yan N. Effect of moisture content on curing kinetics of pMDI resin and wood mixtures. *Int J Adhes Adhes* 2005; 25: 450-5.
- [23] Taki K. 水性ビニルウレタン系接着剤に関する研究 (第4報) イソシアネート化合物による木材の接着 [Studies on Aqueous Vinyl Polymer-Isocyanate Adhesives IV. Adhesion of woods with isocyanate compounds]. *JWRS Journal* 1985; 31: 573-8.
- [24] Gao Z, Wang W, Zhao Z, Guo M. Novel whey protein-based aqueous polymer isocyanate adhesive for glulam. *J Appl Polym Sci* 2011; 120: 220-5.

- [25] Omura Y, 水性高分子-イソシアネート系接着剤の近赤外分光法による接着層の *in-situ* 分析 [*in-situ* analysis of API adhesive glue-line using FT-NIR] (Master thesis). Tokyo: The University of Tokyo; 2012. Japanese.
- [26] Ozaki Y, editor. 赤外分光法 [Infrared Spectroscopy], Tokyo: IPC; 1998. Japanese.
- [27] Burns DA, Ciurczak EW. Handbook of Near-Infrared Analysis. 3rd ed. Boca Raton, London, New York: CRC Press; 2007.
- [28] Weng S. 傅里叶变换红外光谱分析. 第二版 [FT-IR Spectroscopy Analysis. 2nd ed.] Beijing: Chemical Industry Press; 2010.
- [29] Noda I. Two-dimensional infrared (2D IR) spectroscopy: theory and applications. *Appl Spectrosc* 1990; 44: 550-61.
- [30] Peng Y. 二维红外相关光谱在聚合物体系中的应用 [The Application of 2D Correlation IR Spectrum on Polymer] (Doctor thesis). Shanghai: Fudan University; 2006. Chinese.
- [31] Liu H, Xiang B, Qu L. Structure analysis of ascorbic acid using near-infrared spectroscopy and generalized two-dimensional correlation spectroscopy. *J Mol Struct* 2006; 794: 12-17.
- [32] Menard KP. Dynamic mechanical analysis a practical introduction. Boca Raton, London, New York, Washington DC: CRC Press; 2006.
- [33] Sterley M, Trey S, Lundevall Å, Olsson S. Influence of Cure Conditions on the Properties of a One-Component Moisture-Cured Polyurethane Adhesive in the Context of Green Gluing of Wood. *J Appl Polym Sci* 2012; 126: 296-303.
- [34] Taki K, Tomita B, Mizumachi H. 水性ビニルウレタン系接着剤に関する研究 (第2報) 接着剤の架橋密度が広い温度域にわたる物性ならびに接着強度におよぼす影響 [Studies on Aqueous Vinyl Polymer-Isocyanate Adhesives II. Dependence

of mechanical properties and bond strength on the concentration of crosslinks in cured adhesives over a wide temperature range]. JWRS Journal 1982; 28: 150-5.

[35] Holland BJ, Hay JN. The thermal degradation of poly (vinyl alcohol). *polym* 2001; 42: 6775-83.

[36] Tsuchiya Y, Sumi K. Thermal decomposition products of poly (vinyl alcohol). *J Polym Sci, Polym Chem* 1969; 7: 3151-58.

[37] Kwon E, Castaldi M J. Investigation of Mechanisms of Polycyclic Aromatic Hydrocarbons (PAHs) Initiated from the Thermal Degradation of Styrene Butadiene Rubber (SBR) in N<sub>2</sub> Atmosphere. *Environ Sci Technol* 2008; 42: 2175-80.

[38] Chattopadhyay DK, Webster D C. Thermal stability and flame retardancy of polyurethanes. *Prog Polym Sci* 2009; 34: 1068-113.

[39] Herreraa M, Matuscheka G, Kettrup A. Thermal degradation of thermoplastic polyurethane elastomers (TPU) based on MDI. *Polym Degrad Stabil* 2002; 78: 323-31.

[40] Petrovic ZS, Zavargo Z, Flynn JH, Macknight WJ. Thermal degradation of segmented polyurethanes. *J Appl Polym Sci* 1994; 51: 1087-95.

[41] Berta M, Lindsay C, Pans G, Camino G. Effect of chemical structure on combustion and thermal behaviour of polyurethane elastomer layered silicate nanocomposites. *Polym Degrad Stabil* 2006; 91: 1179-91.

[42] Gupta T, Adhikari B. Thermal degradation and stability of HTPB based polyurethane and polyurethaneureas. *Thermochim Acta* 2003; 402: 169-81.

[43] Taki K, Tomita B, Mizumachi H. 水性ビニルウレタン系接着剤に関する研究 (第1報) 接着剤の架橋密度が広い温度域にわたる物性と接着強度 [Studies on Aqueous Vinyl Polymer-Isocyanate Adhesives I. Mechanical properties of base

polymer and bond strength over a wide temperature range]. JWRS Journal 1982; 28: 143-9.

[44] Watanabe K, Miyake T, Okumoto T. 炭素-13 核磁気共鳴法と赤外吸収スペクトル法によるポリウレタン中のイソシアネート化合物のアミンを用いる分解性の評価 [Evaluation for amine-degradation of isocyanate polymerizates in polyurethane networks by  $^{13}\text{C}$ -NMR and IR spectroscopy]. BUNSEKI KAGAKU 1996; 45: 321-6.

[45] Ren D, Frazier C. Structure–property behavior of moisture-cure polyurethane wood adhesives: Influence of hard segment content. Int J Adhes Adhes 2013; 45: 118-24.

[46] Menard KP. Dynamic mechanical analysis a practical introduction. Boca Raton, London, New York, Washington DC: CRC Press; 2006.

[47] Lu Y, Larock RC. Soybean-oil-based waterborne polyurethane dispersions: effects of polyol functionality and hard segment content on properties. Biomacromolecules 2008; 9: 3332-40.

[48] Jiang X. 简明红外光谱识谱法 [Concise analysis of FT-IR Spectrum]. Guangxi: Guangxi Normal University Press; 1992.

[49] Larkin P. IR and Raman Spectroscopy Principles and Spectral Interpretation. Amsterdam, Boston, Heidelberg, London, New York, Oxford, Paris, San Diego, San Francisco, Singapore, Sydney, Toyo: Elsevier; 2011.

[50] 2D shige (c) Shigeaki Morita, Kwansei-Gakuin University, 2004-2005.

[51] Han S, Luan Y, Pang S, Zhang Y. Thermodynamic and Spectroscopic Analysis of The Conformational Transition of Poly (vinyl alcohol) by Temperature-Dependent FTIR. Spectrochim. Acta Part A Mol. Biomol. Spectrosc. 2015; 139: 37-42.

- [52] Macphail RA, Strauss HL, Snyder RG, Elliger CA. C-H Stretching Modes and the Structure of n-Alkyl Chains. 2. Long, All-Trans Chains. *J. Phys. Chem.* 1984; 88: 334-41.
- [53] Wheeler OH. Near infrared spectra of organic compounds. *Chem. Rev.* 1959; 59: 629-60.
- [54] Miller CE, Edelman PG, Ratner BD. Near-Infrared Spectroscopic Analyses of Poly (Ether Urethane Urea) Block Copolymers. Part I: Bulk Composition. *Appl. Spectrosc.* 1990; 44: 576–80.
- [55] Miller, CE, Eichinger BE. Analysis of Rigid Polyurethane Foams by Near-Infrared Diffuse Reflectance Spectroscopy. *Appl. Spectrosc.* 1990; 44: 887–94.
- [56] Taki K, Yagi S, Yamagishi Y. Bond Quality of PVA-Isocyanate Reactive Resin Adhesive. III. Properties of Cured Resin Films. *JWRS Journal* 1980; 26: 81-6. Japanese.
- [57] Taki K, Tomita B, Mizumachi H. Studies on Aqueous Vinyl Polymer-Isocyanate Adhesive III. Reaction Mechanism of The Isocyanate Group. *JWRS journal* 1983; 29: 145-52. Japanese.
- [58] Taki K. Studies on Aqueous Vinyl Polymer-Isocyanate Adhesives IV. Adhesive of Woods with Isocyanate Compounds. *JWRS Journal* 1985; 31: 573-8. Japanese.
- [59] Yamada M, Maeda L, Taki K, Sibuya M. AA 化 PVA 水溶液の pMDI 分散性と木材接着性能(第 1 報)-PVA 水溶液での pMDI の分散性と反応性 [pMDI dispersity and wood bonding property of acetoacetylated PVA (Prat I) dispersity and reactivity of pMDI in PVA aqueous solution]. *J Adh Sco Jpn* 2006; 42: 364-71. Japanese.

[60] Yamada M, Taki K, Shibuya M. Crosslinking Reactions between Isocyanate Compounds and Acetoacetylated PVA in water in Organic Solvent Systems. JWRS Journal 2008; 54: 191-8. Japanese.

[61] Beijing Organic Chemical Plant Research Institute (Compiled by). 聚乙烯醇的性质和应用 [Properties and Applications of Polyvinyl Alcohol]. Beijing: Textile Industry Press; 1979.

[62] Taki K, Mizumachi H, Yamagishi Y. 水性ビニルウレタン系接着剤の接着性 (第2報) 乾湿状態における接着性と接着剤の物性 [Bond Quality of PVA-isocyanate Reactive Resin Adhesive (II) Relation between bond quality at dry and wet state and physical properties of cured resin films. JWRS Journal 1979; 25: 216-24. Japanese.

[63] SPSJ (Compiled by). 高分子と水分 [Polymer and Moisture]. Tokyo: Kyoritsu Shuppan Co., Ltd.; 1995.

[64] SPSJ (Compiled by). 高分子の物性 [Properties of Polymer]. Tokyo: Kyoritsu Shuppan Co., Ltd.; 1997.

[65] Ling Z, Hori N, Iwata T, Akio T. *In-situ* Analysis of Chemical Structure of API Adhesive Using FT-NIR Spectroscopy. J Adh Sco Jpn 2015; 51: 322-31.

[66] Hori T. ポリイソシアネートの誘導体 [Derivatives of polyisocyanate]. ADHESION TECHNOLOGY, JAPAN 2001; 21: 17-26.

[67] Harling S, Meoal G, Schaible S, Schulthess A, Braendli C, Meincke O. Latent reactive polyurethanes based on toluenediisocyanate-uretdione and polycaprolactones. Int J Adhes Adhes 2013; 46: 26-33.

[68] Watanabe K, Miyake T, Okumoto T. Evaluations for amine-degradation of isocyanurate polymerizates in polyurethane networks by  $^{13}\text{C}$ -NMR and IR spectroscopy. *BUNSEKI KAGAKU* 1996; 45: 321-26. Japanese.

[69] Labafzadeh SR, Kavakka JS, Vyavaharkar K, Sievänen K, Kilpeläinen I. Preparation of cellulose and pulp carbamates through a reactive dissolution approach. *RSC Adv* 2014; 4: 22434-41.

[70] Berta M, Lindsay C, Pans G, Camino G. Effect of chemical structure on combustion and thermal behaviour of polyurethane elastomer layered silicate nanocomposites. *Polym. Degrad. Stabil.* 2006; 91: 1179-91.

## **Acknowledgements**

Many people offered me valuable help in the thesis writing.

First, I would like to give my sincere and deepest gratitude to my supervisor, Prof. Akio Takemura, who taught me over all this research with extraordinarily patience. He gave me valuable guidance, great advice and inspiration of idea. Without his strong support, I could not complete this thesis.

My heartfelt thanks also go to Prof. Satoshi Shida, Prof. Tadahisa Iwata, Prof. Yuji Matsumoto and Prof. Yukie Saito who checked my thesis with greet patience and gave me instructive suggestions.

Then thinks to Prof. Daisuke Ishii and Prof. Naruhito Hori who kindly and patiently taught me on my study.

I also would like to thank NIPPON A & L Inc. (Japan) and Nippon Polyurethane Industry Co., Ltd. (Japan) for their generous supply of SBR latex and MR-200.

I am grateful to my lovely colleagues in our laboratory. They helped me and offered a quiet situation to compose the thesis.

Last but not least, my thanks would also go to my parents, elder brother and sister for their boundless love and whole-hearted support over all those past years.